Title
Regulation of immune cell development and effector function mediated by X-linked epigenetic regulator UTX.

Author
Cheng, Mandy

Publication Date
2023

Peer reviewed|Thesis/dissertation

UNIVERSITY OF CALIFORNIA

Los Angeles

Regulation of immune cell development and effector function mediated by X-linked epigenetic regulator UTX.

A dissertation submitted in partial satisfaction of the requirements for the degree Doctor of Philosophy in Molecular Biology

by

Mandy Cheng

2023

ABSTRACT OF THE DISSERTATION

Regulation of immune cell development and

effector function mediated by X-linked epigenetic regulator UTX.

by

Mandy Cheng

Doctor of Philosophy in Molecular Biology

University of California, Los Angeles, 2023

Professor Maureen Su, Chair

Epigenetic regulation, changes in gene expression without alterations to the genetic material, has brought to light another layer of regulatory mechanisms that control immune effector processes in response to immune threats such as viral infection, cancer, and autoimmunity. Elucidating epigenetic regulators driving immune cell differentiation and modulation of effector processes are critical to our understanding of endogenous immune responses. Our studies aim to delineate mechanisms driven by an X-linked epigenetic regulator, UTX, in regulation of natural killer (NK) and T cells, two cell types important in the innate and adaptive arms of our immune system.

Viral infection outcomes are sex-biased, with males generally more susceptible than females. Paradoxically, the numbers of anti-viral NK cells are increased in males. We demonstrate that while numbers of NK cells are increased in male mice, they display decreased effector function

compared to females in mice and humans. These differences were not solely dependent on gonadal hormones, since they persisted in gonadectomized mice. *Kdm6a* (UTX), an epigenetic regulator which escapes X inactivation, was lower in male NK cells, while NK cell-intrinsic UTX deficiency in female mice increased NK cell numbers and reduced effector responses. Furthermore, mice with NK cell-intrinsic UTX deficiency showed increased lethality to mouse cytomegalovirus (MCMV). Integrative multi-omics analysis revealed a critical role for UTX in regulating chromatin accessibility and gene expression critical for NK cell homeostasis and effector function. Collectively, these data implicate UTX as a critical molecular determinant of sex differences in NK cells.

Low oxygen levels, or hypoxia, has been associated with immune defects in multiple contexts. Hypoxia is associated with higher levels of H3K27me3 in CD4+ T cells. T cell-specific deletion of the histone demethylase is sufficient to recapitulate multiple features of hypoxia, including increased H3K27me3 accumulation and decreased production of IFN-γ^+ $CD4^+$ T cells in response to IL-12 cytokine stimulation. T cell specific UTX deletion has functional consequences, as mice are more susceptible to colon cancer and is not responsive to IFN-γ-dependent checkpoint therapy with anti-PD-1 treatment. However, mice with loss of UTX in T cells protected from colitis in which IFN-γ production has been tied with pathogenesis. Concomitant RNA and H3K27me3 CUT&Tag sequencing demonstrate an important role for UTX in removing repressive H3K27me3 marks to promote upregulation of IL12/STAT4 pathway genes including *Il12rb, Tbx21,* and *Ifng*. Together, these data demonstrate that UTX functions through its demethylase activity to promote Th_1 cell differentiation and suggest that hypoxia's HIF-independent effects on Th_1 effector function may be mediated through UTX.

This dissertation of Mandy Cheng is approved.

Timothy O'Sullivan

Gay Crooks

Steven Bensinger

Manish Butte

Maureen Su, Committee Chair

University of California, Los Angeles

2023

This dissertation is dedicated to:

My loving family, friends, and partner in life.

Table of Contents

List of Figures

Chapter 2

Chapter 3

ACKNOWLEDGMENTS

First and foremost, I would like to thank my mentor, Maureen Su. Maureen has far exceeded any expectations I had as a graduate student by having the most infectious passion and drive for science. As a mentor, she broadened my perspective on how to approach research at every angle and inspired me every day with her enthusiasm and astute thoughts on how to progress my project. As a prominent and successful female scientist, she set an incredible example not only on how to perform cutting edge research, but also how to carry yourself as a professional in the field. When I first started graduate school, Maureen had just moved her lab over from UNC Chapel Hill, and was gracious enough to accept me as a rotation student even before she had finished moving in. From our first of many one-on-one meetings where we would always lose track of time talking about science and about life in general, I knew she would be the best mentor for me. I thank her for always putting my needs and career development first during my graduate training. I am beyond grateful for her time and patience she gives me since as a clinician she has a very packed schedule, yet she always prioritized me whenever I needed her guidance. Maureen is unique in her capability to gauge the mentoring style that is needed from each student and delivers it with patience and grace. The most valuable trait she has given me is confidence as a scientist. Confidence to speak up and ask questions even when I am nervous, confidence to stand my ground when I feel strongly about something, and confidence to overcome the imposter syndrome that plagued a part of my graduate studies. Through the ups and downs of my time in graduate school, I will always be thankful that Maureen was a constant and unwavering support in my growth. I would be nowhere near who I am today as a scientist if it weren't for all the time and energy she dedicated to my training.

Next, I want to thank Tim O'Sullivan, who has also been a strong mentor for me throughout graduate school. As a major collaborator in my thesis project, Tim has given a lot of his time and effort into developing this project. When I first met Tim during my interviews I was really excited about all the science we discussed during our talk. So much so that I decided to rotate with him once I got in. Tim has welcomed me into the world of NK cells and I will be forever grateful for all the knowledge and experimental techniques he has passed down to me. He taught me a lot from presenting skills to always coming up with innovative ideas to approach science. I am thankful everything Tim has invested into my own development as a scientist as well as our collaborative project.

I would like to thank Peter Bradley for being an incredible introduction into graduate school as my home area director. I distinctly remember that he already memorized my name during the interviews and always tried to introduce me to PIs that he thought I would like to speak with. His warmth and dedication to the program was a large reason for my choice to attend UCLA. Peter was so good gauging my personality that he introduced me to Maureen and said "I think you two would really get along". I am thankful to peter that during my first year of rotations, he was indispensable for my time adjusting to graduate school, and I always felt comfortable talking to him. Furthermore, I would also like to thank both Peter and Patricia Johnson for allowing me to be a part of the microbial pathogenesis training grant program for 2 years.

Many thanks to Melissa Lechner and Lisa Kohn for being incredible colleagues and pillars of support for me throughout the years. Melissa and Lisa joined the Su lab shortly after I officially started working with Maureen. For some time, it was just the 3 of us in lab together. I want to thank Melissa for always lending an ear when I needed her. Also, Melissa is another incredible female physician scientist that was not only a great collaborator in lab projects together but is also

a kind and giving person. I want to thank Lisa for the time we spent together and for our talks we would have about science and life. Lisa is one of the most compassionate and caring people I have had the ability to interact with.

I want to thank all our lab technicians, Kevin Joung, Natalie Yakobian, Lily Guo, Aline Hoang, Michael Astourian, and Ethan McCarthy, that have worked with me throughout the years to help me with experiments and mouse handling. Special thanks to Kevin and Natalie for all emotional support and coffee breaks we would have during my second year. Thanks to Natalie for not only being an incredible lab mate but one of my closest friends throughout graduate school (and beyond!). I appreciate all the late nights together for long experiments and the uplifting attitude that was always brought to lab. Thanks to Aline for being a bright and infectiously happy person in lab. I am thankful for Aline for boosting morale in the lab and being an incredible person to work with. Finally, I am thankful for Ethan who has supported me both as a scientist and by taking care of the mice, which are critical for my experiments.

Thanks to my undergraduate students Scott Chin and Bryan Chen who have worked very diligently with me over the years. Thanks to Scott for reaching out to me by being one of the few students to consistently come to my office hours when I TA'ed. Thanks to Scott for all the long hours for large mouse experiments together and for learning bioinformatics once we went into the pandemic and had to become virtual. Thanks to Bryan who mainly worked remotely on additional bioinformatic analysis that was instrumental in both projects. I appreciate his willingness to learn, even with no prior bioinformatic analysis experience.

Also, thanks to O'Sullivan lab members Joey Li and Luke Riggan for collaborating on the NK cell project together. Thanks for the guidance by Luke on initial experiments and thanks to Joey for his hard work and diligence on pushing out all the large experiments that were needed.

Additionally, thanks to Joey for all the support and time dedicated to working on this project together.

Thanks to my undergraduate lab mentor, Daniel Portnoy and the postdoctoral scholar I worked with at the time, Gabriel Mitchell. Gabe is one of the first driving factors in my decision to attend graduate school. He allowed me intellectual freedom and had an abundance of patience towards me as a very young scientist. I am also thankful to Dan for his straightforward and rigorous approach to science, which taught me a lot as my first experience with research. I am also grateful to the rest of the Portnoy lab members who allowed me to develop a strong foundation of basic research and presentation skills that I carried throughout my graduate studies.

I would like to acknowledge additional collaborators during my time here at UCLA. Thanks to Feiyang Ma and Matteo Pellegrini for help on bioinformatic analysis for ATAC-sequencing data. Thanks to Haley Hrncir and Arthur Arnold for supplying four core genotype mice for our project. Thanks to Lee Hong and Shezhad Sheikh from UNC, Chapel Hill for contributing to the *in vivo* colitis data sets presented. Thanks to collaborators from UNC Chapel Hill Jason Whitmire, Ageliki Tsagaratou, Karl Shpargel and Onyinye Iweala for helpful discussion in monthly meetings. I also acknowledge my thesis committee members: Steven Bensinger, Timothy O'Sullivan, Gay Crooks and Manish Butte for thoughtful discussion and always pushing me to see different perspectives on my research.

We thank the UCLA Technology Center for Genomics and Bioinformatics for RNA sequencing library preparation and the Cedars Sinai Applied Genomics, Computation, and Translational Core Facility for ATAC sequencing library preparation. Maureen Su is supported by the NIH (NS107851, AI143894, DK119445) Department of Defense (USAMRAA PR200530), and National Organization of Rare Diseases. Tim O'Sullivan is supported by the NIH (AI145997)

and UC CRCC (CRN-20-637105). I am supported by Ruth L. Kirschstein National Research Service Awards (GM007185 and AI007323), and Whitcome Fellowship from the Molecular Biology Institute at UCLA.

Lastly, I would like to thank my loving family and friends who have always given unconditional love and support. Thanks to my mom, who has always valued education over everything else, who has put everything she has ever worked for into supporting me throughout my journey. Thanks to my dad who has always been kind and patient with me even through hard times. Thanks to both my parents for giving me everything I have ever needed to succeed, even though it meant working long, hard hours to get me there. To my grandmother, may she rest in peace after the many years of looking after me and our family. Thanks to my brother who has always been there for me and loves me unconditionally, even if he doesn't always show it. Thanks to my partner, Keita Yada for being there for me through all the good and the bad times and for being my number 1 supporter, all the time (with Molly too). Thanks to all my friends here in LA (Jennifer Lin, Sunny Kim, Francois Yap, Naomi Lee, Daniel Ra, Bao Lam, Jeff Cho, Noah Schlenk), back in SF from college (Judy Lai and Jennifer Tang), and back home in Miami (Ainara Bruno, Michelle Mariano, and Lauren Losada) for the community that has carried me through graduate school.

VITA

Education

2013-2017	University of California, Berkeley Berkeley, CA	B.A.	Molecular Cell Biology Emphasis: Immunity and Pathogenesis
2018-Present	University of California, Los Angeles, CA Advancement to Candidacy: November 16, 2021	Ph.D.	Molecular Biology Focus: Immunity, Microbes, and Molecular Pathogenesis

Professional Experience

2014-18 Research Technician, Laboratory of Dr. Daniel Portnoy, UC Berkeley, CA
2016 Research Intern, Immunology and IMR Discovery Department, Merck, Palo Alto, CA
2013-15 Undergraduate Lab Technician, Laboratory of Dr. Nicole King, UC Berkeley, CA

Professional Societies

2021-present Member, American Association of Immunologists (AAI)
2022-present Member, Society for Natural Immunity (SNI)
2022-present Member, Federation of Clinical Immunology Societies (FOCiS)
2022-present Member, International Cytokine and Interferon Society (ICIS)

Conference/Abstract Awards

May 2022 2022 AAI Trainee Abstract Award

Research Fellowships Received

Whitcome Pre-Doctoral Fellowship in Molecular Biology June 2022-2023 $3,125/mo
University of California, Los Angeles

T32 Ruth L. Kirschstein National Research Service Award June 2022-2023 $26,352
University of California, Los Angeles Microbial Pathogenesis Training Grant (AI007323)

Schering Award June 2022 $10,000
Microbiology, Immunology, and Molecular Genetics | University of California, Los Angeles

Mitsuo Takasugi Award July 2022 $1,000
University of California, Los Angeles

T32 Ruth L. Kirschstein National Research Service Award June 2021- 2022 $25,836
University of California, Los Angeles Microbial Pathogenesis Training Grant (AI007323)

Whitcome Pre-Doctoral Fellowship in Molecular Biology June 2020 - June 2021 $8,680
University of California, Los Angeles

T32 Ruth L. Kirschstein National Research Service Award June 2020 – June 2021 $25,320
University of California, Los Angeles Cellular and Molecular Biology Training Grant (GM007185)

Peer Reviewed Publications

1. **Cheng, M. I.,** Chen, C., Engström, P., Portnoy, D. A., & Mitchell, G. (2018). Actin-based motility allows Listeria monocytogenes to avoid autophagy in the macrophage cytosol. *Cellular Microbiology*, *20*(9). https://doi.org/10.1111/cmi.12854
2. Mitchell, G., **Cheng, M. I.**, Chen, C., Nguyen, B. N., Whiteley, A. T., Kianian, S., … Portnoy, D. A. (2017). Listeria monocytogenes triggers noncanonical autophagy upon phagocytosis, but avoids subsequent growth-restricting xenophagy. *Proceedings of the National Academy of Sciences of the United States of America*, *115*(2).
3. Nguyen, B. N.*, Chávez-Arroyo, A.*, **Cheng, M. I.,** Krasilnikov, M., Louie, A., & Portnoy, D. A. (2020). TLR2 and endosomal TLR-mediated secretion of IL-10 and immune suppression in

response to phagosome-confined Listeria monocytogenes. *PLOS Pathogens*, *16*(7), e1008622. https://doi.org/10.1371/journal.ppat.1008622

4. Wolbert, J.*, **Cheng, M. I.***, Horste, G. M. zu, & Su, M. A. (2020). Deciphering immune mechanisms in chronic inflammatory demyelinating polyneuropathies. *JCI Insight*, *5*(3). https://doi.org/10.1172/jci.insight.132411
5. Wang, Y.*, Guo, L.*, Yin, X.*, McCarthy, E. C., **Cheng, M. I.**, Hoang, A. T, Chen, H., Patel, A.Y, Trout, D.A., Xu, E., Yakobian, N., Hugo, W., Howard, J.F., Sheu, K.M., Hoffmann, A., Lechner, M.G., Su, M. A. (2022). Pathogenic TNF-α drives peripheral nerve inflammation in an Aire-deficient model of autoimmunity. *Proceedings of the National Academy of Sciences*, *119*(4), e2114406119. https://doi.org/10.1073/pnas.2114406119
6. Lechner, M. G., **Cheng, M. I.,** Patel, A. Y., Hoang, A.T., Yakobian, N., Astourian, M., Pioso, M. S., Hugo, W., Angell, T. E., ,.. Su, M. A. (2022). Inhibition of the IL-17A Protects against Thyroid Immune-Related Adverse Events while Preserving Checkpoint Inhibitor Anti-tumor Efficacy. *The Journal of Immunology,* 2022.01.19.476844. https://doi.org/10.1101/2022.01.19.476844

Manuscripts *in Press*

1. **Cheng, M.I.,** Li, J.H., Riggan, L., Yakhshi Tafti, R., Chin, S., Ma, F., Pellegrini, M., Hrncir, H., Arnold, A.P., O'Sullivan, T.E., Su, M.A. The X-linked epigenetic regulator UTX controls NK cell-intrinsic sex differences. *In Press at Nature Immunology NI-A34021C*.

Poster Presentations/Abstracts

1. **Cheng, M.I.*,** Riggan, L., O'Sullivan, T.E., Su, M.A. (September 5, 2020). Epigenetic regulation of Natural Killer Cell Effector Function. *Molecular Biology Institute Annual Retreat and Research Conference,* Los Angeles, CA, USA.
2. **Cheng, M.I.*,** Riggan, L., O'Sullivan, T.E., Su, M.A. (May 11, 2022). Sex differences in NK cells mediated by X-linked UTX. *American Association of Immunologists Conference,* Portland, OR, USA.
3. **Cheng, M.I.*,** Riggan, L., O'Sullivan, T.E., Su, M.A. (May 16, 2022). Sex differences in NK cells mediated by X-linked UTX. *Society for Natural Immunity Conference,* Bonita Springs, FL, USA.
4. **Cheng, M.I.*,** Riggan, L., O'Sullivan, T.E., Su, M.A. (June 22, 2022). **"**Sex differences in NK cells mediated by X-linked epigenetic regulator UTX". *Federation of Clinical Immunology Societies,* San Francisco, CA, USA.
5. **Cheng, M.I.*,** Riggan, L., O'Sullivan, T.E., Su, M.A. (September 6, 2022). **"**Sex differences in NK cells mediated by X-linked epigenetic regulator UTX". *Molecular Biology Interdepartmental Retreat,* Los Angeles, CA, USA.
6. **Cheng, M.I.*,** Riggan, L., O'Sullivan, T.E., Su, M.A. (September 11, 2022 – Virtual iPoster and September 25 – In-Person Poster). **"**Sex differences in NK cells mediated by X-linked epigenetic regulator UTX". *4th International Conference of Innate Lymphoid Cells, Big Island,* HI, USA.

Selected Oral Presentations

1. "Epigenetic regulation of natural killer cell development and effector function" – Molecular Biology Interdepartmental Program Student Seminar Series (March 1, 2020)
2. "Sex differences in NK cells mediated by X-linked UTX" **-** I3T Research In Progress Seminar Series (February 1, 2022)
3. **"**Sex differences in NK cells mediated by X-linked epigenetic regulator UTX". *American Association of Immunologists Conference,* Portland, OR, USA. (Block Symposia Presentation May 10, 2022)
4. **"**Sex differences in anti-viral effector functions of NK cells by X-linked epigenetic regulator UTX". Microbial Pathogenesis Training Grant Research Symposium (May 12, 2022)
5. **"**Sex differences in NK cells mediated by X-linked epigenetic regulator UTX". *Federation of Clinical Immunology Societies,* San Francisco, CA, USA. (June 22, 2022)

Chapter 1: Introduction

Introduction

Our immune system is made up of two major arms, the innate and adaptive immune responses. The innate immune arm is comprised of cell types that are constantly surveying the body to rapidly to the foreign threat such a pathogen or tumor. Cells of the innate immune system keep many pathogens at bay and produce proinflammatory cytokines and chemokines to attract adaptive immune cells to the site of infection or malignancy. This allows the adaptive immune system time to develop a specific and targeted response to clear the malignancy. The major cell types we are investigating part of the innate immune system, natural killer (NK) cells and the adaptive immune response, T cells. Recently, epigenetic regulation, changes in gene expression without alterations to the genetic material, has brought to light another layer of regulatory mechanisms that control immune effector processes.

UTX, an epigenetic regulator, has been recently implicated as important for control of multiple developmental and effector programs[1-3]. UTX is an X-linked protein encoded by the gene *Kdm6a* and possesses intrinsic catalytic H3K27me3 demethylase activity. In addition to UTX's H3K27me3 demethylase activity, UTX binds to additional epigenetic regulators and transcription factors to form large multiprotein complexes to carry out multiple functions such as H3K4 methyltransferase and general chromatin unwinding[4-6]. UTX is an X-linked gene that escapes X-inactivation, which results in differential expression in females vs. males[7]. Thus, in Chapter 2, we further investigate the role of UTX in determining sex differences in immune cells.

Sexual dimorphism in the composition and function of the immune system results in sex bias in susceptibility to infections, autoimmunity, and malignancies[8,9]. Thus, delineation of molecular mediators which drive sex differences in the immune response is important for development of precise therapeutic strategies to boost endogenous immune responses against

pathogenesis. A notable example is the well-described sex difference in composition of natural killer (NK) cells, a cytotoxic innate lymphoid cell that rapidly responds to immune threats. In humans and mice, NK cell numbers are higher in males compared to females[10]. In Chapter 2, we explore additional sex differences in NK cells and identify an epigenetic regulator, Kdm6a (UTX), which escapes X-inactivation in both humans and mice and is expressed at lower levels in male NK cells, as a critical regulator of sex differences in NK cells. Deletion of a single copy of UTX in female NK cells of mice, which mimics lower UTX levels in NK cells from male mice, phenocopies multiple features of male NK cells such as increased numbers and decreased effector function. As an epigenetic regulator, UTX controls multiple genes involved in regulation of NK cell numbers (e.g.*Bcl2*) and effector responses (e.g. *Ifng*) through modulating chromatin accessibility. Taken together, these data implicate UTX as a molecular determinant of sex differences in NK cells. Ultimately, our study provides a deeper mechanistic understanding of sex differences in NK cell biology which is critical in optimizing immune-modulating and anti-viral therapeutics.

In addition to the findings in NK cells, in Chapter 3, we explore the role of UTX in an additional cell type, CD4+ T cells, which also play an important role in the adaptive arm of the immune response against cancer while also identified as the pathogenic cell type in multiple autoimmune diseases. As a member of the 2-oxoglutarate (OG)-dependent dioxygenase (2-OGDD) family of enzymes, UTX has recently been shown to be oxygen-sensitive. Specifically, hypoxia inactivates UTX's demethylase activity in a HIF independent manner[11,12], which results in global H3K27me3 hypermethylation. We focused on UTX as a potential oxygen sensor in CD4+ T cells due to its previous links with immune cell differentiation[2], evidence of H3K27me3 accumulation in hypoxic tumor tissue[11], and because of its potential for therapeutic manipulation[13].

In Chapter 3, we show that hypoxia is associated with higher levels of H3K27me3 in CD4+ T cells. T cell-specific deletion of the histone demethylase is sufficient to recapitulate multiple features of hypoxia, including increased H3K27me3 accumulation and decreased production of IFN-γ^+ $CD4^+$ T cells in response to IL-12 cytokine stimulation. T cell specific UTX deletion has functional consequences, as mice are more susceptible to colon cancer and is not responsive to IFN-γ-dependent checkpoint therapy with anti-PD-1 treatment. However, mice with loss of UTX in T cells protected from colitis in which IFN-γ production has been tied with pathogenesis. Concomitant RNA and H3K27me3 CUT&Tag sequencing demonstrate an important role for UTX in removing repressive H3K27me3 marks to promote upregulation of IL12/STAT4 pathway genes including *Il12rb, Tbx21,* and *Ifng*. Together, these data demonstrate that UTX functions through its demethylase activity to promote Th1 cell differentiation and suggest that hypoxia's HIF-independent effects on Th1 effector function may be mediated through UTX.

References

1. Mitchell, J.E. *et al*. UTX promotes CD8(+) T cell-mediated antiviral defenses but reduces T cell durability. *Cell Rep* **35**, 108966 (2021).

2. Cook, K.D. *et al*. T Follicular Helper Cell-Dependent Clearance of a Persistent Virus Infection Requires T Cell Expression of the Histone Demethylase UTX. *Immunity* **43**, 703-714 (2015).

3. Beyaz, S. *et al*. The histone demethylase UTX regulates the lineage-specific epigenetic program of invariant natural killer T cells. *Nat Immunol* **18**, 184-195 (2017).

4. Gozdecka, M. *et al*. UTX-mediated enhancer and chromatin remodeling suppresses myeloid leukemogenesis through noncatalytic inverse regulation of ETS and GATA programs. *Nat Genet* **50**, 883-894 (2018).

5. Wang, C. *et al*. UTX regulates mesoderm differentiation of embryonic stem cells independent of H3K27 demethylase activity. *Proc Natl Acad Sci U S A* **109**, 15324-15329 (2012).

6. Wang, S.P. *et al*. A UTX-MLL4-p300 Transcriptional Regulatory Network Coordinately Shapes Active Enhancer Landscapes for Eliciting Transcription. *Mol Cell* **67**, 308-321 e306 (2017).

8. Fang, H., Disteche, C.M. & Berletch, J.B. X Inactivation and Escape: Epigenetic and Structural Features. *Front Cell Dev Biol* **7**, 219 (2019).

8. Wilkinson, N.M., Chen, H.C., Lechner, M.G. & Su, M.A. Sex Differences in Immunity. *Annu Rev Immunol* (2022).

9. Klein, S.L. & Flanagan, K.L. Sex differences in immune responses. *Nat Rev Immunol* **16**, 626-638 (2016).

10. Menees, K.B. *et al*. Sex- and age-dependent alterations of splenic immune cell profile and NK cell phenotypes and function in C57BL/6J mice. *Immune Ageing* **18**, 3 (2021).

11. Chakraborty, A. A., *et. al.,* Histone demethylase KDM6A directly senses oxygen to control chromatin and cell fate. *Science* 363, 1217-1222, (2019).

12. Prickaerts, P., *et al*. Hypoxia increases genome-wide bivalent epigenetic marking by specific gain of H3K27me3. *Epigenetics Chromatin* 9, 46, (2016).

13. Kruidenier, L., *et al*. A selective jumonji H3K27 demethylase inhibitor modulates the proinflammatory macrophage response. *Nature* 488, 404-408, (2012).

Chapter 2:

The X-linked epigenetic regulator UTX controls NK cell-intrinsic sex differences

The X-linked epigenetic regulator UTX controls NK cell-intrinsic sex differences

Mandy I. Cheng[1,2,], Joey H. Li[1,2], Luke Riggan[1,2,], Bryan Chen[1], Rana Yakhshi Tafti[1,2], Scott Chin[1], Feiyang Ma[3,4], Matteo Pellegrini[3,4], Haley Hrncir[5], Arthur P. Arnold[5], Timothy E. O'Sullivan[1,2,*] and Maureen A. Su[1,2,6,*]

[1]Department of Microbiology, Immunology, and Molecular Genetics, David Geffen School of Medicine at UCLA, Los Angeles, CA 90095
[2]Molecular Biology Institute, University of California, Los Angeles, Los Angeles, CA 90095, USA
[3]Department of Molecular, Cell, and Developmental Biology, University of California, Los Angeles, California, USA.
[4]Institute for Genomics and Proteomics, University of California, Los Angeles, California, USA.
[5]Department of Physiological Science, Laboratory of Neuroendocrinology of the Brain Research Institute, University of California, Los Angeles, CA 90095-1606, USA
[6]Department of Pediatrics, David Geffen School of Medicine at UCLA, Los Angeles, CA 90095, USA

[*]*Corresponding Authors*

Correspondence:

Timothy E. O'Sullivan, PhD
David Geffen School of Medicine at UCLA
615 Charles E. Young Drive South, BSRB 245F
Los Angeles, CA 90095
Phone: 310-825-4454
Email: tosullivan@mednet.ucla.edu

Maureen A. Su, MD
David Geffen School of Medicine at UCLA
615 Charles E. Young Drive South, BSRB 290C
Los Angeles, CA 90095
Phone: 310-825-2130
Email: masu@mednet.ucla.edu

Abstract

Viral infection outcomes are sex-biased, with males generally more susceptible than females. Paradoxically, the numbers of anti-viral natural killer (NK) cells are increased in males. We demonstrate that while numbers of NK cells are increased in male mice, they display decreased effector function compared to females in mice and humans. These differences were not solely dependent on gonadal hormones, since they persisted in gonadectomized mice. *Kdm6a* (UTX), an epigenetic regulator which escapes X inactivation, was lower in male NK cells, while NK cell-intrinsic UTX deficiency in female mice increased NK cell numbers and reduced effector responses. Furthermore, mice with NK cell-intrinsic UTX deficiency showed increased lethality to mouse cytomegalovirus (MCMV). Integrative multi-omics analysis revealed a critical role for UTX in regulating chromatin accessibility and gene expression critical for NK cell homeostasis and effector function. Collectively, these data implicate UTX as a critical molecular determinant of sex differences in NK cells.

Introduction

Evolutionarily conserved sex differences exist in both innate and adaptive immune responses[1, 2]. While males are less susceptible to autoimmunity, they also mount a less potent anti-viral immune response than females[3]. For instance, males have a higher human cytomegalovirus (HCMV) burden after infection, suggesting increased susceptibility to viral threats[4]. This has also been recently illustrated during the COVID-19 pandemic, in which the strong male bias for severe disease has been postulated to reflect sex differences in immune responses[5]. Multiple studies in humans and mice have recently reported differences in immune cell distribution and/or function in males vs. females[6, 7, 8, 9, 10]. However, the molecular basis for these differences, and the mechanisms by which these differences influence disease outcomes, remain poorly understood.

Sex differences in mammals are defined not only by divergent gonadal hormones, but also by sex chromosome dosage[1]. Expression of a subset of X-linked genes, for example, is higher in females (XX) than males (XY)[11]. While females undergo random X chromosome inactivation (XCI) to maintain similar levels of X-linked protein expression between sexes, XCI is incomplete, with 3-7% of X chromosome genes escaping inactivation in mice and 20-30% escaping inactivation in humans[11, 12, 13]. As such, differential levels of X-linked gene expression in females vs. males have been linked to sex differences in a wide range of conditions including neural tube defects[14] and autoimmune disease[15, 16].

As circulating type 1 innate lymphocytes, NK cells serve as an early line of defense against herpesvirus family members[17]. The importance of NK cells in anti-viral immunity is illustrated in patients with defective NK cell numbers or functionality, who are highly susceptible to infection by herpesviruses such as HCMV and Epstein-Barr virus (EBV)[18, 19]. In mice, NK cells are required for the control of mouse cytomegalovirus (MCMV) and other viral infections[20, 21, 22]. Mice with

either genetic deficiency in NK cell function or loss of NK cell numbers have a significant increase in viral titers and mortality following MCMV infection[21, 22, 23, 24, 25, 26, 27]. Thus, NK cells are critical in anti-viral immunity in both mice and humans.

Given the potent antiviral function of NK cells, it was therefore unexpected that virus-susceptible males display higher numbers of NK cells[6, 7, 8, 9, 10]. Beyond NK cell numbers, other previously unappreciated sexually dimorphic NK cell feature(s) may instead account for sex differences during viral infection. We demonstrate that while male NK cells display enhanced cellular fitness in mice, they show decreased effector function in mice and humans. These sex biases in NK cell composition and function were not completely due to hormonal differences, since they persisted in gonadectomized mice. Through expression screening, we identified the epigenetic regulator and known XCI escapee UTX (encoded by gene *Kdm6a*) expressed at significantly lower levels in both mouse and human male NK cells. UTX regulated both NK cell fitness and effector function in a dose-dependent manner, because UTX haploinsufficiency in female NK cells was sufficient to increase NK cell numbers while impairing cytokine production and cytotoxicity. Female UTX-deficient NK cells displayed enhanced persistence *in vivo* and resistance to apoptosis *ex vivo*, as well as increased susceptibility to MCMV infection. These effects were independent of UTX's intrinsic demethylase activity, as NK cell numbers and IFN-γ production were unaltered in mice expressing a "demethylase dead" UTX mutant. Integrative analysis of assay for transposase-accessible chromatin using sequencing (ATAC-seq), bulk RNA sequencing (RNA-seq), and UTX CUT&Tag of WT and UTX^{NKD} NK cells revealed a critical role for UTX in regulating expression of gene loci involved in NK cell fitness and effector responses. Our findings identify UTX as a major driver of sex differences in NK cell homeostasis and effector function through demethylase-independent modulation of gene expression.

Results

NK cell sexual dimorphism is independent of gonadal sex hormones.

A recent investigation examining spleens of C57BL/6 mice reported increased numbers of NK cells in males vs. females[28]. Consistent with these data, we observed that splenic NK cells (identified as $CD3^-$,$TCR\beta^-$,$NK1.1^+$; **Extended Data Fig. 1a**) are increased in frequency **(Fig. 1a,b)** and absolute numbers **(Fig. 1c)** in male C57BL/6 mice compared to females. These findings suggest that other sexually dimorphic features beyond NK cell numbers may account for increased male susceptibility to viral infections. In response to viral infection, NK cells are critical for early production of proinflammatory cytokines, particularly IFN-γ and GM-CSF[29, 30, 31, 32, 68]. To test if sex differences exist in NK cell-intrinsic function, we compared effector cytokine production in NK cells isolated from female vs. male mice *ex vivo*. Stimulation with the pro-inflammatory cytokines IL-12 and IL-15 resulted in lower IFN-γ production by male NK cells **(Fig. 1d,e and Extended Data Fig. 1b)**. Similar results were observed in response to IL-12 and IL-18 **(Extended Data Fig. 1c,d),** suggesting a respective defect in male NK cell responsiveness to cytokine stimulation**.** Additionally, human NK cells ($TCR\beta^-$,$CD3^-$,$CD56^+$) isolated from peripheral blood mononuclear cells (PBMCs) activated with IL-12 and K562 leukemia cells resulted in lower $\%IFN\text{-}\gamma^+$ **(Fig. 1f and Extended Data Fig. 1e)** and IFN-γ MFI **(Fig. 1g)** in male NK cells vs. female**.** Thus, although NK cell numbers are increased, male NK cell effector cytokine production is consistently reduced in both mice and humans in response to pro-inflammatory cytokines induced during viral infection.

Female or male sex is based on a composite of gonadal hormones (e.g., estrogens or androgens) and sex chromosomes (e.g., 46XX or 46XY)[1]. Previous studies demonstrated direct effects of gonadal hormones in regulation of IFN-γ production by NK cells[33], but it remains

possible that NK cell sex differences could also be attributed to cell-intrinsic factors. To identify sex hormone-mediated effects, we examined NK cell abundance and function in gonadectomized mice. Gonadectomy failed to eliminate sex differences in NK cell frequency **(Fig. 1h and Extended Data Fig.1f),** absolute numbers **(Fig. 1i)** and IFN-γ protein production in response to cytokine stimulation **(Fig. 1j,k and Extended Data Fig.1g)**, indicating gonadal hormones are not solely responsible for sex differences in NK cells. While NK cell maturation subsets identified by CD11b and CD27 expression have differential capacities for survival and effector function[34], splenic NK cells derived from either WT or gonadectomized female and male mice did not display significant differences in the frequencies of NK cell maturation subsets **(Extended Data Fig. 1h-k)**. These results indicated that the observed sex biases in NK cell number and effector function are not due to differential maturation states. Thus, we hypothesized that sex chromosome dosage may contribute to differential NK cell abundance and function between sexes.

X-linked UTX escapes X-inactivation and has higher expression in female NK cells.

While 46XX females undergo X chromosome inactivation (XCI) to control dosages of X-linked genes, a subset of genes escapes XCI (termed XCI escapees), often resulting in higher expression in females compared to males[35, 36]. Thus, increased XCI escapee expression in females compared to males could potentially mediate sex differences in NK cells. While different genes escape X-inactivation in humans and mice, five genes (*XIST*, *DDX3X, KDM6A, EIF2S3, KDM5C*) have previously been identified as XCI escapees in both[37]. *XIST* was excluded from further analysis because it is not expressed in male cells due to its known role in X chromosome inactivation in female cells[1]. All 4 remaining genes were significantly downregulated in male vs. female NK cells, in both human **(Fig. 2a)** and mouse **(Fig. 2b).** *Kdm6a* (which encodes the protein UTX) transcript

levels displayed the most sexually dimorphic expression in both human and mouse NK cells **(Fig. 2a,b**). Male NK cells also expressed lower UTX protein levels compared to female NK cells in mice **(Fig. 2c,d)**. These differences in *Kdm6a* transcript levels and UTX protein levels persisted in both gonadectomized mice **(Fig. 2e-g)** and four core genotype (FCG) mice **(Extended Data Fig. 2a)** in which sex chromosome complement (XX or XY) is uncoupled from gonadal sex organ (ovaries or testes)[38]. These data indicate expression levels of *Kdm6a* (UTX) are sex-biased in NK cells and primarily dictated by X chromosome dosage rather than gonadal hormones.

UTX suppresses NK cell fitness.

To determine if UTX mediates the observed sex differences in NK cells, we generated a series of mice with dose-dependent loss of UTX. First, we generated female mice with a heterozygous deletion of UTX in NK cells (*Kdm6a*$^{fl/WT}$ *Ncr1*$^{Cre+}$, hereafter referred to as UTX^{Het}; **Supplementary Data Table 1**) to mimic the single copy of UTX expressed in males. We confirmed similar NK cell UTX protein expression between female UTX^{Het} and male WT (*Kdm6a*$^{fl/y}$ *Ncr1*$^{Cre-}$) mice **(Extended Data Fig. 2b).** Female UTX^{het} mice displayed similar splenic NK cell numbers compared to male WT **(Fig. 3a,b)**, and both displayed increased numbers of NK cells compared to female WT. No significant differences in maturation by CD11b and CD27 expression were observed between NK cells from female WT, male WT, and female UTX^{Het} mice **(Extended Data Fig. 2c).** Thus, loss of one copy of UTX was sufficient to increase NK cell numbers in a maturation-independent manner.

We next produced mice with a homozygous deletion of UTX (*Kdm6a*$^{fl/fl}$ *Ncr1*$^{Cre+}$, hereafter referred to as UTX^{NKD}; **Supplementary Data Table 1**), resulting in loss of both copies of UTX in NK cells. UTX protein expression was significantly lower in female UTX^{NKD} NK cells compared

to female WT NK cells by flow cytometry **(Extended Data Fig. 2b),** as well as lower compared to NK cells with a single UTX copy (i.e., male WT and female UTX^{Het}). The absence of UTX protein at the predicted size (180 kD) in female UTX^{NKD} compared to WT NK cells was confirmed by western blot **(Extended Data Fig. 2d)**. NK cell frequencies and absolute numbers increased with decreasing UTX copy number **(Fig. 3c,d and Extended Data Fig.3a)**. These data implicate UTX in regulating NK cell frequency and absolute numbers in a dose-dependent manner.

To define the mechanisms underlying the increased NK cell numbers in UTX^{NKD} mice ($CD45.2^{+}$), 1:1 mixed bone marrow chimeric (mBMC) mice with WT ($CD45.1^{+}$) were produced. 6 weeks post-reconstitution, we observed a marked competitive advantage of female UTX^{NKD} ($CD45.2^{+}$) NK cells compared to WT in female recipients ($CD45^{1x2}$) following bone marrow transplantation **(Extended Data Fig. 3b-c)**. In contrast to NK cells, T cells from the same donor (UTX^{NKD},$CD45.2^{+}$), which are UTX-sufficient due to NK-specific deletion of UTX, displayed the original injection ratio (1:1) **(Extended Data Fig. 3b,c)**. These data suggest UTX repressed NK cell numbers in a cell-intrinsic manner during development. To test whether this phenotype was driven by differences in proliferation, we analyzed the cell division marker Ki67 in splenic NK cells in WT:UTX^{NKD} mBMC mice, injected at a 4:1 ratio to normalize cell number between genotypes. Paradoxically, UTX^{NKD} NK cells displayed lower frequencies of $Ki67^{+}$ cells and showed less CFSE dilution in response to IL-15 **(Extended Data Fig. 3d,e)**. These results suggested that the higher NK cell numbers observed in UTX^{NKD} mice were not due to increased proliferation.

Given these results, we hypothesized that the elevated frequency of NK cells in UTX^{NKD} mice **(Fig. 3c-d)** could be due to enhanced cellular fitness of NK cells in the absence of UTX expression. To test this possibility, congenically distinct WT ($CD45^{1x2}$) and UTX^{NKD} ($CD45.2^{+}$)

splenic NK cells were labeled with Cell Trace Violet (CTV) and transferred into WT ($CD45.1^+$) recipients at a 1:1 ratio **(Extended Data Fig. 3f)**. On day 7 post-transfer, the transferred population was skewed toward UTX^{NKD} NK cells in recipient spleens **(Fig. 3e,f)**, demonstrating cell-intrinsic UTX suppression of mature NK cell homeostasis. This difference was not due to altered proliferation, because CTV dilution by both transferred populations was minimal on day 7 post-transfer **(Extended Data Fig. 3g).** To test whether UTX repressed NK cell homeostasis through regulation of apoptosis, we compared cleaved caspase 3 expression in sorted NK cells incubated with either IL-15 alone or with IL-15 and an apoptosis inducer, Nutlin-3a[39]. Lower UTX expression correlated with decreased cleaved caspase 3^+ NK cells in the presence of low dose IL-15 and Nutlin-3a treatment **(Fig. 3g,h)**. Moreover, male NK cells also displayed a modest but significant decrease in the frequency of cleaved caspase 3^+ NK cells in response to Nutlin-3a compared to female NK cells which also persisted in gonadectomized mice **(Extended Data Fig. 3h-k**). Moreover, regulation of NK cell apoptosis and survival relies on the relative expression levels of Bcl-2 (anti-apoptotic factor)[40] which can be antagonized by Bim (pro-apoptotic factor)[41]. UTX^{NKD} NK cells showed increased intracellular protein expression of Bcl-2 and a modest increase in Bim **(Fig. 3i,j and Extended Data Fig. 3l)** compared to WT NK cells. This resulted in a significantly increased Bcl-2:Bim ratio in UTX^{NKD} NK cells **(Fig. 3k)**. Male NK cells also displayed a significant increase in Bcl-2:Bim ratio **(Fig. 3l)**, which persisted following gonadectomy **(Fig. 3m)**. Together, these data demonstrate that altered UTX levels may underlie sex differences in NK cell fitness through regulation of Bcl-2 expression.

UTX enhances NK cell effector function.

Since male NK cells exhibited decreased IFN-γ production **(Fig. 1d,e)** independent of gonadal hormones **(Fig. 1j,k)** we next sought to determine if this phenotype was regulated by UTX levels. After cytokine stimulation, frequencies and absolute numbers of IFN-γ-producing cells **(Fig. 4a left, and Extended Data Fig. 4a,b)** as well as IFN-γ MFI (**Fig. 4a, right)** were similar between male WT and female UTX^{Het} NK cells. IFN-γ production by female UTX^{Het} NK cells was intermediate between female WT and female UTX^{NKD} NK cells **(Fig. 4a and Extended Data Fig. 4a,b)**. This trend was also observed by comparing NK cell IFN-γ accumulation by ELISA **(Fig. 4b)**. Moreover, this phenomenon was not specific to IFN-γ, since GM-CSF production, a pro-inflammatory NK effector molecule[68], was also reduced with decreasing UTX copy number in female NK cells **(Fig. 4c)**.

In addition to cytokine production, NK cell cytolytic activity is crucial for anti-viral[42] and anti-tumor defenses[43]. To assess sex differences in NK cell cytotoxicity, we performed killing assays with MHC Class I-deficient MC38 cells as targets. At a 4:1 Effector:Target ratio, male WT NK cells displayed significantly lower lysis of target cells compared to female WT **(Fig. 4d),** which was sustained in gonadectomized mice **(Extended Data Fig. 4c).** Impaired target cell killing by male NK cells was not due to differences in degranulation, since CD107a levels were similar between female and male NK cells **(Extended Data Fig. 4d,e)**. However, males produced significantly lower levels of cytotoxic molecules perforin and granzyme B in response to IL-15 and anti-NK1.1 activating receptor ligation **(Extended Data Fig. 4d,e).** Notably, UTX^{Het} and male WT NK cells showed similar killing capacity **(Fig. 4d)**, which was intermediate between female WT and UTX^{NKD} NK cells **(Fig. 4d).** Together, these data suggest that UTX enhances NK cell cytotoxicity in a dose-dependent manner.

Considering the observed effects of UTX loss on NK cell effector function, we examined whether UTX^{NKD} mice were more vulnerable to viral infection. Rapid IFN-γ and GM-CSF production is critical for NK cell mediated anti-viral control[29]. Strikingly, UTX^{NKD} mice rapidly succumbed to infection (n = 3/8 survived) upon challenge with a sublethal dose of MCMV **(Fig. 4e)**. Moreover, UTX-deficient splenic NK cells displayed a marked defect in IFN-γ production and granzyme B production in total NK cells on day 1.5 post-infection (D1.5 PI) **(Fig. 4f and Extended Data Fig. 4f,g)**. Additionally, a similar defect in IFN-γ production by UTX^{NKD} was observed in all maturation subsets **(Extended Data Figure 4h),** implicating UTX in control of IFN-γ production in a maturation independent manner. To confirm whether dosage of UTX expression in mature NK cells associates with production of IFN-γ during viral infection *in vivo*, we generated transgenic mice to achieve a tamoxifen-inducible UTX deletion (*Kdm6a*$^{fl/fl}$ *Rosa26*$^{ERT2CRE+}$, hereafter referred to as $iUTX^{-/-}$; **Supplementary Data Table 1**). mBMC mice were produced with a 1:1 mix of WT ($CD45.1^+$) and $iUTX^{-/-}$ ($CD45.2^+$) to limit UTX deletion to the hematopoietic compartment. WT:$iUTX^{-/-}$ mBMC mice were treated with tamoxifen immediately prior to infection with MCMV to ablate UTX expression **(Fig. 4g)**. $iUTX^{-/-}$($CD45.2^+$) NK cells produced less IFN-γ compared to their WT counterparts **(Fig. 4h and Extended Data Fig. 4i).** Tamoxifen administration in WT:$iUTX^{-/-}$ mBMC mice resulted in differential degrees of UTX protein loss and displayed a significant positive correlation between intracellular UTX levels and IFN-γ production on D1.5 PI **(Fig. 4i).** These results demonstrate that cell-intrinsic UTX levels in mature NK cells regulate effector molecule production and subsequent protection against MCMV infection.

UTX regulates NK cells in a demethylase-independent manner.

As a histone demethylase, UTX may control NK cell homeostasis and effector gene expression programs by catalyzing the removal of a methyl group from H3K27me3 (a repressive histone mark) to poise chromatin for active gene expression[44]. However, UTX also possesses demethylase-independent activities by interacting with epigenetic regulators and chromatin modifiers to coordinate gene expression[45, 46]. To explore the role of UTX demethylase activity in modulating NK cell homeostasis and effector function, we leveraged mice which express a catalytically inactive UTX (UTX "demethylase-dead" or UTX^{DMD} mice; **Supplementary Data Table 1**) harboring H1146A and E1148A point mutations in the catalytic domain[47]. Interestingly, female UTX^{DMD} and WT mice exhibited similar frequencies and absolute numbers of splenic NK cells (**Fig. 5a-c**), while UTX^{NKD} mice showed increased splenic NK cell numbers compared to both. These findings suggest that UTX's repression of NK cell numbers was demethylase-independent. Moreover, no differences were observed between WT and UTX^{DMD} NK cells in the ability to produce IFN-γ in response to cytokine stimulation (**Fig. 5d-f)**. These results demonstrate that UTX's function in restraining NK cell numbers and promoting IFN-γ production is demethylase-independent.

In addition to a single copy of UTX, males express the catalytically inactive *Kdm6c* (which encodes the protein UTY), the Y-chromosome linked homolog of UTX. We confirmed that UTY is only expressed in male NK cells from humans **(Extended Data Fig. 5a)** and mice **(Extended Data Fig. 5b)** and was not altered by gonadectomy in mice **(Extended Data Fig. 5b).** As discussed above, no differences were seen in NK cell numbers or effector function between male WT (one copy UTX and UTY) and female UTX^{Het} (one copy UTX) mice (**Fig. 3a,b and Fig. 4a, d**), suggesting a limited role for UTY in regulating NK cell homeostasis and effector function.

Additionally, male UTX^{NKD} (*Kdm6a*$^{fl/y}$ *Ncr1*$^{cre+}$) mice showed increased NK cell frequency and absolute numbers **(Extended Data Fig. 5c,d)** and produced less IFN-γ **(Extended Data Fig. 5e-h),** compared to male WT controls, which mirrors changes seen in females with NK cell UTX deficiency. (**Fig. 3a,b and Fig. 4a,b**). Thus, UTX loss in NK cells has similar effects in females and males.

UTX controls the NK cell transcriptome through chromatin remodeling.

Recent studies have identified NK cell regulatory circuitry (regulomes) that prime innate lymphoid cells for swift effector responses even prior to NK cell activation[48, 49]. As an epigenetic modifier, UTX can alter transcription by organizing chromatin at regulatory elements of target gene loci[50]. To investigate the UTX-mediated modifications on chromatin accessibility and gene expression in NK cells, we performed Assay for Transposase-Accessible Chromatin using sequencing (ATAC-seq) in tandem with bulk RNA sequencing (RNA-seq) on sort-purified WT (CD45.1^{+}) and UTX^{NKD} (CD45.2^{+}) NK cells from 4:1 WT:UTX^{NKD} mBMC mice **(Extended Data Fig. 6a)**. Using mBMC mice allowed for an internally controlled experiment and minimized environmental confounding factors. Principal Component Analysis (PCA) of both ATAC-seq and RNA-seq data revealed sample clustering by genotype **(Extended Data Fig. 6b)**. ATAC-seq revealed 3569 peaks decreased and 2113 peaks increased in accessibility in UTX^{NKD} compared to WT NK cells ($\log_2$ fold change > ±0.5, adjusted p-value < 0.05, FDR < 0.05) **(Supplementary Data Table 2)**. Moreover, RNA-seq identified 701 decreased and 554 increased genes in UTX^{NKD} vs. WT ($\log_2$ fold change > ± 0.5, adjusted p-value < 0.05, FDR < 0.05) **(Extended Data Fig. 6c and Supplementary Data Table 3)**. These findings suggest profound changes in both the chromatin landscape and transcriptome of NK cells in the absence of UTX.

Integrative analysis of ATAC-seq and RNA-seq identified 395 genes that are both differentially accessible and expressed with a significant positive correlation (Spearman correlation: $R = 0.62$, $p < 2.2x10^{-16}$) between the mean log_2 fold change of ATAC-seq peaks and log_2 fold change of RNA-seq expression **(Extended Data Fig. 6d)**. Fuzzy c-means clustering[51] of both the ATAC-seq and RNA-seq datasets identified six major clusters which were significantly decreased (Clusters 1, 2, 3, and 6) or increased (Clusters 4 and 5) in accessibility **(Fig. 6a)** and expression **(Fig. 6b)** in UTX^{NKD} NK cells. For functional enrichment analysis, g:Profiler[52] was used to analyze clusters of differentially expressed genes identified by RNA-seq **(Fig. 6c)**. Major pathways such as immune system process, cytokine production, IFN-γ production, lymphocyte activation, and immune effector process were associated with decreased expression in UTX^{NKD} (Clusters 1, 2, 3, and 6) **(Fig. 6c)**. Meanwhile, pathways such as developmental process, biosynthetic process, and metabolic process were significantly associated with increased expression in UTX^{NKD} (Clusters 4 and 5) **(Fig. 6c)**. Of note, analysis of cell death pathway genes revealed multiple genes to be differentially expressed **(Extended Data Fig. 6e).** Notably, expression of the anti-apoptotic gene *Bcl2* was increased while the pro-apoptotic gene *Casp3* was decreased **(Extended Data Fig. 6e)**. Collectively, these findings implicate loss of UTX results in modifications of chromatin accessibility and expression of genes associated with NK cell homeostasis and effector function.

Considering the genome-wide differences in accessibility and gene expression we observed by ATAC-seq and RNA-seq, we also explored direct UTX-mediated effects. We performed anti-UTX CUT&Tag (Cleavage Under Targets and Tagmentation Assay) followed by sequencing, allowing detection of DNA regions bound to UTX using an antibody-based immunoprecipitation method[53]. Anti-UTX CUT&Tag on sort-purified WT and UTX^{NKD} NK cells revealed 5746 UTX-

bound peaks (FDR < 0.01, adjusted p-value < 0.05) **(Fig. 6d and Supplementary Data Table 4)**. Principal Component Analysis (PCA) of both ATAC-seq and RNA-seq data revealed sample clustering by genotype **(Extended Data Fig. 6f).** We identified 191 genes that were UTX-bound, differentially accessible by ATAC-seq, and differentially expressed by RNA-seq **(Fig. 6d)**. Within these 191 genes, a majority of UTX-bound peaks were located in promoter (20.58%), intronic (46.94%), and intergenic (27.4%) regions **(Fig. 6e)**. Noteworthy genes involved in NK cell homeostasis (*Bcl2 and Thy1)* **(Fig. 6f)**[40, 54, 55] and effector function (*Ifng* and *Csf2*) were UTX-bound, differentially accessible, and differentially expressed **(Fig. 6g)**. Moreover, of the 191 UTX-bound genes, 140 genes were decreased in expression, while the remaining 51 genes were increased **(Supplementary Data Table 3)** corroborating a prior report in T cells that UTX functions in both activating and repressing gene transcription[66]. Enrichr pathway analysis[56] on these 191 UTX-bound genes revealed decreased inflammatory response, IFN-γ signaling, and NK cell cytotoxicity pathways in UTX^{NKD} NK cells **(Extended Data Fig. 6g)**. Conversely, increased cellular catabolic process and apoptosis signaling pathways, which include both pro- and anti-apoptotic genes (e.g., *Bcl2, Bbc3, Gadd45*g), were seen in UTX^{NKD} NK cells. Among 865 UTX-bound peaks with UTX-dependent expression and chromatin accessibility differences (191 unique genes), linear regression analysis showed a significant positive correlation (Pearson's R = 0,5165, p <0.0001) between chromatin accessibility and gene expression **(Extended Data Fig. 6h,i)**. UTX occupied regions within the *Bcl2, Thy1, Ifng, and Csf2* gene loci corresponded with regions in which differences in accessibility and gene expression were also noted **(Fig. 6f,g).** These data suggest UTX regulates chromatin accessibility and gene transcription pathways important in regulating NK cell homeostasis and function.

UTX is known to interact with transcription factors (TFs) to orchestrate target gene transcription[50]. To identify putative TF motifs with differential accessibility due to loss of UTX, we performed HOMER (Hypergeometric Optimization of Motif Enrichment)[57] TF motif analysis on differentially accessible peaks identified by ATAC-seq **(Extended Data Fig. 6j).** TFs associated with NK cell effector function (e.g. Runt (Runx1 and Runx2)[58] and T-box (Eomes, T-bet, Tbr1 and Tbx6)[59] family members) were more significant and had a higher percentage of target motifs associated with decreased accessibility in UTX^{NKD} (Clusters 1, 2, 3, and 6) **(Extended Data Fig. 6j)**. Conversely, TFs associated with proliferation, differentiation, and metabolism in the zinc finger and ETS family TFs[60] were more significantly associated with increased accessibility (Clusters 4 and 5) **(Extended Data Fig. 6j)**. Furthermore, TF motif analysis of UTX-bound peaks by UTX CUT&Tag corroborate these results by revealing TFs critical in both NK cell effector processes (T-bet, Eomes, Runx1, Tbx5) and developmental programs (ETS1, AP-1) **(Extended Data Fig. 6k)**. These data suggest both differential accessibility and direct UTX-binding of important TF binding motifs implicated in regulating NK cell fitness and effector processes. These analyses suggest that UTX modulates the chromatin landscape to control expression of genes important in NK cell homeostasis (*Bcl2 and Thy1)* and effector function (*Ifng* and *Csf2*). Ultimately, these findings suggest a model in which differential UTX expression levels may underlie sexual dimorphism in NK cells as a central regulator of NK cell fitness and effector function **(Fig. 6h)**.

Discussion

Sex is a critical biological variable in determining outcomes to viral infections[3]. This was recently illustrated with COVID-19, in which male sex was identified as a major risk factor for severe disease[5]. Moreover, recent studies have linked NK cell dysfunction to severe COVID-19 disease[61]. Given the importance of NK cells in anti-viral immunity, understanding the root causes of sex differences in NK cell biology will have far-reaching implications in optimizing endogenous effector responses. In this study, we demonstrate that lower UTX expression in male NK cells contributes to their increased numbers and decreased effector functionality **(Fig. 6h)**. NK cell UTX is required for controlling NK cell fitness, modulating accessibility of transcription factor binding motifs, increasing chromatin accessibility at effector gene loci, and poising NK cells for rapid response to viral infection.

In addition to NK cells, sexual dimorphism has been reported in B cells, monocytes, neutrophils, $CD4^+$ T cells, and $CD8^+$ T cells[25]. While sex differences in immune cells have previously been reported to be mediated by gonadal sex hormones[62, 63, 64], it remains possible that a subset of these disparities may also be attributed to differential UTX expression. In support of this possibility, UTX deficiency has been associated with decreased T and iNKT cell numbers[65, 66, 67]; and UTX transcripts are lower in male vs. female cells for multiple immune cell types ($CD4^+$ T cells, $CD8^+$ T cells, Monocytes, B cells) queried in the *DICE* database[68] (data not shown). Further phenotypic studies are needed to determine UTX's role in modulating sex differences in other immune cell types.

NK cell-mediated effector functions include cytokine production and cytotoxic molecule expression[69]. Our multi-omic analyses suggest that UTX poises the chromatin landscape of NK cells to quickly respond to viral challenge by increasing accessibility and transcription of effector

loci. These studies revealed 191 genes (including *Ifng,* and *Csf2*[29, 70]) that were simultaneously bound by UTX, differentially accessible, and expressed. Decreased IFN-γ and GM-CSF cytokine production and impaired cytolytic capacity of UTX-deficient NK cells support UTX's role in promoting effector functionality during inflammation. However, there may be additional indirect consequences of UTX-mediated gene regulation that play important roles in NK cell effector function, as evidenced by the additional genes that are differentially expressed but not bound by UTX.

As a H3K27me3 demethylase, UTX poises chromatin for active gene expression[71]. In addition to its catalytic activity, UTX functions in multiprotein complexes with other epigenetic regulators (e.g. SWI/SNF, MLL4/5 and p300) to mediate chromatin remodeling in a demethylase-independent manner[45, 71]. We report demethylase-independent functions of UTX in regulating homeostasis and effector programs in NK cells. This is in contrast to UTX's role in iNKT cells, in which its demethylase activity is required[65]. Thus, the molecular mechanisms by which UTX functions may be lineage specific. In support of this hypothesis, UTX has been reported to interact with lineage specific TFs in T cells to target effector loci[50]. Our HOMER motif analysis revealed potential UTX interactions with Runx1, Runx2, Eomes, and other TFs important for NK cell effector function during viral infection[58, 59]. Moreover, these analyses also point to UTX interactions with KLF1, KLF5, Sp2 and other TFs associated with NK cell proliferation, differentiation, and metabolism[60]. Furthermore, our results support previously published studies in which UTX in other cell types has been reported to coordinate responses with T-bet, Eomes and Tbx5[50], ETS1[46], and AP-1[65]. Finally, Runx1 has been shown to interact with UTX-regulated BRG1 and SWI/SNF complexes[45]. However, due to the correlative nature of HOMER analysis, further studies with co-immunoprecipitation and mass spectrometry are needed to experimentally verify

these interactions *in situ*. Furthermore, as a constitutive XCI escapee, UTX may have cell type specific mechanisms through two possibilities: i) pool of cofactors present and ii) availability of its epigenetic binding partners. UTX relies on byproducts of metabolic pathways for cofactors (e.g., Fe(II), α-ketoglutarate, oxygen) crucial for its enzymatic activity[72]. Thus, dependent on the metabolic state, there are distinct pools of cofactors accessible for UTX's demethylase function, allowing differential levels of catalytic activity based on the cell type. Additionally, UTX's functionality may also be contingent on the activity and expression level of its binding partners (e.g. MLL3/4, SWI/SNF, p300) which are autosomally encoded.

Weighing factors that define patient subsets with different immune responses will allow us to move past a "one-size-fits-all" therapeutic approach to a precision medicine paradigm. UTX deficiency has been associated with Kabuki Syndrome and Turner Syndrome[65, 73], two human conditions associated with immune dysregulation and increased infections. Our findings suggest the possibility that UTX deficiency in human NK cells may contribute to decreased viral immunosurveillance observed in these patients, although future work will be needed to support this hypothesis. Moreover, understanding sex differences in NK cell function is required to incorporate sex as a biological factor in treatment decisions. In males with severe viral illness, for instance, enhancing NK cell UTX activity may provide therapeutic benefit. We expect that these insights will be important not only in the setting of viral infections, but also in other infections and cancer, where NK cells also play an important role. These findings may also have important implications for adoptive cellular therapies, in which NK cells are the subject of intense interest[74, 75].

Acknowledgements

We thank members of the O'Sullivan and Su labs for helpful discussion. We thank the UCLA Technology Center for Genomics and Bioinformatics for RNA sequencing library preparation and the Cedars Sinai Applied Genomics, Computation, and Translational Core Facility for ATAC sequencing library preparation. T.E.O. is supported by the NIH (AI145997) and UC CRCC (CRN-20-637105). M.A.S. is supported by the NIH (NS107851, AI143894, DK119445) Department of Defense (USAMRAA PR200530), and National Organization of Rare Diseases. M.I.C. is supported by Ruth L. Kirschstein National Research Service Awards (GM007185 and AI007323), and Whitcome Fellowship from the Molecular Biology Institute at UCLA. L.R. is supported by the Warsaw fellowship from the MIMG department at UCLA. J.H.L. is supported by the NIH NIAMS (T32AR071307). A.P.A. is supported by NIH (HD100298).

Author Contributions

M.I.C., L.R., J.H.L., R.Y.T., H.H., A.P.A., T.E.O. and M.A.S. designed the study; M.I.C., J.H.L., R.Y.T., L.R., and S.C. performed the experiments; M.I.C., F.M., B.C., and M.P. performed bioinformatics analysis; M.I.C., M.A.S, J.H.L., and T.E.O. wrote the manuscript.

Competing Interests Statement

T.E.O. is a scientific advisor for Modulus Therapeutics, Xyphos Inc. and Celine Therapeutics, companies that have financial interest in human NK cell-based therapeutics.

Figure 1

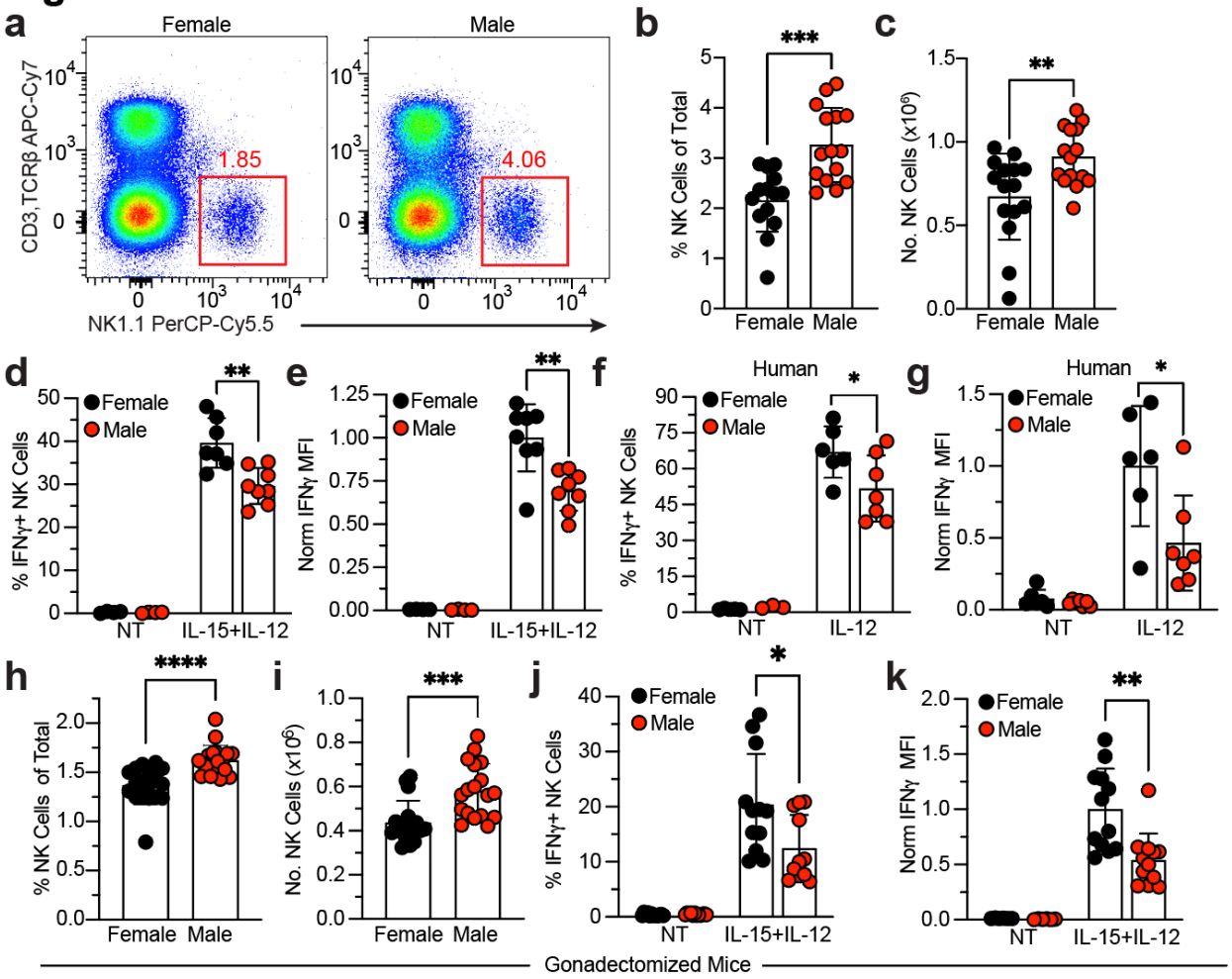

Figure 1: Sex differences in IFN-γ production and NK cell numbers are independent of gonadal hormones. a) Representative dot plots, **b)** frequency, and **c)** absolute numbers of splenic NK cells ($CD3^-$ $TCR\beta^-$ $NK1.1^+$) in female and male C57BL/6 mice (n = 15 per group). **d)** Percentage IFN-γ^+ and **e)** normalized IFN-γ mean fluorescence intensity (MFI) of total splenic NK cells from female vs. male mice cultured with no treatment (NT) or IL-15 (50 ng/mL) and IL-12 (20 ng/mL) for 4 hours, normalized to MFI of female IL-15/12 treatment (n = 8 per group). **f)** Percentage IFN-γ^+ and **g)** normalized IFN-γ MFI of $CD3^-$ $CD56^+$ female (n = 6) and male (n = 7) human NK cells cultured and stimulated with 10 ng/mL of IL-12 for 16 hours in the presence of K562 cells, normalized to MFI of female IL-12 treatment. **h)** Frequency and **i)**

absolute numbers of splenic NK cells in gonadectomized female and male mice (n = 18 per group). **j)** Percentage IFN-γ^+ and **k)** normalized IFN-γ MFI of total splenic NK cells isolated from gonadectomized female and male mice and cultured with no treatment (NT) or IL-15 (50 ng/mL) and IL-12 (20 ng/mL) for 4 hours (n = 12 per group). Data are representative of 2-4 independent experiments. Samples were compared using two-tailed unpaired Student's t test and data points are presented as individual mice with the mean ± SEM (*, $p < 0.05$; **, $p < 0.01$; ***, $p < 0.001$; ****, $p < 0.0001$).

Figure 2

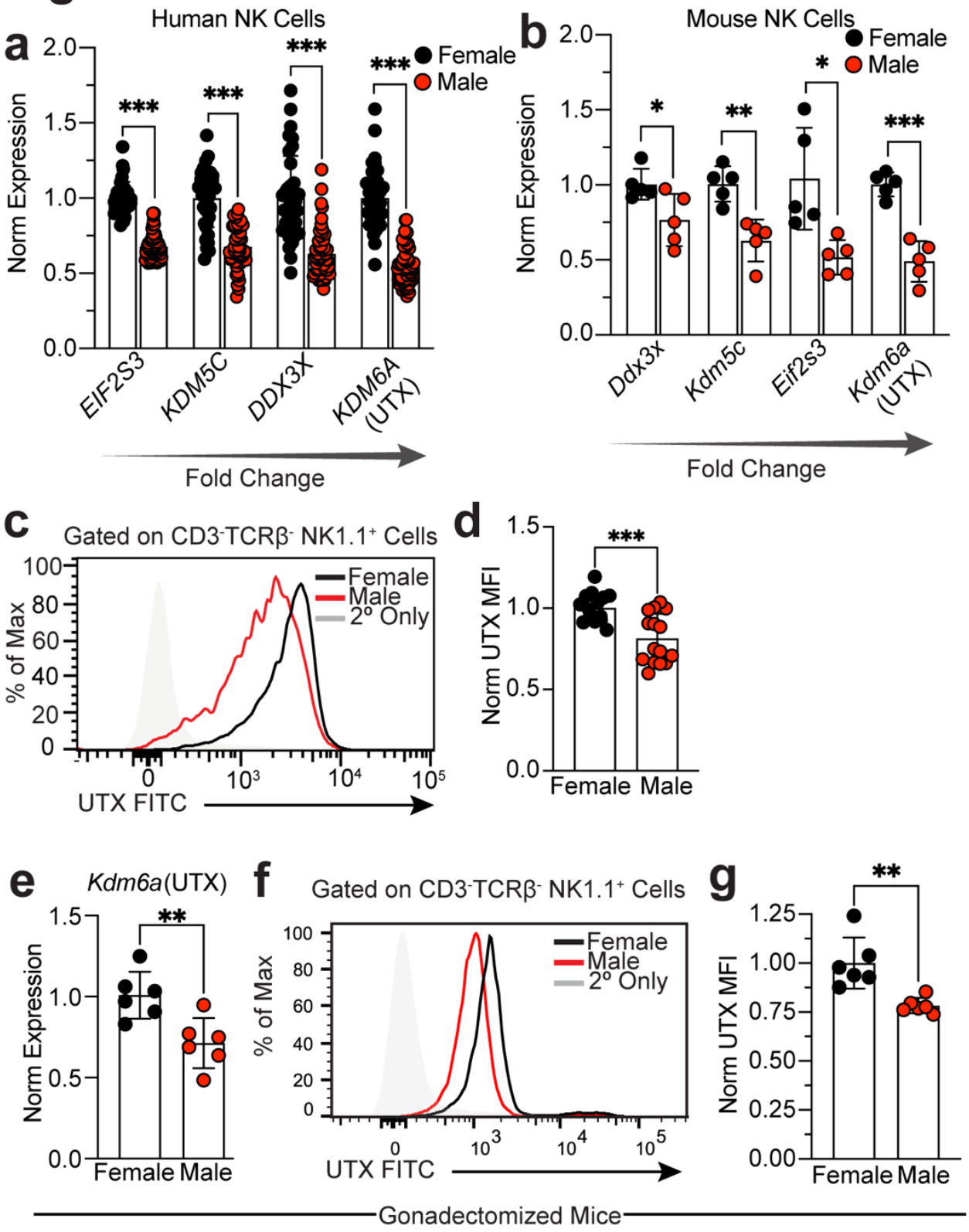
a
Human NK Cells
Norm Expression
2.0
1.5
1.0
0.5
0.0
***
***
***
***
Female
Male
EIF2S3
KDM5C
DDX3X
KDM6A (UTX)
Fold Change
b
Mouse NK Cells
Norm Expression
2.0
1.5
1.0
0.5
0.0
*
**
*
***
Female
Male
Ddx3x
Kdm5c
Eif2s3
Kdm6a (UTX)
Fold Change
c
Gated on CD3-TCRβ- NK1.1+ Cells
% of Max
100
80
60
40
20
0
Female
Male
2º Only
0
10^3
10^4
10^5
UTX FITC
d
Norm UTX MFI
1.5
1.0
0.5
0.0
***
Female
Male
e
Kdm6a(UTX)
Norm Expression
1.5
1.0
0.5
0.0
**
Female
Male
f
Gated on CD3-TCRβ- NK1.1+ Cells
% of Max
100
80
60
40
20
0
Female
Male
2º Only
0
10^3
10^4
10^5
UTX FITC
g
Norm UTX MFI
1.25
1.00
0.75
0.50
0.25
0.00
**
Female
Male
Gonadectomized Mice

Figure 2: X-linked UTX displays sexually dimorphic gene expression independent of sex hormones. a) Normalized expression of X-chromosome inactivation escapee genes using DICE database RNA-seq data on sorted NK cells from human females (n = 36) vs. males (n = 54) normalized to female. **b)** Normalized expression of X chromosome inactivation escapee genes by RT-qPCR in splenic NK cells from female vs. male mice (C57BL/6; 8 week old, n = 5 per group). Genes are ordered by increasing fold change between female and male from left to right. **c)** Representative histogram and **d)** normalized MFI of UTX protein expression in splenic NK cells from naive female vs. male mice by flow cytometry, normalized to MFI of female mice (C57BL/6; 8-week-old; n = 15 per group). **e)** Relative expression of *Kdm6a* (UTX) by RT-qPCR of isolated splenic NK cells normalized to female. **f)** Representative histograms and **g)** relative UTX MFI of NK cells by flow cytometry from spleens of gonadectomized female and male mice (n = 6 per group) normalized to female. Samples were compared using unpaired two-tailed Student's t test and data points are presented as individual mice with the mean ± SEM (*, $p < 0.05$; **, $p < 0.01$; ***, $p < 0.001$).

Figure 3

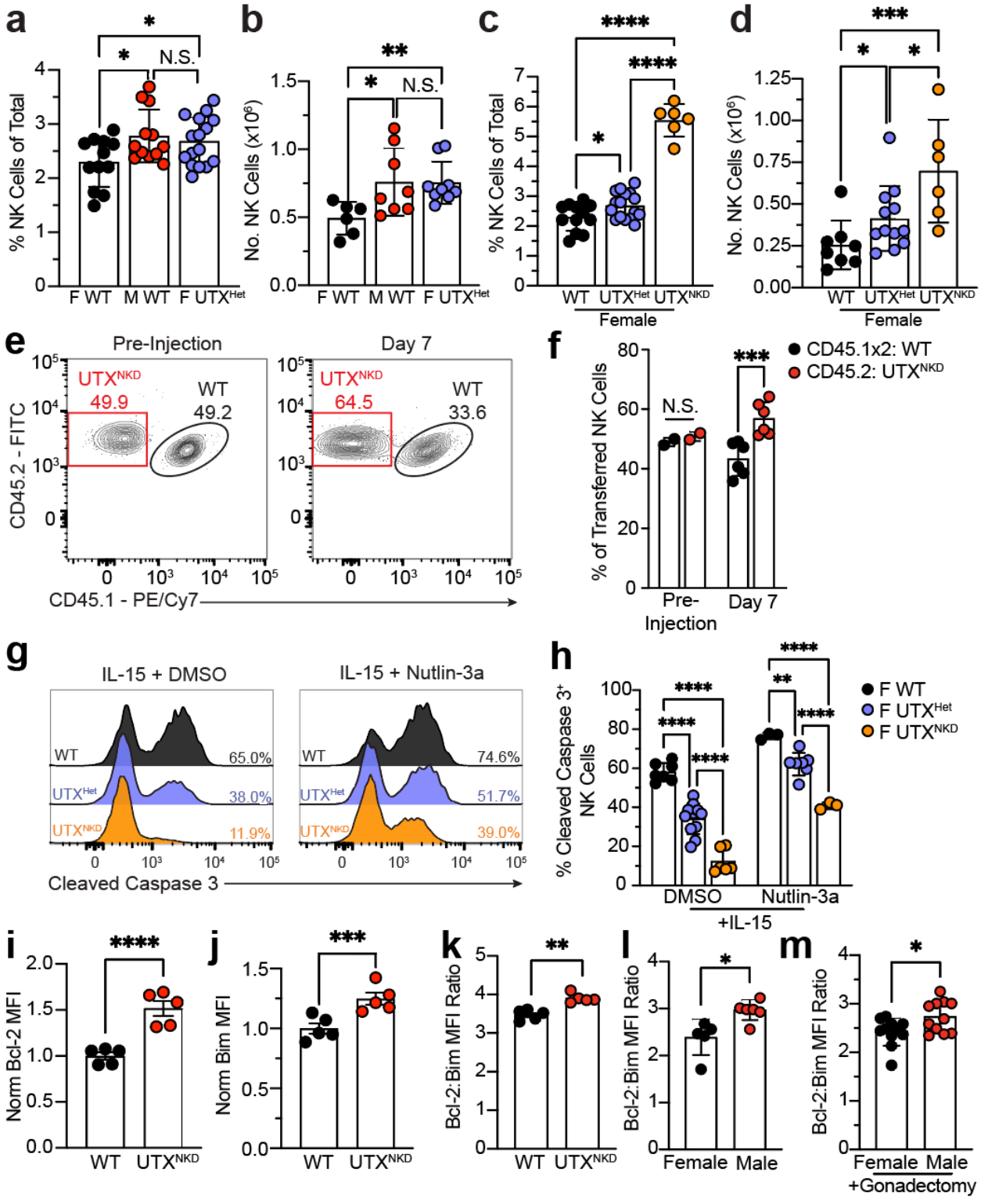
a
b
c
d
% NK Cells of Total
No. NK Cells (x10⁶)
F WT
M WT
F UTXHet
WT
UTXHet
UTXNKD
Female
N.S.
e
Pre-Injection
Day 7
UTXNKD
49.9
WT
49.2
64.5
33.6
CD45.2 - FITC
CD45.1 - PE/Cy7
f
% of Transferred NK Cells
CD45.1x2: WT
CD45.2: UTXNKD
Pre-Injection
Day 7
g
IL-15 + DMSO
IL-15 + Nutlin-3a
WT
UTXHet
UTXNKD
65.0%
38.0%
11.9%
74.6%
51.7%
39.0%
Cleaved Caspase 3
h
% Cleaved Caspase 3+ NK Cells
F WT
F UTXHet
F UTXNKD
DMSO
Nutlin-3a
+IL-15
i
Norm Bcl-2 MFI
j
Norm Bim MFI
k
Bcl-2:Bim MFI Ratio
l
Female
Male
m
+Gonadectomy

Figure 3: UTX suppresses NK cell fitness.

a) Frequency and **b)** absolute numbers of NK cells in spleen of female wild type (WT), male WT, and female UTX^{Het} mice (n = 12-16 per group). **c)** Frequency and **d)** absolute numbers of NK cells in spleen of female WT, UTX^{Het} and UTX^{NKD} mice. **e)** Representative contour plots showing frequencies of congenically distinct WT ($CD45^{1x2}$) and UTX^{NKD} ($CD45.2^{+}$) NK cells transferred into WT ($CD45.1^{+}$) recipients at a 1:1 ratio before injection (left) and on day 7 post transfer (right). **f)** Frequency of WT and UTX^{NKD} cells in the spleen of recipient mice on day 7 post transfer compared to pre-injection ratio (n = 6 per group). **g)** Representative histograms and **h)** quantification of percentage of cleaved caspase 3^{+} NK cells of female WT, UTX^{Het}, and UTX^{NKD} cultured with IL-15 (5 ng/mL) and either DMSO or 2.5 uM Nutlin-3a for 24 hours (n = 3-11 per group). **i-k)** Normalized **i)** Bcl-2 MFI, **j)** Bim MFI, and **k)** Bcl-2:Bim MFI ratio in splenic NK cells from female WT and UTX^{NKD} mice (n = 5 per group). **l-m)** Bcl-2:Bim MFI ratio in splenic NK cells from **l)** female WT and male WT mice (n = 6 per group) and **m)** gonadectomized female and male mice (n = 11 per group). Data are representative of 2-4 independent experiments. Samples were compared using **a-d)** ordinary one-way ANOVA, **h)** two-way ANOVA with Tukey's correction for multiple comparisons, or **f, i-m)** unpaired two-tailed Student's t test and data points are presented as individual mice with the mean ± SEM (N.S., Not Significant; *, $p < 0.05$; **, $p < 0.01$; ***, $p < 0.001$; ****, $p < 0.0001$).

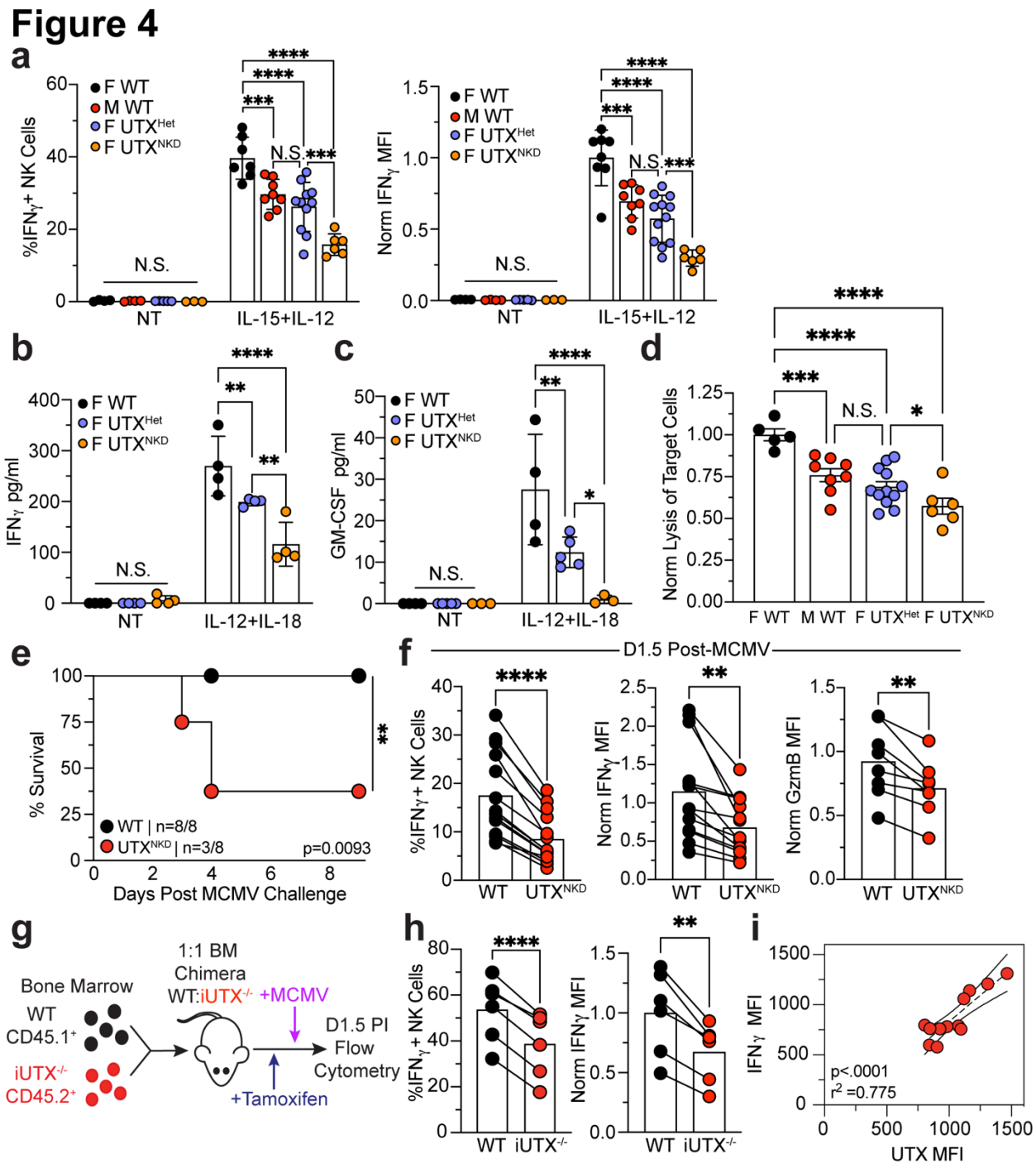

Figure 4: UTX enhances NK cell effector function and is required for survival against viral infection. a) Percentage IFN-γ+ and normalized IFN-γ MFI of total NK cells from female WT, male WT, female UTX^{Het}, and female UTX^{NKD} mice with no treatment (NT) or cultured with IL-15 (50 ng/mL) and IL-12 (20 ng/mL) for 4 hours (n = 6-10 per group), normalized to MFI of

female IL-15/12 treatment. **b)** IFN-γ and **c)** GM-CSF concentrations measured by ELISA in culture supernatants from female WT, UTX^{Het}, and UTX^{NKD} NK cells with no treatment (NT) or stimulated with IL-12 (20 ng/mL) and IL-18 (10 ng/mL) for 4 hours (n = 3-5 per group). **d)** Specific lysis of MHCI-deficient MC38 Target cells by female WT, male WT, female UTX^{Het}, or female UTX^{NKD} NK (Effector) cells for 16 hours at a 4:1 Effector:Target ratio, normalized to percent specific lysis by female WT NK cells (n = 5-12 per group). **e)** Kaplan-Meier survival curves of WT and UTX^{NKD} mice infected with MCMV (n = 8 per genotype). Mantel-Cox test (**, p=0.0093). **f)** Flow cytometric analysis of percentage IFN-γ^+, normalized IFN-γ MFI, and normalized granzyme B (GzmB) MFI relative to WT in splenic NK cells on D1.5 post MCMV infection of 4:1 WT:UTX^{NKD} mixed bone marrow chimeras (mBMCs) (n = 6-14). **g)** Schematic showing generation of 1:1 WT:$iUTX^{-/-}$ mBMCs. WT ($CD45.1^+$) and $iUTX^{-/-}$ ($CD45.2^+$) bone marrow was transferred at a 1:1 ratio into busulfan depleted hosts and treated with 1 mg tamoxifen daily for 3 days prior to MCMV infection. **h)** Percentage IFN-γ^+ and normalized IFN-γ MFI of NK cells derived from 1:1 WT:$iUTX^{-/-}$ mBMC mice on day 1.5 post MCMV infection, normalized to WT (n = 6). **i)** Correlation of IFN-γ vs. UTX MFI of total splenic NK cells (n = 12). Two-tailed correlation of XY data performed. Pearson's r^2 =0.775, and p <0.0001. Data are representative of 2-3 independent experiments. Samples were compared using **a-c)** two-way ANOVA or **d)** one-way ANOVA with Tukey's correction for multiple comparisons or **f,h)** paired two-tailed Student's t test. Data points are presented as individual mice with the mean ± SEM (*, p<0.05; **, p<0.01; ***, p<0.001; ****, p<0.0001).

Figure 5

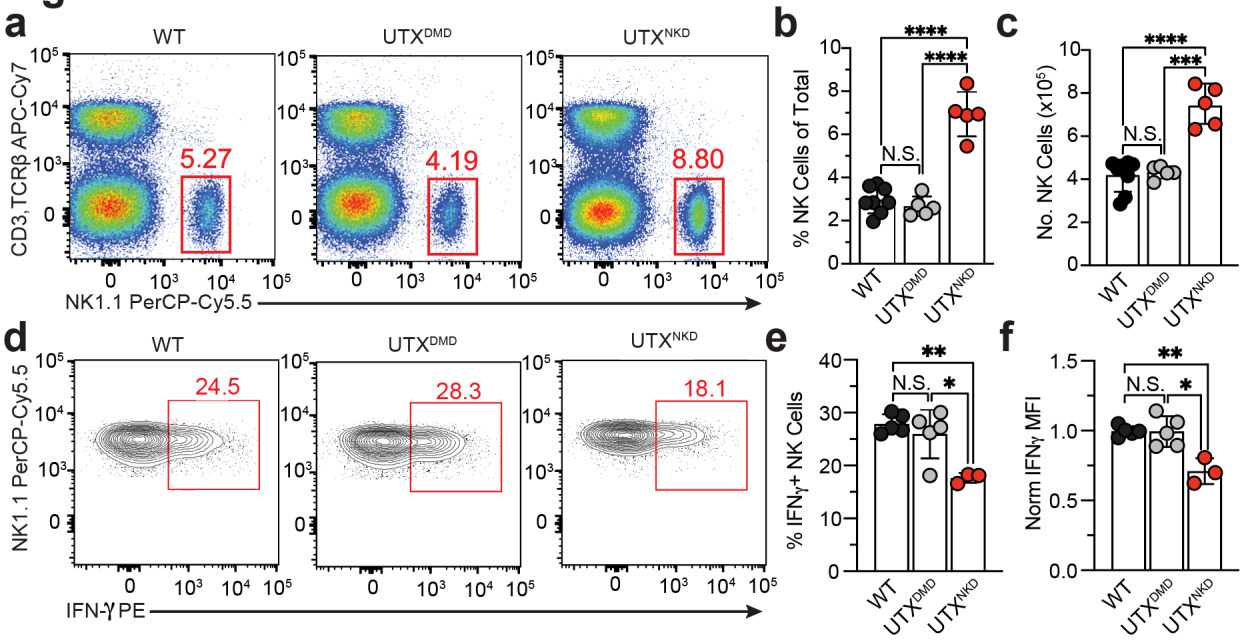

Figure 5: UTX controls NK cell homeostasis and IFN-γ production independent of demethylase activity. a) Representative density plots, **b)** frequency, and **c)** number of NK cells in the spleen of female WT, UTX^{DMD}, and UTX^{NKD} mice (n = 5 per group). **d)** Representative contour plots, **e)** percentage IFN-γ^{+}, and **f)** normalized IFN-γ MFI of female WT, UTX^{DMD}, and UTX^{NKD} NK cells (n = 5 per group) normalized to WT. Data are representative of 2-3 independent experiments. Samples were compared using one-way ANOVA with Tukey's correction for multiple comparisons**.** Data points are presented as individual mice with the mean ± SEM (N.S., Not Significant; *, p <0.05; **, p <0.01; ***, p<0.001; ****, p<0.0001).

Figure 6

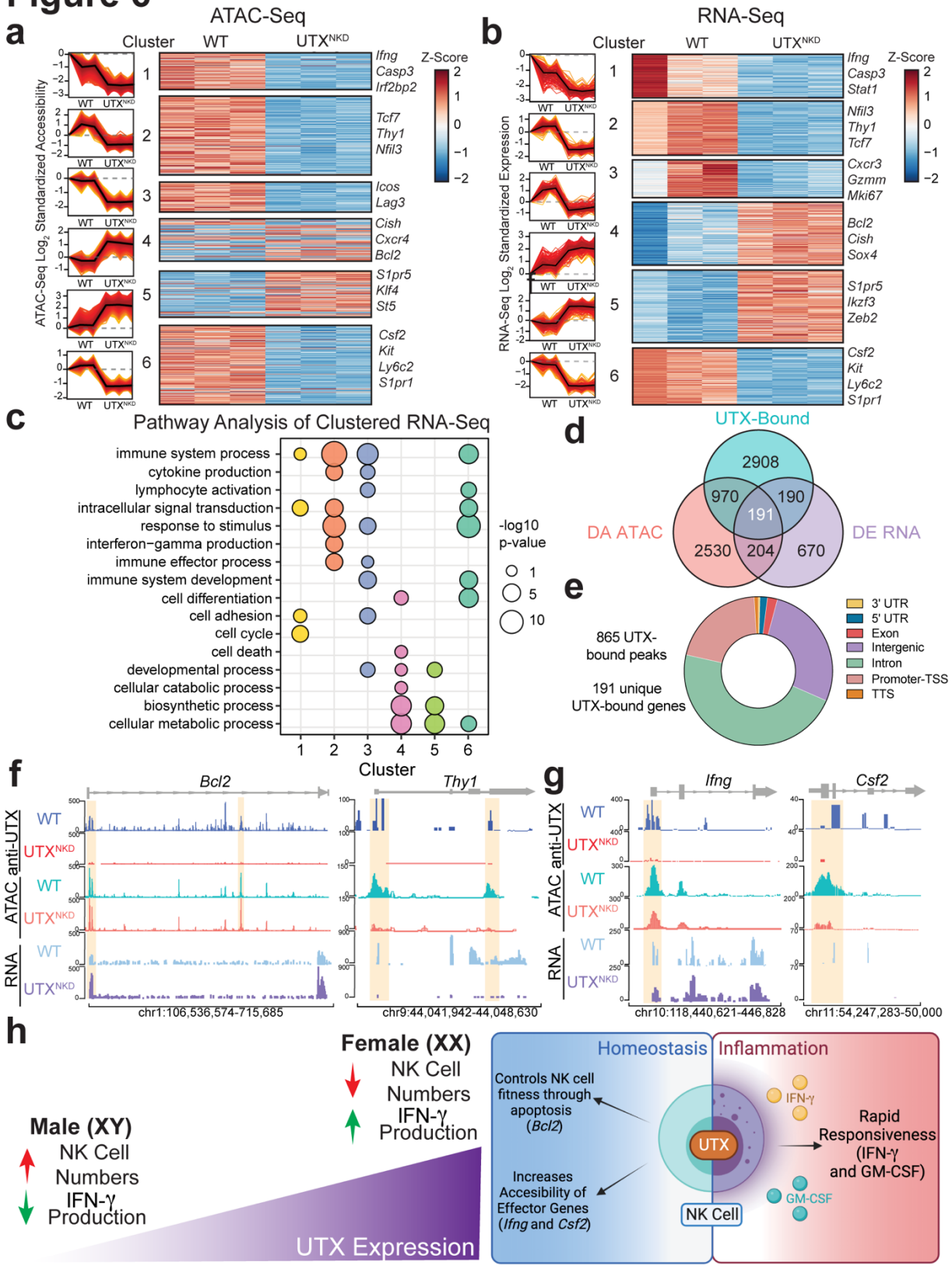
a
ATAC-Seq
Cluster
WT
UTX^NKD
ATAC-Seq Log2 Standardized Accessibility
Z-Score
Ifng
Casp3
Irf2bp2
Tcf7
Thy1
Nfil3
Icos
Lag3
Cish
Cxcr4
Bcl2
S1pr5
Klf4
St5
Csf2
Kit
Ly6c2
S1pr1
b
RNA-Seq
RNA-Seq Log2 Standardized Expression
Stat1
Cxcr3
Gzmm
Mki67
Sox4
Ikzf3
Zeb2
c
Pathway Analysis of Clustered RNA-Seq
immune system process
cytokine production
lymphocyte activation
intracellular signal transduction
response to stimulus
interferon−gamma production
immune effector process
immune system development
cell differentiation
cell adhesion
cell cycle
cell death
developmental process
cellular catabolic process
biosynthetic process
cellular metabolic process
-log10 p-value
d
UTX-Bound
2908
970
190
191
DA ATAC
DE RNA
2530
204
670
e
865 UTX-bound peaks
191 unique UTX-bound genes
3' UTR
5' UTR
Exon
Intergenic
Intron
Promoter-TSS
TTS
f
Bcl2
Thy1
ATAC anti-UTX
RNA
chr1:106,536,574-715,685
chr9:44,041,942-44,048,630
g
Ifng
Csf2
chr10:118,440,621-446,828
chr11:54,247,283-50,000
h
Male (XY)
NK Cell Numbers
IFN-γ Production
Female (XX)
NK Cell Numbers
IFN-γ Production
UTX Expression
Homeostasis
Inflammation
Controls NK cell fitness through apoptosis (Bcl2)
Increases Accesibility of Effector Genes (Ifng and Csf2)
UTX
NK Cell
IFN-γ
GM-CSF
Rapid Responsiveness (IFN-γ and GM-CSF)

Figure 6: Global changes in NK cell chromatin accessibility and transcription mediated by UTX. a-c) WT:UTX^{NKD} mBMCs were generated by transferring WT (CD45.1^{+}) and UTX^{NKD} (CD45.2^{+}) bone marrow into lymphodepleted host mice (CD45^{1x2}) and allowed to reconstitute for 6 weeks. Splenic NK cells were sorted for ATAC-seq and RNA-seq library preparation (n=3 per group). **a, b)** Line graphs (left) and heatmap (right) of fuzzy c-means clustered **a)** differentially accessible peaks identified by ATAC-seq and **b)** differentially expressed genes identified by RNA-seq of splenic NK cells from WT:UTX^{NKD} mBMCs (adjusted p-value < 0.05 and membership score > 0.5)**.** Line graphs show mean (black line) and standard deviation (red ribbon) of mean-centered normalized $\log_2$ values of significant (FDR and adjusted p-value < 0.05). **c)** Pathway analysis of significant fuzzy c-means clustered RNA-seq genes using g:Profiler with point size indicating -$\log_{10}$(p-value). **d-g)** Anti-UTX CUT&Tag was performed in WT and UTX^{NKD} NK cells and identified 5746 unique UTX-bound peaks (n=3 per group). **d)** Location of UTX-bound peaks. **e)** Venn diagram outlining overlapping differentially accessible (DA) genes identified by ATAC-seq and differentially expressed (DE) genes identified by RNA-seq. **f-g)** Representative gene tracks from UCSC Integrated Genome Browser of anti-UTX CUT&Tag ("anti-UTX"), ATAC-seq, and RNA-seq of **f)** *Bcl2* and *Thy1* and **g)** *Ifng* and *Csf2* ; Y-axis depicts counts per million (CPM). **h)** Schematic of how differential UTX expression levels underlie sexual dimorphism in NK cell composition and function (left). Diagram of how UTX may be regulating gene programs involved in NK cell numbers and effector function during homeostasis and viral infection (right).

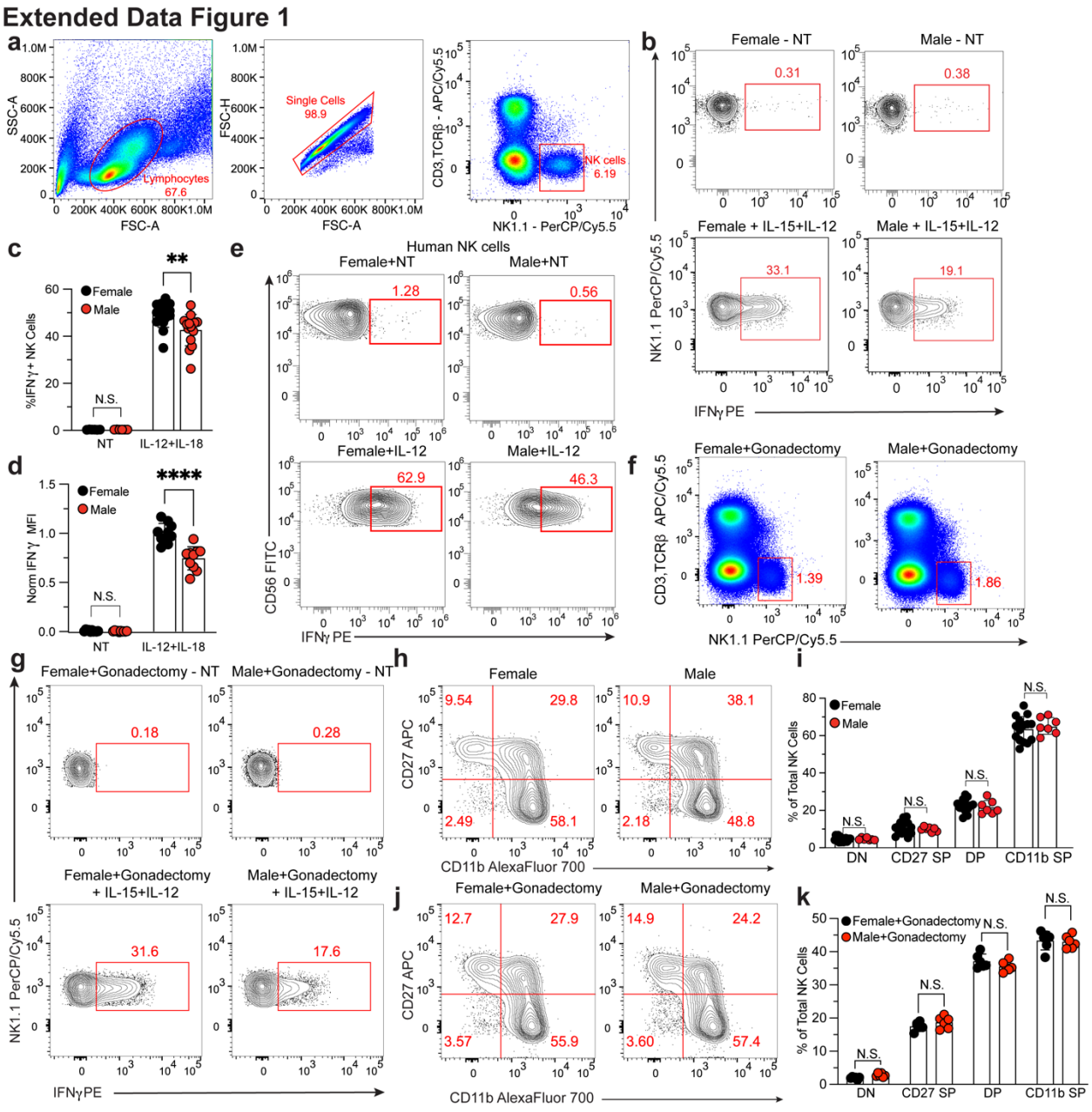

Extended Data Figure 1: Sex differences in IFN-γ production in response to IL-12/18. a) Representative dot plots showing gating strategy to identify $CD3^-$ $TCR\beta^-$ $NK1.1^+$ mouse NK cells. **b)** Representative contour plots, **(c)** percentage IFN-γ^+, and **(d)** normalized IFN-γ MFI of female and male WT NK cells with cultured no treatment (NT) or IL-12 (20 ng/mL) and IL-18 (10 ng/mL) for 4 hours (n = 14 per group). **e)** Representative contour plots of $CD3^-$ $CD56^+$ female (n = 6) and male (n = 7) human NK cells cultured and stimulated with 10 ng/mL of IL-12 for 16 hours in the

presence of K562 cells. **f)** Representative dot plots of splenic NK cells ($CD3^-$ $TCR\beta^-$ $NK1.1^+$) in gonadectomized female and male mice. **g)** Representative contour plots of total splenic NK cells isolated from gonadectomized female and male mice and cultured with no treatment (NT) or IL-15 (50 ng/mL) and IL-12 (20 ng/mL) for 4 hours. **h)** Representative contour plots and **i)** percentage $CD27^-CD11b^-$ (DN), $CD27^+CD11b^-$ (CD27 SP), $CD27^+CD11b^+$ (DP), and $CD27^-CD11b^+$ (CD11b SP) of total splenic NK cells from female and male mice (n = 7 per group). **j)** Representative contour plots and **k)** percentage $CD27^-CD11b^-$ (DN), $CD27^+CD11b^-$ (CD27 SP), $CD27^+CD11b^+$ (DP), and $CD27^-CD11b^+$ (CD11b SP) of total splenic NK cells from gonadectomized mice (n = 6 per group). Data are representative of 2-3 independent experiments. Samples were compared using unpaired two-tailed Student's t test and data points are presented as individual mice with the mean ± SEM (N.S., Not Significant; **, $p < 0.01$; ****, $p < 0.0001$).

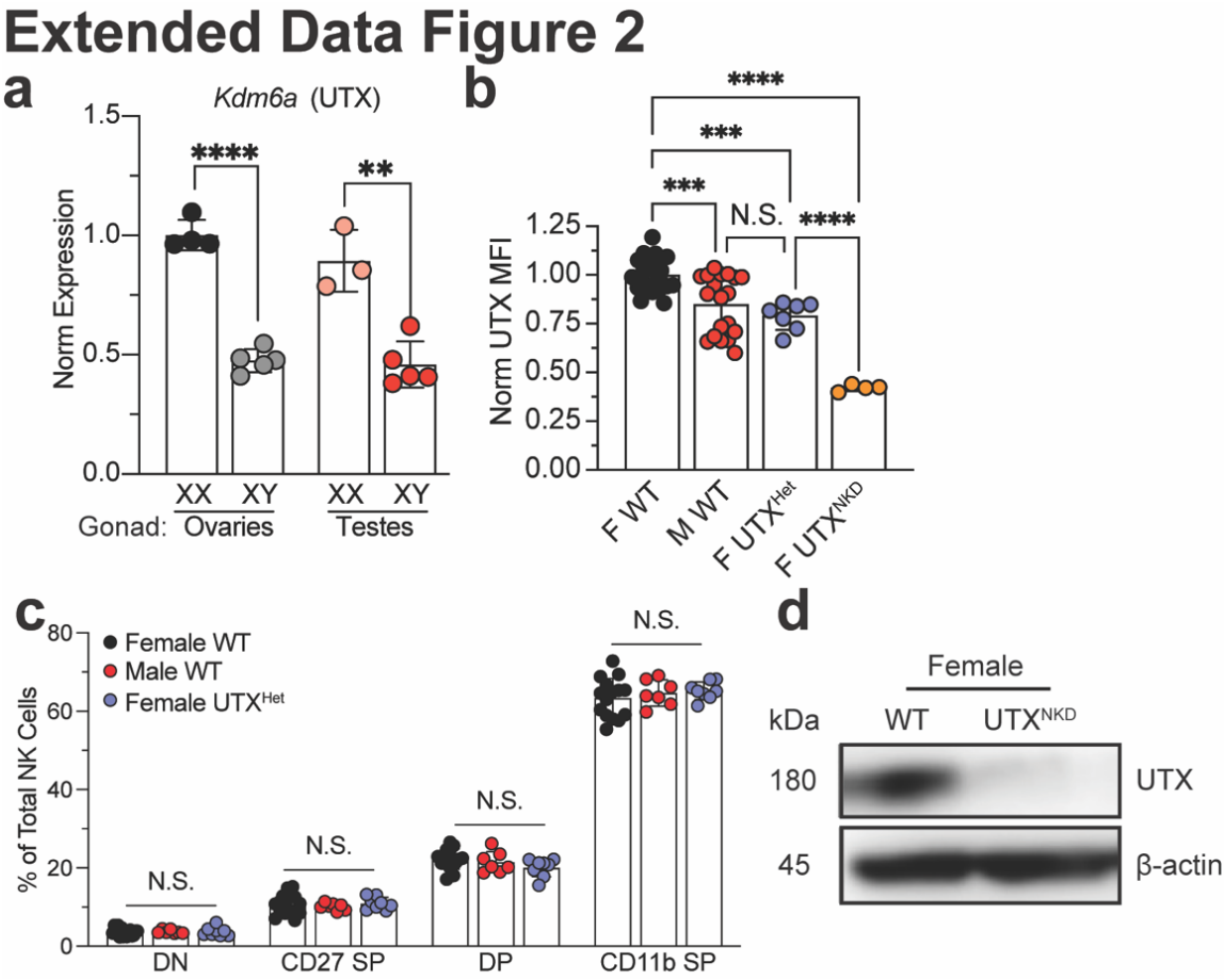

Extended Data Figure 2: UTX expression in Four Core Genotype mice and maturation in UTX mouse models. a) Relative expression of *Kdm6a* (UTX) by RT-qPCR in Four Core Genotype mice, in which male or female gonads present are independent of XX or XY chromosome composition, normalized to female WT expression (XX with ovaries) (n = 3-5 per group). **b)** Relative UTX MFI in splenic NK cells isolated from female WT, male WT, female UTX^{Het}, and female UTX^{NKD} mice (n = 4-19 per group). **c)** CD11b and CD27 expression within NK cells isolated from female WT, male WT, and female UTX^{Het} mice (n = 7-13 per group). **d)** Representative western blot showing protein expression of UTX in NK cells isolated from female WT and UTX^{NKD} mice compared to β-actin loading control. Data are representative of 2-3

independent experiments. Samples were compared using **a)** unpaired two-tailed Student's t test, **b,c)** one-way ANOVA with Tukey's correction for multiple comparisons. Data points are presented as individual mice with the mean ± SEM (N.S., Not Significant; **, $p < 0.01$; ***, $p < 0.001$; ****, $p < 0.0001$).

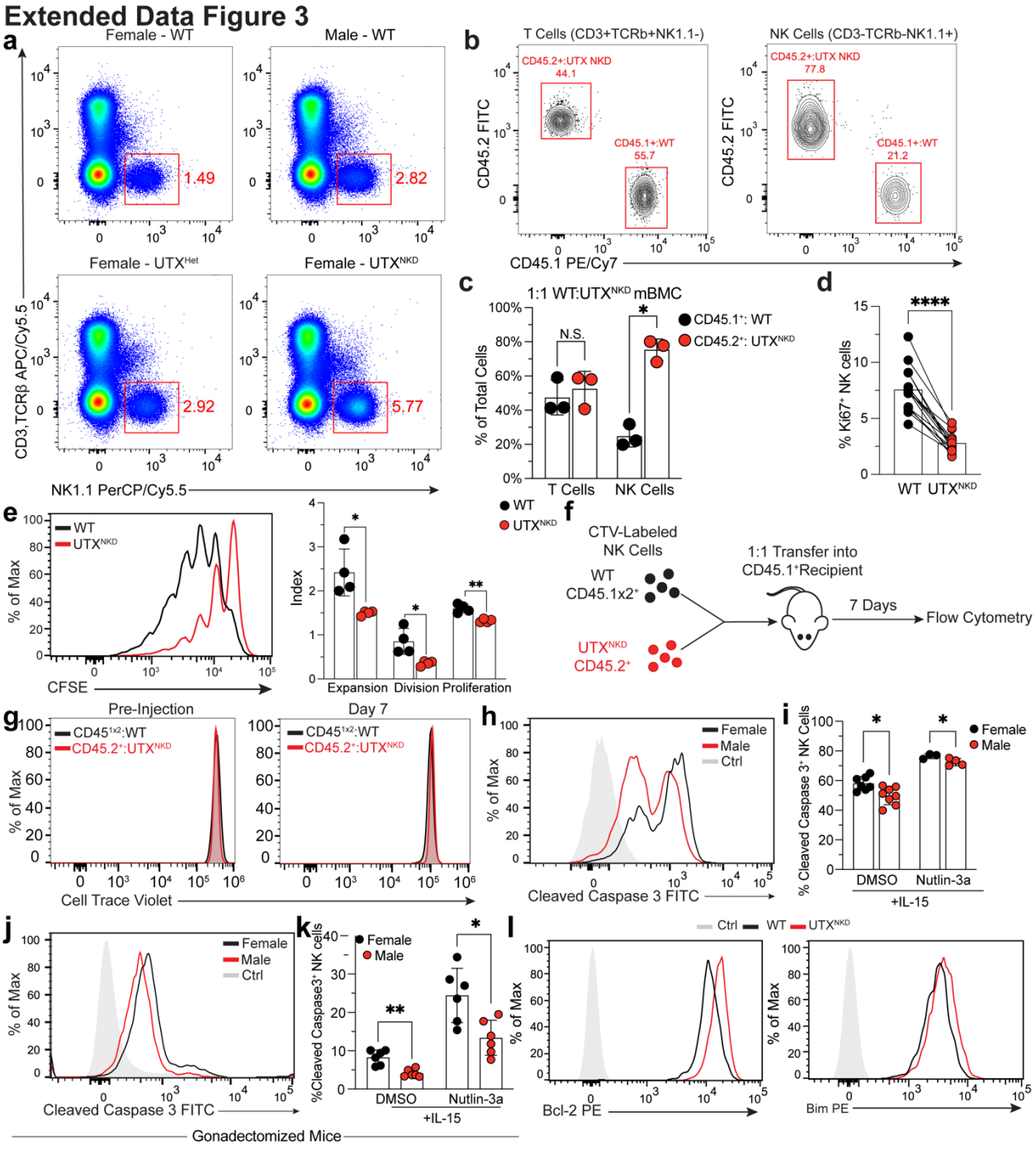

Extended Data Figure 3: UTX regulates NK cell fitness. a) Representative flow cytometry dot plots of NK cells in spleen of female wild type (WT), male WT, and female UTX^{Het}, and female UTX^{NKD} mice. **b)** Representative contour plots and **c)** percent of WT CD45.1^{+} or UTX^{NKD} CD45.2^{+} cells of total splenic T cells (left) and NK cells (right) in 1:1 WT:UTX^{NKD} mBMC mice (n=3). **d)**

Percentage of Ki67^{+} cells in blood of 4:1 WT:UTX^{NKD} mBMCs (n=28) ratio used to normalize WT and UTX^{NKD} NK cell numbers. **e)** Representative histogram (left) and quantification (right) of CFSE expansion, division and proliferation indexes calculated using FlowJo's Proliferation tool of CFSE-labeled splenic NK cells isolated from WT and UTX^{NKD} mice stimulated *ex vivo* with IL-15 (50 ng/mL) for 4 days. **f)** Schematic showing adoptive transfer of CTV-labeled congenically distinct WT (CD45^{1x2}) and UTX^{NKD} (CD45.2^{+}) NK cells transferred into WT (CD45.1^{+}) recipients at a 1:1 ratio with analysis of CTV dilution and WT:UTX^{NKD} ratio on D7 by flow cytometry. **g)** Representative histograms showing CTV dilution of congenically distinct WT (CD45^{1x2}) and UTX^{NKD} (CD45.2^{+}) NK cells transferred into WT (CD45.1^{+}) recipients before transfer (left) and on day 7 post transfer (right). **h)** Representative histograms and **i)** percentage of cleaved caspase 3^{+} splenic NK cells from female WT and male WT (n = 3-8 per group) treated *ex vivo* with IL-15 (5 ng/mL) and DMSO or 2.5 uM Nutlin-3a for 24 hours. **j)** Representative histograms and **k)** percentage of cleaved caspase 3^{+} splenic NK cells from gonadectomized female and male mice (n = 6 per group) treated *ex vivo* with IL-15 (5 ng/mL) and DMSO or 2.5 uM Nutlin-3a for 24 hours. **l)** Representative histograms of Bcl-2 (left) and Bim (right) of flow cytometry in splenic NK cells from female WT and UTX^{NKD} mice (n = 5 per group). "Ctrl" refers to matched unstained flow cytometry controls. Data are representative of 2-3 independent experiments. Samples were compared using unpaired two-tailed Student's t test with Welch's correction and data points are presented as individual mice with the mean ± SEM (N.S., Not Significant; *, $p<0.05$; **, $p<0.01$; ****, $p<0.0001$).

Extended Data Figure 4

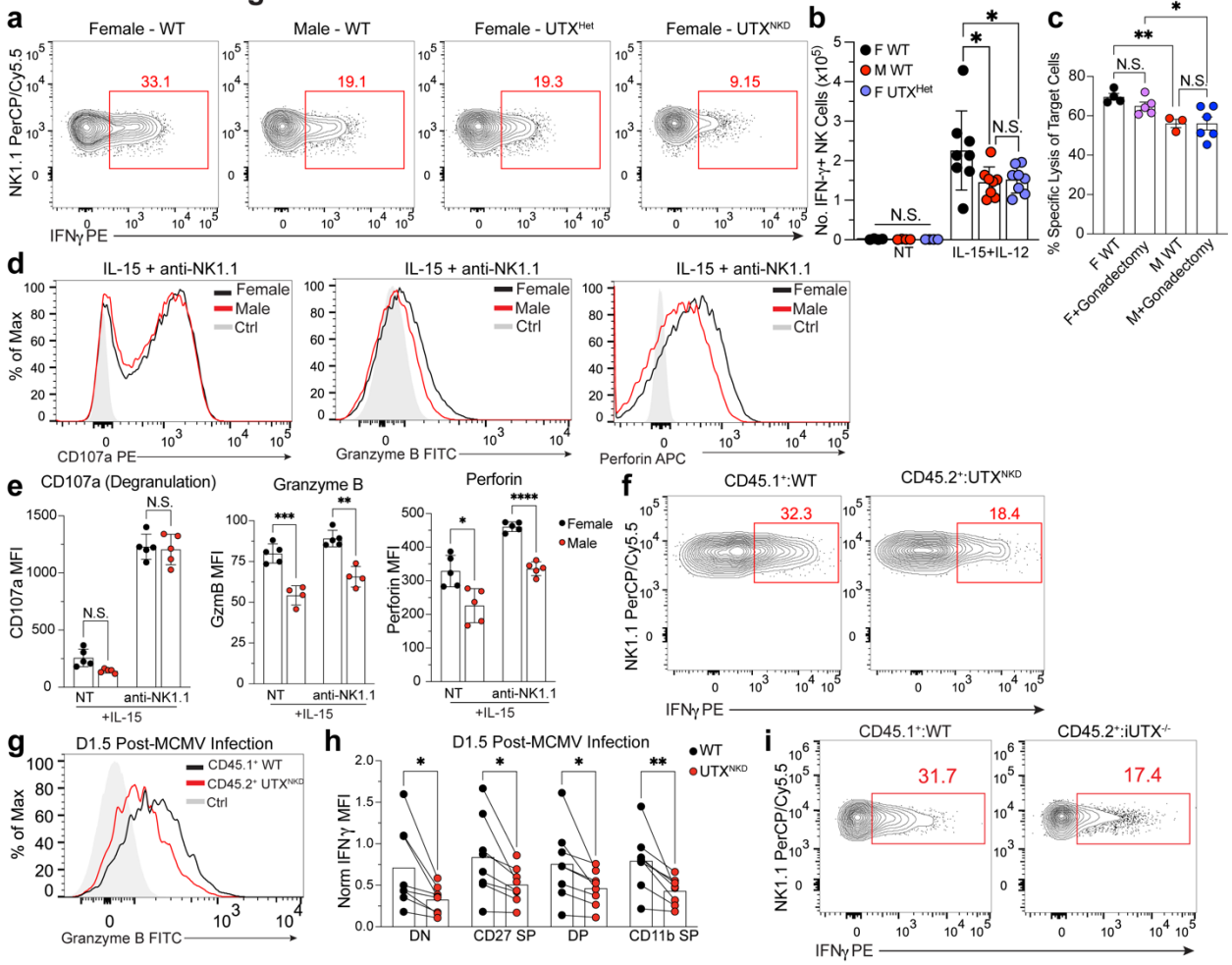

Extended Data Figure 4: UTX enhances effector function independent of gonadal hormone and maturation. a) Representative contour plots of total NK cells from female WT, male WT, female UTX^{Het}, and female UTX^{NKD} mice cultured with IL-15 (50 ng/mL) and IL-12 (20 ng/mL) for 4 hours. **b)** Absolute number of IFN-γ^{+} NK cells from female WT, male WT, and female UTX^{Het} mice stimulated with either no treatment (NT) or IL-15 (50 ng/mL) and IL-12 (20 ng/mL) for 4 hours (n = 8 per group). **c)** Specific lysis of MHC Class I deficient MC38 cells (Target cells) by female WT, male WT, and gonadectomized female and male NK cells for 16 hours at a 4:1 effector:target ratio, normalized to percent specific lysis by female WT NK cells (n = 3-6 per group). **d)** Representative histograms and **e)** MFI of CD107a, granzyme b (GzmB), and perforin

of female WT and male WT NK cells incubated with IL-15 (50 ng/mL) only or additionally stimulated with plate-bound anti-NK1.1 antibody (PK136) (n = 4-5 per group). "Ctrl" refers to matched unstained control for flow cytometry. Representative **f)** contour plots of IFN-γ and **g)** histogram of GzmB expressing total splenic NK cells on D1.5 post MCMV infection of 4:1 WT:UTX^{NKD} mixed bone marrow chimeras (mBMCs), ratio used to normalize cell numbers between genotypes. **h)** IFN-γ protein production in UTX^{NKD} compared to WT NK cells within maturation subsets: CD27^{-}CD11b^{-} (DN), CD27^{+}CD11b^{-} (CD27 SP), CD27^{+}CD11b^{+} (DP), and CD27^{-}CD11b^{+} (CD11b SP) isolated from 4:1 WT:UTX^{NKD} mBMC 1.5 days post-MCMV infection (n = 6)**. i)** Representative contour plots of total NK cells derived from 1:1 WT:iUTX$^{-/-}$ mBMC mice on day 1.5 post MCMV infection, normalized to WT (n = 6). Data are representative of 2-3 independent experiments. Samples were compared using paired two-tailed Student's t test and data points are presented as individual mice with the mean ± SEM (N.S., Not Significant; *, $p<0.05$; **, $p<0.01$; ***, $p<0.001$; ****, $p<0.0001$).

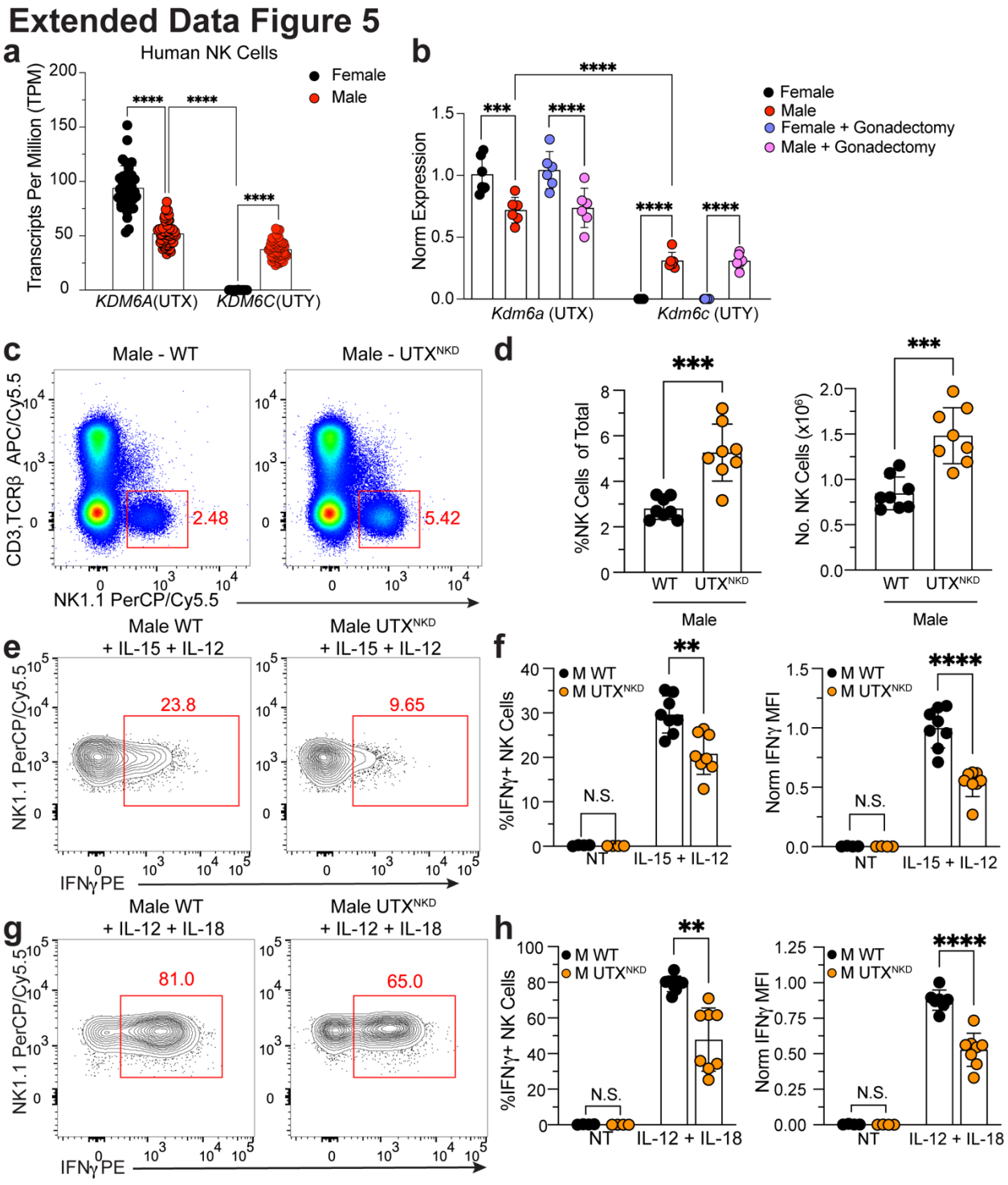

Extended Data Figure 5: UTY is expressed but not sufficient to compensate for loss of UTX in NK cell homeostasis and effector function. a) Expression in transcripts per million of *KDM6A* (UTX) and *KDM6C* (UTY) using DICE database RNA-seq data on sorted NK cells from human

females (n = 36) vs. males (n = 54). **b)** Relative expression of *Kdm6a* (UTX) and *Kdm6c* (UTY) by RT-qPCR in splenic NK cells isolated from female WT, male WT, and gonadectomized female and male mice (n = 6 per group). **c)** Representative flow cytometry dot plots and quantification of **d)** frequency and absolute numbers of NK cells in spleen of male WT and UTX^{NKD} mice (n = 8 per group). **e)** Representative flow cytometry contour plots and quantification of **f)** percentage IFN-γ^+ and normalized IFN-γ MFI of total NK cells from male WT vs. male UTX^{NKD} mice with no treatment (NT) or in response to IL-15 (50 ng/mL) and IL-12 (20 ng/mL) stimulation for 4 hours *ex vivo*, MFI normalized to male WT (n = 8 per group). **g)** Representative flow cytometry contour plots and quantification of **h)** percentage IFN-γ^+ and normalized IFN-γ MFI of total NK cells from male WT vs. male UTX^{NKD} mice with no treatment (NT) or in response to IL-12 (20 ng/mL) and IL-18 (10 ng/mL) stimulation for 4 hours *ex vivo*, MFI normalized to male WT (n = 8 per group). Data are representative of 2-3 independent experiments. Samples were compared using paired two-tailed Student's t test and data points are presented as individual mice with the mean ± SEM (N.S., Not Significant; **, p <0.01; ***, p <0.001; ****, p<0.0001).

Extended Data Figure 6

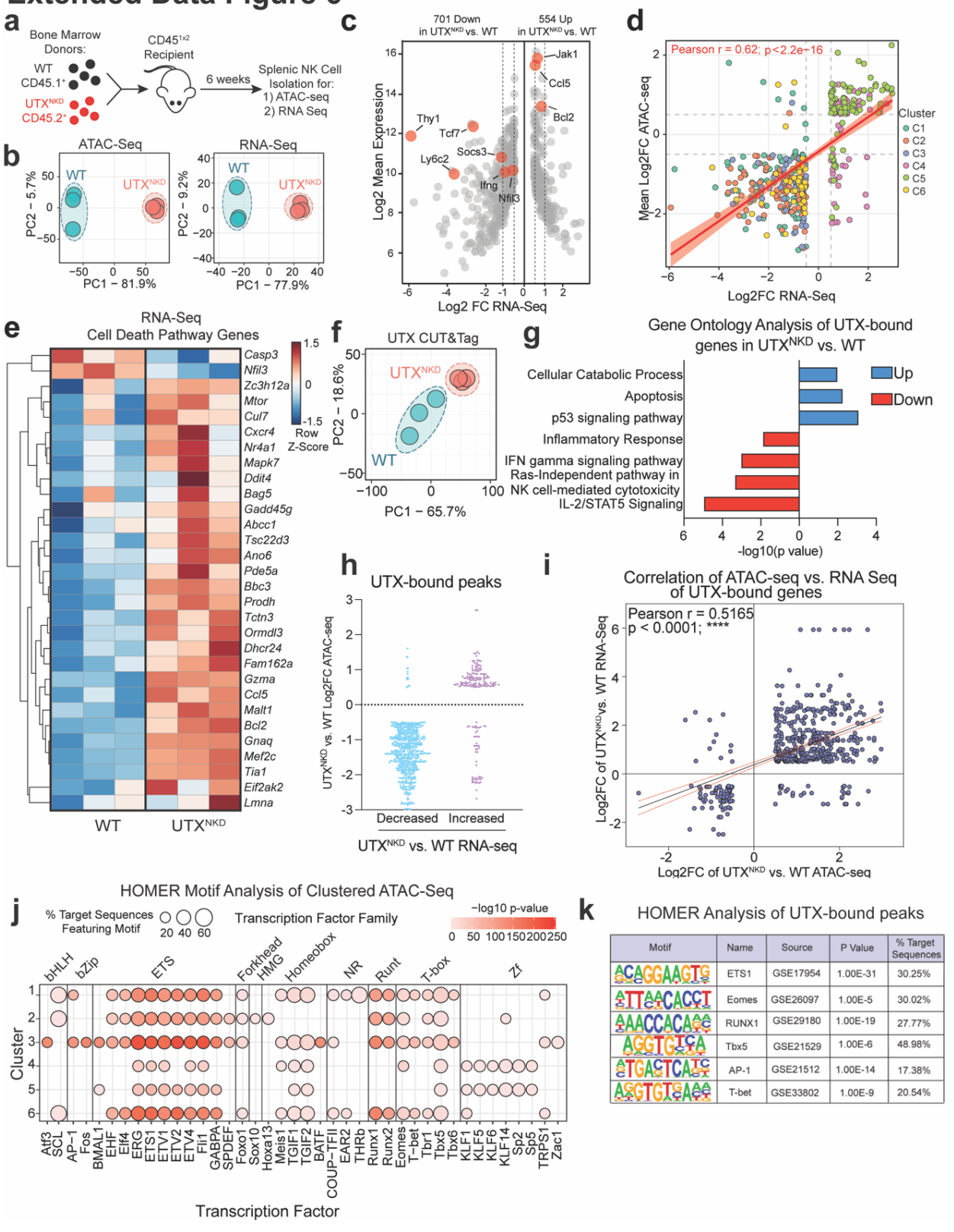

Motif	Name	Source	P Value	% Target Sequences
	ETS1	GSE17954	1.00E-31	30.25%
	Eomes	GSE26097	1.00E-5	30.02%
	RUNX1	GSE29180	1.00E-19	27.77%
	Tbx5	GSE21529	1.00E-6	48.98%
	AP-1	GSE21512	1.00E-14	17.38%
	T-bet	GSE33802	1.00E-9	20.54%

Extended Data Figure 6: Integrative ATAC, RNA, anti-UTX CUT&Tag sequencing analysis reveal concomitant changes in chromatin accessibility and transcription mediated by UTX. **a)** Schematic of mBMC mice generated by transferring a mixture of WT ($CD45.1^+$) and UTX^{NKD} ($CD45.2^+$) bone marrow into a lymphodepleted host ($CD45^{1x2}$) and allowed to reconstitute for 6 weeks. NK cells were sorted from spleens of mBMC mice for ATAC-seq and RNA-seq library preparation. **b)** Principal component analysis (PCA) of (left) chromatin accessibility (ATAC-seq) and (right) transcriptional (RNA-seq) changes in WT and UTX^{NKD} NK cells at steady state. **c)** Volcano plot of significant differentially expressed genes by RNA-seq plotted by Log2FC of UTX^{NKD} vs. WT (x-axis) and Log2 Mean Expression (y-axis). Dotted lines represent different Log2FC cut offs (0.5 and 1). Red dots are highlighted genes of interest for NK cell effector and developmental pathways. **d)** Scatter plot highlighting genes that were differentially accessible and expressed (FDR and adjusted p-value < 0.05) colored by fuzzy c-means cluster (see **Fig. 6**). Y-axis depicts mean $\log_2$ fold change of ATAC accessibility peaks and x-axis depicts $\log_2$ fold change of RNA-seq transcript levels. Best fit regression line (red) with standard error (light red ribbon). Positive correlation calculated by Spearman correlation of dataset ($R=0.62$, $p<2.2x10^{-16}$). **e)** Heatmap displaying differentially expressed cell death pathway genes between WT and UTX^{NKD} NK cells. All genes displayed in heatmap met the following threshold of significance: FDR < 0.05, adjusted p-value < 0.05, and $\log_2$ fold change > 0.5. **f)** PCA analysis of anti-UTX CUT&Tag in sort-purified WT and UTX^{NKD} NK cells (n=3 per group). **g)** Functional gene ontology pathway analysis on UTX-bound genes that are decreased (red) or increased (blue) by expression by RNA-seq using Enrichr. **h)** Log2FC in UTX^{NKD} vs. WT of ATAC accessibility (y-axis) plotted by either decreased (>-0.5 Log2FC) (blue) or increased (>+0.5 Log2FC) (purple) expression by RNA-seq (x-axis) of the UTX bound genes with significant changes in accessibility and expression. **i)**

Correlation plot of Log2FC of UTX^{NKD} vs. WT RNA-seq values compared to corresponding ATAC-seq values for each specific UTX-bound gene. Linear regression was performed to allow for the best-fit line to be plotted (black line through graph) with the confidence intervals plotted (dotted red lines). Pearson's correlation was performed with r = 0.5165 with a significant p value < 0.0001. **j)** HOMER motif analysis of significant fuzzy c-means clustered ATAC-seq peaks grouped by transcription factor family (top) and transcription factor (bottom). Point size indicates percentage of target sequences featuring motif and red gradient indicates $-\log_{10}$(p-value) of enrichment. **k)** HOMER Motif analysis performed on UTX-bound peaks. % Target Sequences refers to percent of target motifs identified by the HOMER algorithm out of the background motifs.

Supplementary Data Table 1: Mouse Strains Used in this Study				
Mouse Strain Name (abbreviation)	Genotype	Genetic Background	Description	Reference
UTX^{NKD}	*Kdm6a*$^{flox/flox}$ *Ncr1*$^{cre+}$	C57BL/6	Homozygous UTX KO in NKp46 expressing cells.	Generated *De Novo*
UTX^{Het}	*Kdm6a*$^{flox/WT}$ *Ncr1*$^{cre+}$	C57BL/6	Heterozygous deletion of UTX in NKp46 expressing cells.	Generated *De Novo*
$iUTX^{-/-}$	*Kdm6a*$^{flox/flox}$ *Rosa26*$^{ERT2cre+}$	C57BL/6	Mouse with full body Tamoxifen-inducible deletion of UTX.	Generated *De Novo* with Jackson Lab Strain ID #:008463
UTX^{DMD}	$UTX^{H1146A+E1148A}$	C57BL/6	Mouse harboring full body copy of a demethylase dead UTX	PMID: 22949634
Four Core Genotype Mice (FCG)	XX - Ovary XY – Ovary XX – Testes XY - Testes	C57BL/6	Mice with sex chromosomes independent of gonadal composition	PMID: 19028515

Contact for Reagent and Resource Sharing

Further information and requests for resources and reagents should be directed and will be fulfilled by the Corresponding Authors, Timothy O'Sullivan (tosullivan@mednet.ucla.edu) and Maureen Su (masu@mednet.ucla.edu)

Method Details

Mice

Mice were bred at UCLA in accordance with the guidelines of the institutional Animal Care and Use Committee (IACUC). The following mouse strains were used in this study: C57BL/6

(CD45.2$^+$) (Jackson Labs, #000664), B6.SJL (CD45.1$^+$) (Jackson Labs, #002114), *Rosa26*^{ERT2Cre} (Jackson Labs, #008463), *Ncr1*^{Cre} [76], *Kdm6a*$^{fl/fl}$ [64], UTX$^{H1146A+E1148A}$ (UTX^{DMD})[47], and Four Core Genotype mice[31]. For experiments with gonadectomy, procedure was performed by Jackson Laboratories Surgical Services. To generate UTX^{NKD} and UTX^{Het} mice *de novo* for this study, *Ncr1*$^{Cre/WT}$ mice were crossed to *Kdm6a*$^{fl/fl}$ mice to generate either *Ncr1*$^{Cre/WT}$*Kdm6a*$^{fl/fl}$ (UTX^{NKD}) or *Ncr1*$^{Cre/WT}$*Kdm6a*$^{fl/WT}$ (UTX^{Het}) offspring. To generate iUTX$^{-/-}$ mice with a full body tamoxifen-inducible deletion of UTX *de novo*, *Rosa26*^{ERT2Cre} mice were crossed to *Kdm6a*$^{fl/fl}$ mice to generate F2 progeny *Rosa26*$^{ERT2Cre/+}$*Kdm6a*$^{fl/fl}$ offspring. CD45^{1x2} mice were generated *de novo* by crossing CD45.1$^+$ B6.SJL and CD45.2$^+$ C57BL/6 mice. For all mouse experiments in 6-8 week old age-matched littermates were used in accordance with approved institutional protocols. mBMC mice were generated by depleting host CD45^{1x2} mice by intraperitoneal (i.p.) injection of busulfan (1mg/mL) at 20mg/kg for 3 consecutive days, followed by reconstitution 24 hours later with various mixtures (specified for each experiment in figure legends) of bone marrow cells from WT (CD45.1$^+$) and knockout (CD45.2$^+$) donor mice in the presence of an anti-NK1.1 antibody (1 mg/ml; clone: PK136) to deplete any remaining mature NK cells. For inducible deletion of UTX in iUTX$^{-/-}$ mice, mBMC mice produced with WT and iUTX$^{-/-}$ bone marrow were treated with 1 mg tamoxifen i.p. daily for 3 days prior to MCMV infection.

MCMV infection

MCMV (Smith strain)[77] was serially passaged through BALB/c hosts three times, and then salivary gland viral stocks were prepared with a dounce homogenizer for dissociating the salivary glands of infected mice 3 weeks after infection. Experimental mice in studies were infected with MCMV by i.p. injection of 7.5 x 10^3 plaque-forming units (PFU) in 0.5 mL of PBS. Mice were monitored

and weighed daily and sacrificed when body weight dropped over 20% from initial weight. "Sub-lethal dose" of MCMV was determined by infection of mice with different dosages to identify the dose in which WT C57BL/6 would survive after 7 days.

Isolation and enrichment of mouse NK cells

Mouse spleens, livers, lungs, and blood were harvested and prepared into single cell suspensions as described previously[78]. Splenic single cell suspensions were lysed in red blood cell lysis buffer and resuspended in EasySep™ buffer (StemCell). To avoid depleting $Ly6C^+$ NK cells we developed a custom antibody cocktail as follows: splenocytes were labeled with 10 μg per spleen of biotin conjugated antibodies against CD3 (17A2), CD19 (6D5), CD8 (53-6.7), CD88 (20/70), Ly6G (1A8), SiglecF (S17007L), TCRβ (H57-597), CD20 (SA275A11), CD172a (P84) and magnetically depleted from total splenocyte suspensions with the use of anti-biotin coupled magnetic beads (Biolegend)[40].

Ex vivo stimulation of mouse NK cells

For cytokine stimulation experiments, 2 x 10^4 mouse NK cells were stimulated for 4 hours in CR-10 (RPMI 1640 + 25 mM HEPES + 10% FBS, 1% L-glutamine, 1% 200 mM sodium pyruvate, 1% MEM-NEAA, 1% penicillin-streptomycin, 0.5% sodium bicarbonate, 0.01% 55 mM 2-mercaptoethanol), Brefeldin A (1:1000; BioLegend) and Monensin (2 uM; BioLegend) with or without recombinant mouse IL-15 (50 ng/mL; Peprotech), mouse IL-12 (20 ng/mL; Peprotech), and/or recombinant mouse IL-18 (10 ng/mL; Peprotech). Cells were cultured in CR-10 media alone as a negative control (No Treatment or NT). Absolute number of IFN-γ producing NK cells were determined by acquiring and counting individual cells with an Attune NxT after intracellular

flow cytometry staining to determine cell count of IFN-γ^+ out of the 2 x 10^4 cells plated total. For plate-bound antibody stimulation experiments, 2 x 10^4 isolated NK cells per condition were stimulated with 4 mg/mL precoated antibody against NK1.1 (PK136) for 4 hours in complete media containing Brefeldin A (1:1000; BioLegend) and Monensin (2uM; BioLegend). Cells were cultured in media alone as a negative control (No Treatment or NT).

Proliferation assays

CellTrace™ CFSE (Thermo) stock solution was prepared per the manufacturers' instructions and diluted at 1:10,000 in 37C PBS. Isolated NK cells were incubated in 0.5mL of diluted CFSE solution for 5 minutes at 37°C. The solution was quenched with 10X the volume of CR-10 media. Cells were then washed and plated at 50 ng rmIL-15 (Peprotech) and cultured for 4 days to assess proliferation.

Human NK cell culture and stimulation

Human peripheral blood mononuclear cells (PBMCs) from anonymous healthy donors were obtained from leukoreduction filters after platelet apheresis from the UCLA Virology Core. NK cells were isolated using the EasySep Human NK Cell Isolation Kit (Stem Cell Technologies) following manufacturer instructions. Following isolation, cells were maintained in 24-well G-Rex plates (Wilson Wolf) in NK MACS media (Miltenyi Biotech) supplemented with human IL-2 (100 IU/mL, Peprotech) and human IL-15 (20 ng/mL, Peprotech) at a plating density of 5 x 10^6 cells per well. For cytokine stimulation, either freshly isolated human NK cells or cells activated for 14 days with IL-2/IL-15 were plated with K562 leukemia cells at an E:T ratio of 2.5:1 in addition to human IL-2 (100 IU/mL, Peprotech), human IL-15 (20 ng/mL, Peprotech), human IL-12 (10

ng/mL, Peprotech), and/or human IL-18 (100 ng/mL, Peprotech) in CR-10 media. NK cells were stimulated with cytokines for 16 hours before analysis by flow cytometry.

Cleaved caspase 3 induction

2 x 10^4 mouse NK cells were cultured in CR-10 media with 5 ng/mL recombinant mouse IL-15 (Peprotech) and control DMSO or 2.5 μM Nutlin-3a (MedChem Express; Cat# HY-10029) for 24 hours before intracellular staining for cleaved caspase 3.

Adoptive transfer of NK cells

Freshly isolated congenically distinct NK cells were labeled with CellTrace™ Violet (CTV) (ThermoFisher; Cat#C34557) following manufacturer instructions. CTV labeled cells were mixed at a 50:50 ratio, resuspended in PBS, and injected 5x10^5 cells i.v. into wild type recipient mice.

Tumor killing assays

Low passage MHC Class I deficient MC38 tumor cells were labeled with CTV (ThermoFisher; Cat#C34557) following manufacturer instructions. Freshly isolated splenic NK cells were cultured with 1 x 10^4 β2M$^{-/-}$ MC38 cells per well at effector:target (E:T) ratios of 4:1, 2:1, and 1:1 in the presence of 50 ng/mL recombinant mouse IL-15 (Peprotech; Cat#210-15) for 16 hours. Remaining CTV positive tumor cells were quantified by flow cytometry using the Attune NxT Acoustic Focusing cytometer and data were analyzed with FlowJo v10.7.2 software (TreeStar).

Flow cytometry and cell sorting

Cells were analyzed for cell surface markers using fluorophore-conjugated antibodies (BioLegend, eBioscience). Cell surface staining was performed in FACS Buffer (2% FBS and 2 mM EDTA in PBS) and intracellular staining was performed by fixing and permeabilizing using the eBioscience Foxp3/Transcription Factor kit for intranuclear proteins or BD Cytofix/Cytoperm kits for cytokines. Flow cytometry was performed using the Attune NxT Acoustic Focusing cytometer (Thermo) and data were analyzed with FlowJo v10.7.2 software (TreeStar). Cell surface and intracellular staining was performed using the following fluorophore-conjugated antibodies: CD45.1 (A20), CD45.2 (104), NK1.1 (PK136), TCRβ (H57-597), CD3 (17A2), IFN-γ (XMG1.2), Ly6C (HK1.4), Bcl-2 (BCL/10C4), CD11b (M1/70), CD27 (LG.3A10), granzyme b (GB11), UTX (N2C1 - GeneTex), Goat anti-rabbit H&L (Abcam - ab6717), Bim (c34c5), Ki-67 (16A8), CD107a (1D4B), cleaved caspase 3 (Asp175), human CD56 (TULY56), human CD3 (UCHT1), and human IFN-γ (B27). Isolated splenic NK cells were sorted using Aria-H Cytometer (BD) to >95% purity.

Quantitative PCR

For quantitative PCR experiments, up to 5 x 10^5 cells were isolated using NK EasySep magnetic Isolation kit (StemCell; Cat#19855) as detailed above. RNA was isolated from cells using Quick-RNA Micro-prep kit (Zymo; Cat#R1051). Then, RNA was quantified using a NanoDrop and used up to 1 ug to synthesize cDNA using High-Capacity cDNA Reverse Transcription Kit (ThermoFisher; Cat# 4368813). Then 1 ul of undiluted cDNA was directly used in a Taqman Real-Time PCR assay in a 386 well plate. Each sample was plated at a minimum of 3 technical replicates per taqman probe. Taqman probes (*Ifng*: Mm01168134_m1, *Csf2*: Mm01290062_m1, *Kdm6a (Utx):* Mm00801998_m1, *Eif2s3:* Mm01236979_g1, *Kdm5c*: Mm00840032_m1, *Kdm6c (Uty):* Mm00447710_m1, *Ddx3x: Mm04207948_gH*), were ordered from ThermoFisher Taqman probe

catalog (Cat# 4331182). Normalized expression was calculated as follows: 1) β-actin was used as a housekeeping gene and used to normalize the amount of each sample for each probe, then 2) each sample was normalized to female WT for each gene.

ELISA

2 x 10^4 mouse NK cells were stimulated with recombinant mouse IL-12 (20 ng/mL; Peprotech) and recombinant mouse IL-18 (10 ng/mL; Peprotech) for 4 hours before conditioned media was harvested and stored at -80°C. Mouse IFN-γ and GM-CSF were detected using Legend Max ELISA kits (Biolegend) following manufacturer's instructions.

Western blot

Protein was extracted from enriched primary splenic NK cells using Pierce RIPA buffer (Thermo-Fisher) with Halt protease inhibitor cocktail (Thermo-Fisher) and protein concentration was quantified using the Pierce BCA Protein Assay kit (Thermo-Fisher). Samples were electrophoresed on NuPage Novex 4–12% Bis-Tris Protein Gels, transferred to PVDF membranes, and blocked overnight at 4°C with 5% w/v nonfat milk in 1X TBS and 0.1% Tween-20. Immunoblots were performed using rabbit anti-UTX (anti-UTX Cell Signaling Rabbit mAb #33510), rabbit anti-β-actin (Cell Signaling CST4970), and goat anti-rabbit horseradish peroxidase secondary antibody (Thermo-Fisher 31466). Proteins were detected using the SuperSignal West Pico PLUS ECL kit (Thermo-Fisher) and visualized using the Azure Biosystems c280 imager.

RNA-seq library construction

RNA was isolated from 50,000 sort-purified NK cells per sample using RNeasy Mini kit (Qiagen). RNA quality was verified using High Sensitivity RNA Screen Tape and excluded samples with a RINe <6.0. RNA-seq libraries were sequenced using Illumina HighSeq 4000 platform (single end, 50bp).

ATAC-seq library construction

ATAC-seq libraries were produced by the Applied Genomics, Computation, and Translational Core Facility at Cedars Sinai in the following manner: 50,000 cells per sample were lysed to collect nuclei and treated with Tn5 transposase (Illumina) for 30 minutes at 37°C with gentle agitation. The DNA was isolated with DNA Clean & Concentrator Kit (Zymo) and PCR amplified and barcoded with NEBNext High-Fidelity PCR Mix (New England Biolabs) and unique dual indexes (Illumina). The ATAC-Seq library amplification was confirmed by real-time PCR, and additional barcoding PCR cycles were added as necessary while avoiding overamplification. Amplified ATAC-Seq libraries were purified with DNA Clean & Concentrator Kit (Zymo). The purified libraries were quantified with Kapa Library Quant Kit (KAPA Biosystems) and quality assessed on 4200 TapeStation System (Agilent). The libraries were pooled based on molar concentrations and sequenced on an Illumina HighSeq 4000 platform (paired end, 100bp).

CUT&Tag Library Preparation

For anti-UTX CUT&Tag library preparation, nuclei were isolated with cold nuclear extraction buffer (20 mM HEPES, pH 7.9, 10 mM KCl, 0.1% Triton X-100, 20% glycerol, 0.5 mM spermidine in 1X protease inhibitor buffer) and incubated with activated concanavalin A (ConA) coated magnetic beads (Polysciences - 86057-3) in PCR strip tubes at room temperature for 10

minutes. A 1:100 dilution of primary antibody (anti-UTX Cell Signaling Rabbit mAb #33510 or IgG Isotype Control: Cell Signaling Technology #3900S) in antibody buffer (20 mM HEPES pH 7.5; 150 mM NaCl; 0.5 mM Spermidine; 1X Protease inhibitor cocktail (Roche) ; 0.05% Digitonin, 2 mM EDTA, 0.1% BSA) was added and nuclei were incubated with primary antibodies overnight at 4C. The next day, the strip tubes were incubated on a magnetic tube holder and supernatants were discarded. Secondary antibody (Guinea Pig anti-Rabbit IgG Fisher Scientific - NBP172763) was added diluted 1:100 in Dig-Wash (20 mM HEPES pH 7.5; 150 mM NaCl; 0.5 mM Spermidine; 1X Protease inhibitor cocktail; 0.05% Digitonin) and nuclei were incubated for 1 hour at room temperature. Nuclei were washed four times in Dig-Wash and then incubated with a 1:20 dilution of pAG-Tn5 adapter complex (EpiCypher) in Dig-300 buffer (1x Protease inhibitor cocktail, 20 mM HEPES pH 7.5, 300 mM NaCl, 0.5 mM spermidine) for 1 hour at room temperature. To stop tagmentation, 25 uL Dig-300 buffer with 10 uL 1 M MgCl, 7.5 uL 0.5 M EDTA, 2.5 uL 10% SDS, and 5 uL 10 mg/mL proteinase K was added to each reaction and incubated at 55 degrees for 1 hour. DNA was extracted by phenol:chloroform:isoamyl alcohol separation. DNA was barcoded and amplified using the following conditions: a PCR mix of 25 uL NEBNext 2X mix, 2 uL each of barcoded forward and reverse 10 uM primers, and 21 uL of extracted DNA was amplified at: 58C for 5 min, 72C for 5 min, 98C for 45 sec, 16x 98C for 15 sec followed by 63C for 10 sec, 72C for 1 min. Amplified DNA libraries were purified by adding 1.3x volume of KAPA pure SPRI beads (Roche) to each sample and incubated for 10 minutes at room temperature. Samples were placed on a magnet and unbound liquid was removed. Beads were rinsed twice with 80% ethanol, and DNA was eluted with 25 uL TE buffer. All individually i7-barcoded libraries were mixed at equal molar proportions for sequencing on an Illumina NovaSeq 6000 sequencer.

Sequencing Data Analysis

ATAC-seq and anti-UTX CUT&Tag fastq files were trimmed to remove low-quality reads and adapters using Cutadapt[79] (version 2.3). The reads were aligned to the reference mouse genome (mm10) with bowtie2[80] (version 2.2.9). Peak calling was performed with MACS2[81] (version 2.1.1). Peaks/regions identified as UTX-bound (UTX CUT&Tag) and differentially accessible (ATAC-seq) were annotated using the annotatepeaks.pl function from the HOMER analysis package. To determine the distance to the nearest TSS (transcription start site), we used the default settings in annotatepeaks.pl, which utilizes RefSeq transcription start sites to determine the closest TSS. For genomic annotation, we used the "Basic Annotation" output provided by the assignGenomeAnnotation program in annotatePeaks.pl. The TSS was defined from -1kB to +100bp, and TTS (transcription termination site) was defined from -100 bp to +1kB. "Basic Annotation" is based on alignments of RefSeq transcripts to the UCSC hosted mouse genome file (mm10). HTseq[82] (version 0.9.1) was used to count the number of reads that overlap each peak per sample. The peak counts for ATAC-seq were analyzed with DESeq2 [83] (version 1.24.0) to identify differentially accessible genomic regions. Peaks with adjusted p-value < 0.05 were considered significantly differentially accessible. UTX CUT&Tag peak counts were trimmed for low counts <50 and WT was compared with UTX^{NKD} as a control for background signal. The peak counts for ATAC and anti-UTX CUT&Tag were visualized with Integrated Genome Browser (version 9.1.8) using mouse genome 2011. RNA sequencing analysis was carried out by first checking the quality of the reads using FastQC. Then, they were mapped with HISAT2 (version 2.2.1) to the mouse genome (mm10). The counts for each gene were obtained by HtSeq[82]. Differential expression analyses were carried out using DESeq2[83] (version 1.24.0) with default parameters. Genes with

adjusted p value <0.05 were considered significantly differentially expressed. Sequencing depth normalized counts were used to plot the expression values for individual genes.

Fuzzy c-means clustering was used for both ATAC-seq and RNA-seq using significant (adjusted p-value andFDR <0.05, $\log_2$ fold change +/- 0.5) normalized counts generated from DESeq2. Mfuzz package (version 3.14) within R was used to perform this analysis into 6 clusters with a membership score of > 0.5. The differentially accessible ATAC peaks were analyzed using the findMotifsGenome.pl function from HOMER[57] (version 4.9.1) of each cluster to identify enriched cis-regulatory motifs of transcription factors. Pathway analysis of clustered RNA-seq data was performed using g:Profiler using the g:GOSt function. Top relevant pathways were selected from KEGG Biological Pathways and Gene Ontology Pathways (Biological Processes and Molecular Function).

DICE Expression Data Analysis

Gene expression data in sorted human NK cells by donor sex was provided by the Database of Immune Cell Expression, Expression quantitative trait loci (eQTLs) and Epigenomics (DICE) Project[68]. Expression data was downloaded as transcripts per million per sorted immune cell type and male or female sex. Expression was then normalized to the average of females.

Statistical Analyses

For graphs, data are shown as mean ± SEM, and unless otherwise indicated, statistical differences were evaluated using a student's t test. For graphs containing multiple groups, either one-way (one treatment or condition) or two-way (multiple treatments or conditions) ANOVA with Tukey's correction for multiple comparisons was used as stated. For Kaplan-Meir survival curve, samples

were compared using the Log-rank (Mantel-Cox) test with correction for testing multiple hypotheses. A p-value < 0.05 was considered significant. Graphs were produced and statistical analyses were performed using GraphPad Prism and ggplot2 library in R. Spearman Correlation on best fit regression line was performed using ggpubr library in R.

Data Availability

Sequencing datasets are accessible from GEO with accession number GSE185065.

References

1. Wilkinson, N.M., Chen, H.C., Lechner, M.G. & Su, M.A. Sex Differences in Immunity. *Annu Rev Immunol* (2022).

2. Klein, S.L. & Flanagan, K.L. Sex differences in immune responses. *Nat Rev Immunol* **16**, 626-638 (2016).

3. Pardue, M.-L. & Wizemann, T.M. Exploring the biological contributions to human health: does sex matter? (2001).

4. Gianella, S. *et al*. Sex Differences in CMV Replication and HIV Persistence During Suppressive ART. *Open Forum Infect Dis* **7**, ofaa289 (2020).

5. Takahashi, T. & Iwasaki, A. Sex differences in immune responses. *Science* **371**, 347-348 (2021).

6. Abdullah, M. *et al*. Gender effect on in vitro lymphocyte subset levels of healthy individuals. *Cell Immunol* **272**, 214-219 (2012).

7. Lee, B.W. *et al*. Age- and sex-related changes in lymphocyte subpopulations of healthy Asian subjects: from birth to adulthood. *Cytometry* **26**, 8-15 (1996).

8. Melzer, S. *et al*. Reference intervals for leukocyte subsets in adults: Results from a population-based study using 10-color flow cytometry. *Cytometry B Clin Cytom* **88**, 270-281 (2015).

9. Patin, E. *et al*. Natural variation in the parameters of innate immune cells is preferentially driven by genetic factors. *Nat Immunol* **19**, 302-314 (2018).

10. Huang, Z. *et al*. Effects of sex and aging on the immune cell landscape as assessed by single-cell transcriptomic analysis. *Proc Natl Acad Sci U S A* **118** (2021).

11. Talebizadeh, Z., Simon, S.D. & Butler, M.G. X chromosome gene expression in human tissues: male and female comparisons. *Genomics* **88**, 675-681 (2006).

12. Hyde, D.M. *et al*. Peribronchiolar fibrosis in lungs of cats chronically exposed to diesel exhaust. *Lab Invest* **52**, 195-206 (1985).

13. Fang, H., Disteche, C.M. & Berletch, J.B. X Inactivation and Escape: Epigenetic and Structural Features. *Front Cell Dev Biol* **7**, 219 (2019).

14. Chen, X. *et al*. Sex difference in neural tube defects in p53-null mice is caused by differences in the complement of X not Y genes. *Dev Neurobiol* **68**, 265-273 (2008).

15. Smith-Bouvier, D.L. *et al*. A role for sex chromosome complement in the female bias in autoimmune disease. *J Exp Med* **205**, 1099-1108 (2008).

16. Souyris, M. *et al*. TLR7 escapes X chromosome inactivation in immune cells. *Sci Immunol* **3** (2018).

17. Hammer, Q., Ruckert, T. & Romagnani, C. Natural killer cell specificity for viral infections. *Nat Immunol* **19**, 800-808 (2018).

18. Orange, J.S. Natural killer cell deficiency. *J Allergy Clin Immunol* **132**, 515-525 (2013).

19. Biron, C.A., Nguyen, K.B., Pien, G.C., Cousens, L.P. & Salazar-Mather, T.P. Natural killer cells in antiviral defense: function and regulation by innate cytokines. *Annu Rev Immunol* **17**, 189-220 (1999).

20. Scalzo, A.A., Fitzgerald, N.A., Simmons, A., La Vista, A.B. & Shellam, G.R. Cmv-1, a genetic locus that controls murine cytomegalovirus replication in the spleen. *J Exp Med* **171**, 1469-1483 (1990).

21. Bukowski, J.F., Warner, J.F., Dennert, G. & Welsh, R.M. Adoptive transfer studies demonstrating the antiviral effect of natural killer cells in vivo. *J Exp Med* **161**, 40-52 (1985).

22. Bukowski, J.F. & Welsh, R.M. Inability of interferon to protect virus-infected cells against lysis by natural killer (NK) cells correlates with NK cell-mediated antiviral effects in vivo. *J Immunol* **135**, 3537-3541 (1985).

23. Brown, M.G. *et al*. Vital involvement of a natural killer cell activation receptor in resistance to viral infection. *Science* **292**, 934-937 (2001).

24. Welsh, R.M., Brubaker, J.O., Vargas-Cortes, M. & O'Donnell, C.L. Natural killer (NK) cell response to virus infections in mice with severe combined immunodeficiency. The stimulation of NK cells and the NK cell-dependent control of virus infections occur independently of T and B cell function. *J Exp Med* **173**, 1053-1063 (1991).

25. Daniels, K.A. *et al*. Murine cytomegalovirus is regulated by a discrete subset of natural killer cells reactive with monoclonal antibody to Ly49H. *J Exp Med* **194**, 29-44 (2001).

26. Shellam, G.R., Allan, J.E., Papadimitriou, J.M. & Bancroft, G.J. Increased susceptibility to cytomegalovirus infection in beige mutant mice. *Proc Natl Acad Sci U S A* **78**, 5104-5108 (1981).

27. Bancroft, G.J., Shellam, G.R. & Chalmer, J.E. Genetic influences on the augmentation of natural killer (NK) cells during murine cytomegalovirus infection: correlation with patterns of resistance. *J Immunol* **126**, 988-994 (1981).

28. Menees, K.B. *et al*. Sex- and age-dependent alterations of splenic immune cell profile and NK cell phenotypes and function in C57BL/6J mice. *Immun Ageing* **18**, 3 (2021).

29. Mujal, A.M., Delconte, R.B. & Sun, J.C. Natural Killer Cells: From Innate to Adaptive Features. *Annu Rev Immunol* **39**, 417-447 (2021).

30. Loh, J., Chu, D.T., O'Guin, A.K., Yokoyama, W.M. & Virgin, H.W.t. Natural killer cells utilize both perforin and gamma interferon to regulate murine cytomegalovirus infection in the spleen and liver. *J Virol* **79**, 661-667 (2005).

31. Tyznik, A.J., Verma, S., Wang, Q., Kronenberg, M. & Benedict, C.A. Distinct requirements for activation of NKT and NK cells during viral infection. *J Immunol* **192**, 3676-3685 (2014).

32. Orange, J.S., Wang, B., Terhorst, C. & Biron, C.A. Requirement for natural killer cell-produced interferon gamma in defense against murine cytomegalovirus infection and enhancement of this defense pathway by interleukin 12 administration. *J Exp Med* **182**, 1045-1056 (1995).

33. Nakaya, M., Tachibana, H. & Yamada, K. Effect of estrogens on the interferon-gamma producing cell population of mouse splenocytes. *Biosci Biotechnol Biochem* **70**, 47-53 (2006).

34. Chiossone, L. *et al*. Maturation of mouse NK cells is a 4-stage developmental program. *Blood* **113**, 5488-5496 (2009).

35. Wainer Katsir, K. & Linial, M. Human genes escaping X-inactivation revealed by single cell expression data. *BMC Genomics* **20**, 201 (2019).

36. Yang, F., Babak, T., Shendure, J. & Disteche, C.M. Global survey of escape from X inactivation by RNA-sequencing in mouse. *Genome Res* **20**, 614-622 (2010).

37. Berletch, J.B. *et al*. Escape from X inactivation varies in mouse tissues. *PLoS Genet* **11**, e1005079 (2015).

38. Arnold, A.P. Four Core Genotypes and XY* mouse models: Update on impact on SABV research. *Neurosci Biobehav Rev* **119**, 1-8 (2020).

39. Hasegawa, H. *et al*. Activation of p53 by Nutlin-3a, an antagonist of MDM2, induces apoptosis and cellular senescence in adult T-cell leukemia cells. *Leukemia* **23**, 2090-2101 (2009).

40. Riggan, L. *et al*. The transcription factor Fli1 restricts the formation of memory precursor NK cells during viral infection. *Nat Immunol* (2022).

41. Min-Oo, G., Bezman, N.A., Madera, S., Sun, J.C. & Lanier, L.L. Proapoptotic Bim regulates antigen-specific NK cell contraction and the generation of the memory NK cell pool after cytomegalovirus infection. *J Exp Med* **211**, 1289-1296 (2014).

42. Bjorkstrom, N.K., Strunz, B. & Ljunggren, H.G. Natural killer cells in antiviral immunity. *Nat Rev Immunol* **22**, 112-123 (2022).

43. Smyth, M.J. *et al*. Perforin is a major contributor to NK cell control of tumor metastasis. *J Immunol* **162**, 6658-6662 (1999).

44. Van der Meulen, J., Speleman, F. & Van Vlierberghe, P. The H3K27me3 demethylase UTX in normal development and disease. *Epigenetics* **9**, 658-668 (2014).

45. Wang, S.P. *et al*. A UTX-MLL4-p300 Transcriptional Regulatory Network Coordinately Shapes Active Enhancer Landscapes for Eliciting Transcription. *Mol Cell* **67**, 308-321 e306 (2017).

46. Gozdecka, M. *et al*. UTX-mediated enhancer and chromatin remodeling suppresses myeloid leukemogenesis through noncatalytic inverse regulation of ETS and GATA programs. *Nat Genet* **50**, 883-894 (2018).

47. Wang, C. *et al*. UTX regulates mesoderm differentiation of embryonic stem cells independent of H3K27 demethylase activity. *Proc Natl Acad Sci U S A* **109**, 15324-15329 (2012).

48. Sciume, G. *et al*. Rapid Enhancer Remodeling and Transcription Factor Repurposing Enable High Magnitude Gene Induction upon Acute Activation of NK Cells. *Immunity* **53**, 745-758 e744 (2020).

49. Shih, H.Y. *et al*. Developmental Acquisition of Regulomes Underlies Innate Lymphoid Cell Functionality. *Cell* **165**, 1120-1133 (2016).

50. Miller, S.A., Mohn, S.E. & Weinmann, A.S. Jmjd3 and UTX play a demethylase-independent role in chromatin remodeling to regulate T-box family member-dependent gene expression. *Mol Cell* **40**, 594-605 (2010).

51. Dembele, D. & Kastner, P. Fuzzy C-means method for clustering microarray data. *Bioinformatics* **19**, 973-980 (2003).

52. Raudvere, U. *et al*. g:Profiler: a web server for functional enrichment analysis and conversions of gene lists (2019 update). *Nucleic Acids Res* **47**, W191-W198 (2019).

53. Kaya-Okur, H.S. *et al*. CUT&Tag for efficient epigenomic profiling of small samples and single cells. *Nat Commun* **10**, 1930 (2019).

54. Kupz, A. *et al*. Contribution of Thy1+ NK cells to protective IFN-gamma production during Salmonella typhimurium infections. *Proc Natl Acad Sci U S A* **110**, 2252-2257 (2013).

55. Gillard, G.O. *et al*. Thy1+ NK [corrected] cells from vaccinia virus-primed mice confer protection against vaccinia virus challenge in the absence of adaptive lymphocytes. *PLoS Pathog* **7**, e1002141 (2011).

56. Chen, E.Y. *et al*. Enrichr: interactive and collaborative HTML5 gene list enrichment analysis tool. *BMC Bioinformatics* **14**, 128 (2013).

57. Heinz, S. *et al*. Simple combinations of lineage-determining transcription factors prime cis-regulatory elements required for macrophage and B cell identities. *Mol Cell* **38**, 576-589 (2010).

58. Rapp, M. *et al*. Core-binding factor beta and Runx transcription factors promote adaptive natural killer cell responses. *Sci Immunol* **2** (2017).

59. Simonetta, F., Pradier, A. & Roosnek, E. T-bet and Eomesodermin in NK Cell Development, Maturation, and Function. *Front Immunol* **7**, 241 (2016).

60. Presnell, J.S., Schnitzler, C.E. & Browne, W.E. KLF/SP Transcription Factor Family Evolution: Expansion, Diversification, and Innovation in Eukaryotes. *Genome Biol Evol* **7**, 2289-2309 (2015).

61. Kramer, B. *et al*. Early IFN-alpha signatures and persistent dysfunction are distinguishing features of NK cells in severe COVID-19. *Immunity* **54**, 2650-2669 e2614 (2021).

62. D'Agostino, P. *et al*. Sex hormones modulate inflammatory mediators produced by macrophages. *Ann N Y Acad Sci* **876**, 426-429 (1999).

63. Lu, F.X. *et al*. The strength of B cell immunity in female rhesus macaques is controlled by CD8+ T cells under the influence of ovarian steroid hormones. *Clin Exp Immunol* **128**, 10-20 (2002).

64. Singh, R.P. & Bischoff, D.S. Sex Hormones and Gender Influence the Expression of Markers of Regulatory T Cells in SLE Patients. *Front Immunol* **12**, 619268 (2021).

65. Cook, K.D. *et al*. T Follicular Helper Cell-Dependent Clearance of a Persistent Virus Infection Requires T Cell Expression of the Histone Demethylase UTX. *Immunity* **43**, 703-714 (2015).

66. Beyaz, S. *et al*. The histone demethylase UTX regulates the lineage-specific epigenetic program of invariant natural killer T cells. *Nat Immunol* **18**, 184-195 (2017).

67. Mitchell, J.E. *et al*. UTX promotes CD8(+) T cell-mediated antiviral defenses but reduces T cell durability. *Cell Rep* **35**, 108966 (2021).

68. Schmiedel, B.J. *et al*. Impact of Genetic Polymorphisms on Human Immune Cell Gene Expression. *Cell* **175**, 1701-1715 e1716 (2018).

69. Pomeroy, C., Delong, D., Clabots, C., Riciputi, P. & Filice, G.A. Role of interferon-gamma in murine cytomegalovirus infection. *J Lab Clin Med* **132**, 124-133 (1998).

70. Louis, C. *et al*. NK cell-derived GM-CSF potentiates inflammatory arthritis and is negatively regulated by CIS. *J Exp Med* **217** (2020).

71. Bosselut, R. Pleiotropic Functions of H3K27Me3 Demethylases in Immune Cell Differentiation. *Trends Immunol* **37**, 102-113 (2016).

72. Hong, S. *et al*. Identification of JmjC domain-containing UTX and JMJD3 as histone H3 lysine 27 demethylases. *Proc Natl Acad Sci U S A* **104**, 18439-18444 (2007).

73. Van Laarhoven, P.M. *et al*. Kabuki syndrome genes KMT2D and KDM6A: functional analyses demonstrate critical roles in craniofacial, heart and brain development. *Hum Mol Genet* **24**, 4443-4453 (2015).

74. Rezvani, K. Adoptive cell therapy using engineered natural killer cells. *Bone Marrow Transplant* **54**, 785-788 (2019).

75. Angelo, L.S. *et al*. Phenotypic and Functional Plasticity of CXCR6(+) Peripheral Blood NK Cells. *Front Immunol* **12**, 810080 (2021).

76. Eckelhart, E. *et al*. A novel Ncr1-Cre mouse reveals the essential role of STAT5 for NK-cell survival and development. *Blood* **117**, 1565-1573 (2011).

77. Smith, L.M., McWhorter, A.R., Masters, L.L., Shellam, G.R. & Redwood, A.J. Laboratory strains of murine cytomegalovirus are genetically similar to but phenotypically distinct from wild strains of virus. *J Virol* **82**, 6689-6696 (2008).

78. Weizman, O.E. *et al*. ILC1 Confer Early Host Protection at Initial Sites of Viral Infection. *Cell* **171**, 795-808 e712 (2017).

79. Kechin, A., Boyarskikh, U., Kel, A. & Filipenko, M. cutPrimers: A New Tool for Accurate Cutting of Primers from Reads of Targeted Next Generation Sequencing. *J Comput Biol* **24**, 1138-1143 (2017).

80. Langmead, B. & Salzberg, S.L. Fast gapped-read alignment with Bowtie 2. *Nat Methods* **9**, 357-359 (2012).

81. Zhang, Y. *et al*. Model-based analysis of ChIP-Seq (MACS). *Genome Biol* **9**, R137 (2008).

82. Anders, S., Pyl, P.T. & Huber, W. HTSeq--a Python framework to work with high-throughput sequencing data. *Bioinformatics* **31**, 166-169 (2015).

83. Love, M.I., Huber, W. & Anders, S. Moderated estimation of fold change and dispersion for RNA-seq data with DESeq2. *Genome Biol* **15**, 550 (2014).

Chapter 3:

UTX regulates T cell effector responses in hypoxia during cancer and autoimmunity

UTX regulates T cell effector responses in hypoxia during cancer and autoimmunity

Mandy I. Cheng[1,2,], Lee Hong[2], Melissa Lechner[1], Bryan Chen[1], Scott Chin[1], Shezhad Sheikh, and Maureen A. Su[1,2,3,*]

[1]*Department of Microbiology, Immunology, and Molecular Genetics, David Geffen School of Medicine at UCLA, Los Angeles, CA 90095*
[2]*Molecular Biology Institute, University of California, Los Angeles, Los Angeles, CA 90095, USA*
[3]*Department of Pediatrics, David Geffen School of Medicine at UCLA, Los Angeles, CA 90095, USA*

Correspondence:

Maureen A. Su, MD
David Geffen School of Medicine at UCLA
615 Charles E. Young Drive South, BSRB 290C
Los Angeles, CA 90095
Phone: 310-825-2130
Email: masu@mednet.ucla.edu

Abstract

Low oxygen levels, or hypoxia, has been associated with immune defects in multiple contexts. Hypoxia is associated with higher levels of H3K27me3 in CD4+ T cells. T cell-specific deletion of the histone demethylase is sufficient to recapitulate multiple features of hypoxia, including increased H3K27me3 accumulation and decreased production of IFN-γ^+ $CD4^+$ T cells in response to IL-12 cytokine stimulation. T cell specific UTX deletion has functional consequences, as mice are more susceptible to colon cancer and is not responsive to IFN-γ-dependent checkpoint therapy with anti-PD-1 treatment. However, mice with loss of UTX in T cells protected from colitis in which IFN-γ production has been tied with pathogenesis. Concomitant RNA and H3K27me3 CUT&Tag sequencing demonstrate an important role for UTX in removing repressive H3K27me3 marks to promote upregulation of IL12/STAT4 pathway genes including *Il12rb, Tbx21,* and *Ifng*. Together, these data demonstrate that UTX functions through its demethylase activity to promote Th1 cell differentiation and suggest that hypoxia's HIF-independent effects on Th1 effector function may be mediated through UTX.

Introduction

Hypoxia occurs when oxygen demand outstrips supply and is a feature of multiple pathological immune niches, including tumors and sites of tissue inflammation. The consequences of hypoxia can be potentially dire, with sustained hypoxia in pathologic sites leading to metabolic crisis and cell death. As a consequence, multiple oxygen sensing mechanisms have evolved that mediate an adaptive response to low oxygen conditions. Central to these hypoxia-induced pathways is the stabilization of the transcription factor HIF (hypoxia-inducible factor), which promotes expression of genes important in adaptation to low oxygen levels in multiple tissue types. In addition, multiple HIF-*independent* oxygen sensing mechanisms have recently been identified, including those that alter histone methylation to induce transcriptional changes in hypoxia[1]. In support of an important role for hypoxia in disease development, hypoxia in pathologic immune niches has been linked to disease outcome. For instance, hypoxia in tumors has been linked with poor outcomes with cancer[2]. Strong evidence now exists that hypoxic tumor microenvironment limits effective anti-tumor immune responses, suggesting that hypoxia's immunosuppressive effect is a major contributor to poor outcomes[3]. At the same time, hypoxia in inflamed colon tissue is associated with protection in a mouse model of colitis[4]. Although the mechanisms underlying these associations remain incompletely defined, it is possible that they may also reflect hypoxia-induced immunosuppression.

Hypoxia has been associated with alterations in the differentiation and effector function of immune cells. For instance, multiple studies have reported that hypoxic conditions decrease the proportion of T cells that produce IFN-γ[5,6]. In these studies, this decrease has been attributed to stabilization of T cell HIF-1a, since genetic deletion of HIF-1a in T cells resulted in increased IFN-γ secretion[6]. Moreover, hypoxia-induced changes in IFN-γ production were abolished in HIF-1a

deficient $CD4^+$ T cells, suggesting that upregulation of HIF-1a is responsible for the hypoxia-induced changes. Importantly, however, because the changes were incompletely attenuated with HIF-1a deficiency, these data also suggested the existence of an additional, distinct oxygen-sensing pathways important in regulating hypoxia-induced changes.

UTX (ubiquitously transcribed tetratricopeptide repeat protein on the X chromosome; transcribed by the gene *Kdm6a*) is an epigenetic regulator that catalyzes the demethylation of repressive trimethylated histone 3 lysine 27 (H3K27me3) marks to activate gene transcription[7]. As a member of the 2-oxoglutarate (OG)-dependent dioxygenase (2-OGDD) family of enzymes, UTX has recently been shown to be oxygen-sensitive. Specifically, hypoxia inactivates UTX's demethylase activity in a HIF independent manner[8,9] which results in global H3K27me3 hypermethylation. We focused on UTX as a potential oxygen sensor in $CD4^+$ T cells due to its previous links with immune cell differentiation[10,11] evidence of H3K27me3 accumulation in hypoxic tumor tissue[6] and because of its potential for therapeutic manipulation[7].

Here, we show that hypoxia is associated with histone hypermethylation in CD4+ T cells. T cell-specific deletion of the histone demethylase UTX (encoded by the gene *Kdm6a*) is sufficient to recapitulate multiple features of hypoxia, including decreased proportion of IFN-γ^+ $CD4^+$ T cells. Concomitant RNA and H3K27me3 CUT&Tag sequencing demonstrate an important role for UTX in removing repressive H3K27me3 marks to promote upregulation of IL12/STAT4 pathway genes including *IL12rb, Tbx21,* and *Ifng*. T cell specific UTX deletion has functional consequences, as mice are more susceptible to colon cancer but protected from colitis. Together, these data demonstrate that UTX functions through its demethylase activity to promote Th_1 cell differentiation and suggest that hypoxia's HIF-independent effects on Th_1 effector function may be mediated through UTX.

Results

Hypoxia and UTX deficiency leads to increased H3K27me3 levels in CD4+ T cells.

Recent work demonstrated H3K27me3 accumulation in an immortalized cell line in hypoxia[8]. Consistent with this, our results indicate this phenomenon translates to primary T cells due to increased global H3K27me3 levels in T cells incubated in hypoxia (1% O_2) compared to normoxia (20% O_2) **(Fig. 1a)**. Since UTX is an epigenetic regulator harboring intrinsic H3K27me3 demethylase activity, we hypothesized loss of UTX catalytic activity under low oxygen conditions may be causing the accumulation of H3K27me3 levels in T cells. To interrogate this, we produced mice with a T cell specific deletion of UTX (*Kdm6a*$^{flox/flox}$ *Lck*$^{cre+}$) hereafter referred to as UTX^{TCD} mice. Flow cytometric analysis revealed an increase in H3K27me3 levels in naïve splenic CD4+ T cells in UTX^{TCD} mice compared to WT **(Fig. 1b)**. Together, these data suggest that loss of UTX in T cells recapitulates the accumulation of H3K27me3 levels observed in hypoxic conditions.

Hypoxia and UTX deficiency both result in decreased CD4+ T cell IFN-γ production.

Hypoxia has previously been associated with decreased CD4$^+$ T cell IFN-γ production[6]. In line with this, our flow cytometric analysis of mouse CD4+ T cells stimulated with proinflammatory cytokines IL-2 and IL-12, showed lower IFN-γ production with hypoxia (1% O2) compared to normoxia (20%) **(Fig. 1c,d)**. Remarkably, UTX deficiency in CD4+ T cells phenocopied this hypoxia-associated finding, with significantly lower proportion of UTX^{TCD} CD4+ T cells producing IFN-γ, compared to WT **(Fig. 1c,d)**. Additionally, UTX deficiency abolished hypoxia-induced decrease in IFN-γ production since there were no significant differences between IFN-γ production during normoxia or hypoxia by UTX^{TCD} T cells **(Fig. 1c,d).** Moreover, there is no significant difference in IFN-γ production between WT T cells in hypoxia and UTX^{TCD} T cells in

normoxia. Taken together, these data suggest loss of UTX in T cells phenocopies IFN-γ production during hypoxia conditions and eliminates the oxygen sensitivity of the T cells as seen in WT.

T cell specific UTX deficiency protects against autoimmune colitis.

Given decreased IFN-γ production by UTX-deficient $CD4^+$ T cells *in vitro*, we next sought to determine how T cell specific UTX deficiency affects disease development. We utilized two different mouse models of colitis, in which pathologic hypoxia is well-characterized and IFN-γ producing $CD4^+$ T cells have been identified as a pathogenic cell type[12]. The first mouse model of autoimmune colitis we tested was an acute high-dose injection of an activating antibody against CD3 (anti-CD3, clone: 2C11), which has been reported to result in colonic T helper cells expansion and differentiation[13] **(Fig. 2a)**. In accordance with our *in vitro* findings, flow cytometric analysis of the small intestine of anti-CD3 challenged mice revealed decreased IFN-γ producing $CD4^+$ T cells in UTX^{TCD} compared to WT **(Fig. 2b,c)**. These data suggest loss of UTX in T cells also results in defective IFN-γ production and Th_1 differentiation *in vivo* in response to anti-CD3 treatment.

Furthermore, to determine long-term effects in survival and disease progression due to loss of UTX in T cells, a $CD4^+$ T cell adoptive transfer colitis model was used **(Fig. 2d)**[14]. Naïve $CD4^+$ T cells ($CD3^+$ $TCR\beta^+$ $CD4^+$ $CD45RB^{hi}$) cells from either WT or UTX^{TCD} mice were transferred into mice lacking T or B cells ($Rag2^{-/-}$), and recipients were monitored for IFN-γ production, weight loss, and survival **(Fig. 2d)**. Similar to the acute colitis model, recipients of UTX^{TCD} T cells showed significantly decreased IFN-γ production by $CD4^+$ T cells compared to WT in the lamina propria **(Fig. 2e,f)**. Notably, recipients of UTX^{TCD} T cells were protected from pathologies associated with colitis such as weight loss and lethality (defined by >20% weight loss), suggesting that UTX deficiency in $CD4^+$ T cells is sufficient to protect from colitis **(Fig. 2g,h)**. Moreover,

recipients of UTX^{TCD} T cells had decreased inflammatory colitis as measured by colon weight to length ratios **(Fig. 2i)**.Hematoxylin and eosin staining of colons revealed diffuse inflammation from the cecum to rectum with infiltration of $CD4^+$ lymphocytes into the lamina propria in the recipients of WT T cells **(Fig. 2j, left)**; however, recipients of UTX^{TCD} T cells had significantly decreased lymphocytic infiltration into the lamina propria, mucosal thickening, transmural spread, and abnormal crypt formation as measured by blinded histopathological scoring **(Fig. 2j, right and Fig. 2k)**. Together, these data suggest loss of UTX in T cells results in decreased IFN-γ production *in vivo* and protection against inflammatory colitis.

UTX deficiency results in increased susceptibility to colon cancer.

In addition to colitis, colon cancer has also been previously characterized to be associated with hypoxic microenvironments[15]. Thus, we tested if loss of UTX in T cells impacted the survival potential of mice challenged with a subcutaneous tumor model of colon cancer (MC38). We transferred $3x10^5$ MC38 colon cancer cells into the flank of either WT or UTX^{TCD} mice and monitored survival (characterized as a tumor of <1000 mm^3 size) and tumor measurements over time. Our results indicate loss of UTX in T cells is detrimental to survival against tumor growth since UTX^{TCD} mice displayed increased lethality **(Fig. 3a)** and tumor size over time **(Fig. 3b)** and on day 25 post MC38 challenge **(Fig. 3c)**. Furthermore, recent developments in tumor immunotherapy indicate treatment with anti-PD-1 is dependent on IFN-γ production by T cells[16]. Thus, we hypothesized that UTX^{TCD} mice would not be responsive to anti-PD-1 therapy due to defective IFN-γ production by UTX-deficient $CD4^+$ T cells **(Fig. 1 and 2)**. To test this, we treated WT or UTX^{TCD} mice challenged with MC38 tumors subcutaneously with either isotype or anti-PD-1 treatment twice a week until the study's endpoint **(Fig. 3d)**. As predicted, WT mice

responded quickly to anti-PD-1 treatment with little to no tumor growth compared to isotype treatment over time **(Fig. 3d,e – pink (WT - anti-PD-1) vs. black (WT - isotype))** and on Day 21 post MC38 tumor challenge (**Fig. 3e**). However, in accordance with our hypothesis, UTX^{TCD} mice showed both higher tumor burden compared to WT **(Fig. 3d,e – red (UTX^{TCD} – isotype) vs. black (WT - isotype))** and did not respond to anti-PD-1 treatment with no significant difference between isotype and anti-PD-1 treatment over time **(Fig. 3d,e – red (UTX^{TCD} - isotype) vs. blue (UTX^{TCD} - anti-PD-1))** and on Day 21 post MC38 tumor challenge (**Fig. 3e**). These results indicate loss of UTX in T cells results is not responsive to anti-PD-1 therapy due to the inability of UTX-deficient T cells to produce robust IFN-γ levels in response to tumor challenge.

T cell specific UTX deficiency results in repressive H3K27me3 accumulation and downregulation of transcription T helper 1 effector gene loci.

A previous report in T cells described differentiation from naïve CD4+ T cells to T helper type 1 cell (Th_1) was associated with removal of H3K27me3 marks at *Ifng, Tbx21,* and other Th_1-associated loci[17]. Erasure of these repressive H3K27me3 marks increases chromatin accessibility at these genetic loci and poises them for active gene transcription to allow to Th_1 differentiation. Since UTX deficiency in T cells results in decreased IFN-γ production by $CD4^+$ T cells, UTX may play a role in catalyzing removal of H3K27me3 at gene loci required for Th1 differentiation. To explore this possibility, we performed bulk RNA sequencing and H3K27me3 CUT&Tag sequencing to identify genetic loci whose transcription may be regulated by UTX's demethylase activity. RNAseq of WT vs. UTX^{TCD} $CD4^+$ T cells showed global changes in transcription, with 660 genes downregulated and 1084 genes upregulated in UTX^{TCD} **(Fig. 4a)**. Gene ontology pathway analysis of the downregulated genes in UTX^{TCD} vs. WT showed Th_1 effector gene

pathways such as “IL-12 and Stat4 dependent signaling” and “Cytokines and Inflammatory Response”. More specifically, examples of downregulated genes in UTX^{TCD} $CD4^{+}$ T cells included Th_1 genes including *Tbx21, Ifng,* and *Il12rb2* **(Fig. 4c)**. At the same time, these genes correlated with increased H3K27me3 levels by CUT&Tag in UTX^{TCD} T cells **(Fig. 4d)**. Further integrative analysis of the RNA-seq and H3K27me3 CUT&Tag datasets revealed a correlation of genes that show decreased expression by RNA-seq with genes that showed higher levels of H3K27me3 (repressive) histone marks **(Fig. 4e)**. Finally, H3K27me3 CUT&Tag showed significantly higher peaks in distal regulatory regions associated with *Ifng* **(Fig. 4f)**, and promoter, intronic, and intergenic regions associated with *Tbx21* and *Il12rb2* **(Fig. 4f)**. These findings suggest UTX regulates Th_1 differentiation from naïve CD4+ T cells by catalyzing the removal of repressive histone marks (H3K27me3) to regulate downstream Th_1 gene expression.

Discussion

We demonstrated both hypoxia and UTX-deficiency results in accumulation of H3K27me3 and decreased IFN-γ production. Furthermore, Th_1 stimulation experiments *in vitro* with IL-12 and *in vivo* with anti-CD3 treatment of UTX-deficient T cells resulted in decreased IFN-γ production by $CD4^+$ T cells. Moreover, UTX deficiency in T cells protects against colitis driven by pathogenic Th_1 cells. At the same time, mice with UTX-deficient T cells are more prone to colon cancer, where IFN-γ producing Th_1 cells are important for responsiveness to anti-tumor checkpoint therapy (anti-PD-1). Finally, global transcriptomics by RNA-seq and H3K27me3 profiling by CUT&Tag in WT or UTX^{TCD} T cells revealed decreased expression of Th1 genes (*Tbx21, Ifng,* and *Il12rb2*) and concomitant increased repressive H3K27me3 at those gene loci. Ultimately, our study suggests UTX is oxygen-sensitive and is required in regulating expression of genes critical for Th_1 differentiation.

Previously, UTX's oxygen sensitivity was demonstrated in accumulation of H3K27me3 in hypoxia (5% O_2) was observed in a mouse hepatoma cell line (mHepa-1 c4) in a Hif1a (hypoxia-inducible factor)-independent manner. Notably, our results demonstrate this is also the case in primary mouse T cells. The specific effect of hypoxia on T cell effector function has been a topic of debate in which a study in 2015 reports decreased IFN-γ production[6] and another study in 2010 reporting increased IFN-γ production in hypoxia[18]. However, cell culturing and hypoxia conditions may be a cause for the discrepancies described in these studies. Furthermore, increased IFN-γ protein production was detected in Balb/c mice meanwhile in C57BL/6 only displayed differences in *Ifng* transcript levels. Our results support the hypothesis that IFN-γ production by $CD4^+$ T cells in C57BL./6 mice is significantly decreased in hypoxic conditions and loss of UTX recapitulates this decrease and displays similar levels despite differences in environmental oxygen conditions.

Since deletion of UTX in T cells phenocopies the increased H3K27me3 accumulation and decreased IFN-γ production, one possible hypothesis is that UTX's demethylase activity is required for promoting IFN-γ production in T cells. However, additional studies using a demethylase-dead mutant of UTX in T cells would be beneficial in determining if these effects are dependent on UTX's catalytic activity. This contrasts with UTX's activity in mouse natural killer (NK) cells in which demethylase activity is dispensable for productive IFN-γ secretion. Similarly, another study in CD8+ T cells determined UTX's catalytic demethylase activity was not required for productive effector function[19]. However, in human NK cells, pharmacological inhibition of UTX and JMJD3's H3K27me3 demethylase activity resulted in decreased IFN-γ production[7]. This indicates UTX may display cell type specific activities.

Furthermore, UTX can also cooperate with additional epigenetic regulators such as BRG1, MLL4/5, SWI/SNF to deposit additional histone marks and modulate general chromatin accessibility in a demethylase-independent manner[20-22]. There may be additional UTX-mediated demethylase-independent functions that play a role during hypoxia in other contexts.

Further studies are needed to elucidate differential UTX-mediated mechanisms based on the cell type. Moreover, additional mechanistic studies are required to identify specific regions that UTX are bound to within the genome in $CD4^+$ T cells to determine direct UTX-mediated effects. Also, other protein-protein interactions between UTX and other transcription factors during hypoxia such as Hif-1α will be important to understand if they co-regulate each other.

Acknowledgements

We thank members of the Su lab for helpful discussion. We thank the UCLA Technology Center for Genomics and Bioinformatics for RNA sequencing library preparation. M.A.S. is supported by

the NIH (NS107851, AI143894, DK119445) Department of Defense (USAMRAA PR200530), and National Organization of Rare Diseases. M.I.C. is supported by Ruth L. Kirschstein National Research Service Awards (GM007185 and AI007323), and Whitcome Fellowship from the Molecular Biology Institute at UCLA.

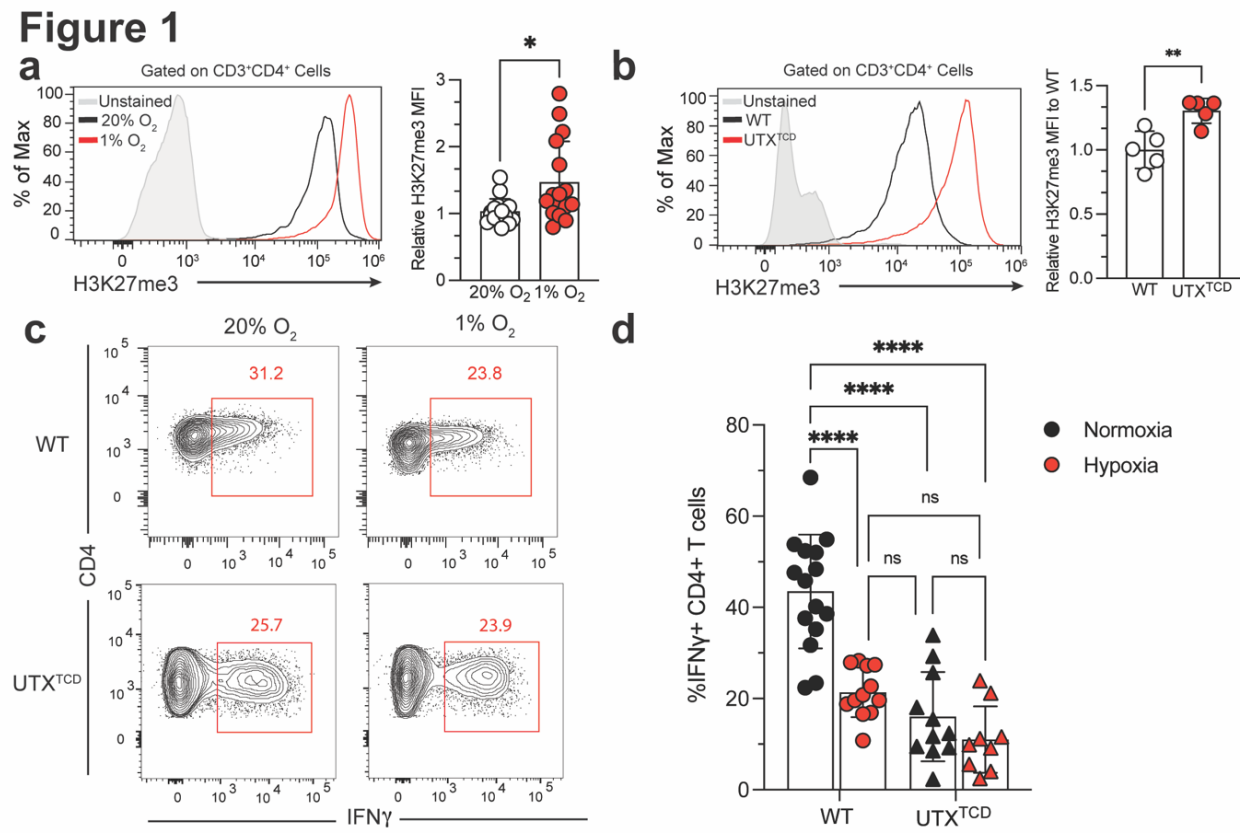

Figure 1: Loss of UTX in CD4+ T cells recapitulates increased H3K27me3 and decreased IFN-γ production in hypoxia. a) Representative histograms (left) and quantification (right) of H3K27me3 MFI in CD4+ T cells from spleens of WT mice in normoxia (20% O_2) compared to hypoxia (1% O_2) (n = 15 per group). **b)** Representative histograms (left) and quantification (right) of H3K27me3 MFI in CD4+ T cells from spleens of WT or UTX^{TCD} mice (n = 5 per group). **c,d)** CD4+ T cells were isolated from spleens of WT or UTX^{TCD} mice and stimulated in the presence of IL-12 (10 ng/ml), IL-2 (5ng/ml), anti-CD28 (0.5 mg/ml), and plate-bound anti-CD3 (10 ug/ml) for 4 days before performing flow cytometry. **c)** Representative contour plots and **d)** quantification of %IFN-γ+ CD4+ T cells cultured in normoxia in normoxia (20% O_2) compared to hypoxia (1% O_2) (n = 12 per group). Data are representative of 2-3 independent experiments. Samples were compared using **a,b)** paired two-tailed Student's t test **c,d)** one-way ANOVA and data points are presented as individual mice with the mean ± SEM (ns, Not Significant; ****, p<0.0001).

Figure 2

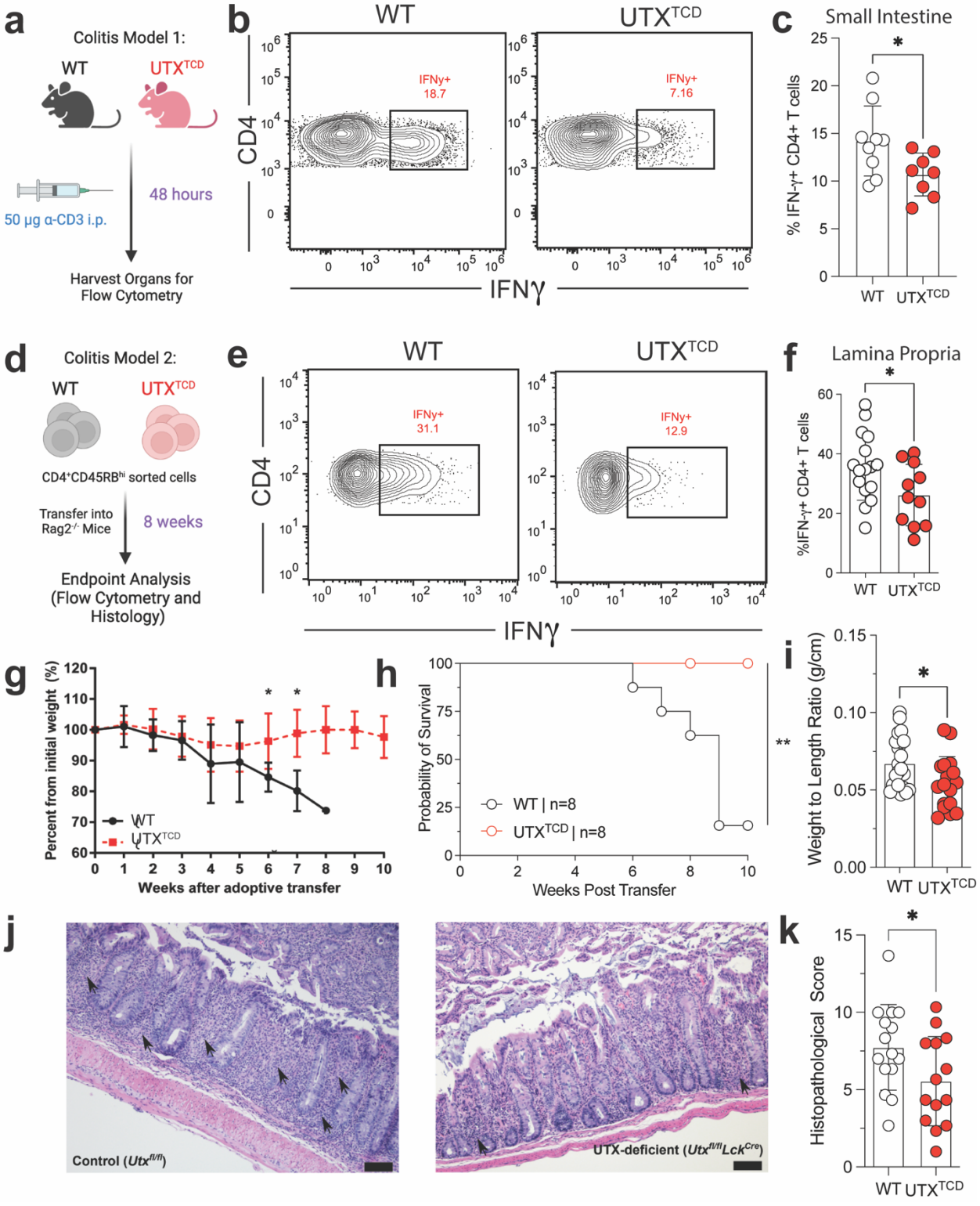
a
Colitis Model 1:
WT
UTXTCD
48 hours
50 µg α-CD3 i.p.
Harvest Organs for Flow Cytometry
b
WT
UTXTCD
IFNγ+ 18.7
IFNγ+ 7.16
CD4
IFNγ
c
Small Intestine
% IFN-γ+ CD4+ T cells
d
Colitis Model 2:
CD4+CD45RBhi sorted cells
Transfer into Rag2-/- Mice
8 weeks
Endpoint Analysis (Flow Cytometry and Histology)
e
IFNγ+ 31.1
IFNγ+ 12.9
f
Lamina Propria
%IFN-γ+ CD4+ T cells
g
Percent from initial weight (%)
Weeks after adoptive transfer
h
Probability of Survival
WT | n=8
UTXTCD | n=8
Weeks Post Transfer
i
Weight to Length Ratio (g/cm)
j
Control (Utxfl/fl)
UTX-deficient (Utxfl/flLckCre)
k
Histopathological Score

Figure 2: Deletion of UTX in T cells is protective in two models of autoimmune colitis.

a) Schematic of experimental design of colitis model 1: WT and UTX^{TCD} mice were injected with 50 ug of anti-CD3 antibody intraperitoneally (i.p.). After 48 hours, the small intestine was harvested for flow cytometry. **b)** Representative contour plots and **c)** quantification of %IFN-γ+ CD4+ T cells from the small intestine of WT or UTX^{TCD} mice (n = 9 per group). **c)** Schematic of experimental design of colitis model 2: $CD4^{+}CD45RB^{hi}$ T cells were FACS sorted from WT or UTX^{TCD} mice and transferred into $Rag2^{-/-}$ recipient mice. Recipients were monitored for 8 weeks and then sacrificed for flow cytometry and histological analysis of the lamina propria. **e)** Representative contour plots and **f)** quantification of %IFN-γ+ CD4+ T cells from the lamina propria of $Rag2^{-/-}$ recipient mice with either WT or UTX^{TCD} transferred cells (n = 16 per group). **g)** Graph of percent weight loss from original weight in recipients with either WT or UTX^{TCD} transferred cells (n = 7-8 per group). **h)** Kaplan-Meier survival curve of $Rag2^{-/-}$ recipient mice of WT or UTX^{TCD} T cells, with survival defined as weight loss <20% (n = 7-8 per group). **i)** Histopathological scoring of colon tissues for inflammation. **j)** Hematoxylin and eosin (H&E) staining of colon tissues of recipient mice at study endpoint. Note extensive infiltration in the lamina propria (black arrows; left) in recipients of control $CD4^{+}CD45RB^{hi}$ cells with relatively mild disease and decreased immune cell infiltration in recipients of UTX-deficient $CD4^{+}CD45RB^{hi}$ cells (black arrows; right). Black scale bar=50um. **k)** Weight-to-length ratios of recipient mice colons harvested at study endpoint, measured as weight (g) divided by length (cm) from the cecum to rectum (n = 10 per group). Data are representative of 2-3 independent experiments. Samples were compared using unpaired two-tailed Student's t and data points are presented as individual mice with the mean ± SEM (ns, Not Significant; ****, $p<0.0001$).

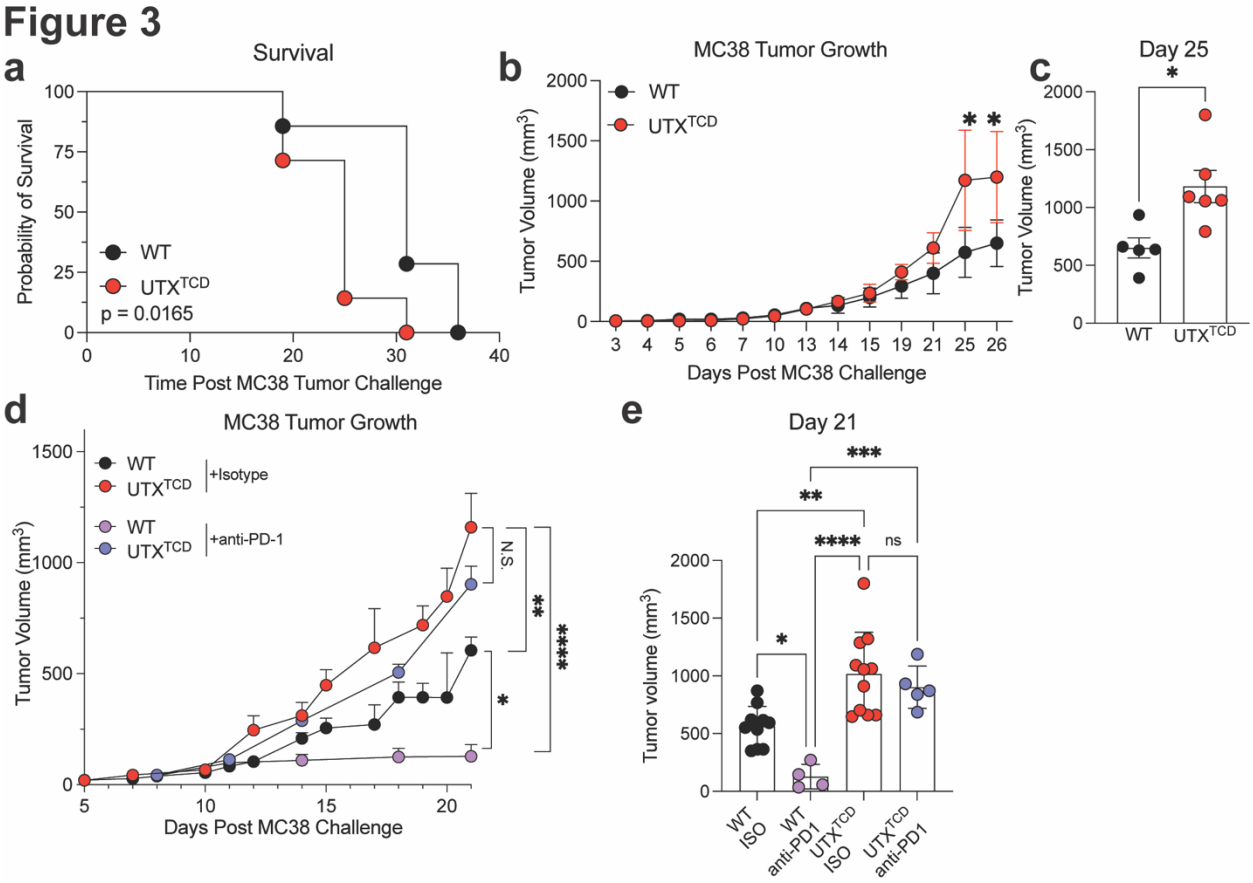

Figure 3: Increased tumorigenicity in mice UTX deficient T cells and is not rescued by treatment with ant-PD-1. a) Kaplan-Meier survival curve, **b)** tumor volume over time, and **c)** Day 25 tumor volumes of WT or UTX^{TCD} mice challenged with $3x10^5$ MC38 tumor cells, with survival defined as weight loss <20% (n = 5-7 per group). **d)** Tumor volume over time and **e)** Day 21 tumor volumes of WT or UTX^{TCD} mice challenged with $3x10^5$ MC38 tumor cells, with either isotype or anti-PD-1 treatment (n = 5-11 per group). Data are representative of 2-3 independent experiments. Samples were compared using **c)** unpaired two-tailed Student's t test **d, e)** one-way ANOVA and data points are presented as individual mice with the mean ± SEM (ns, Not Significant; *, p<0.05; **, p<0.01; ***, p<0.001; ****, p<0.0001).

Figure 4

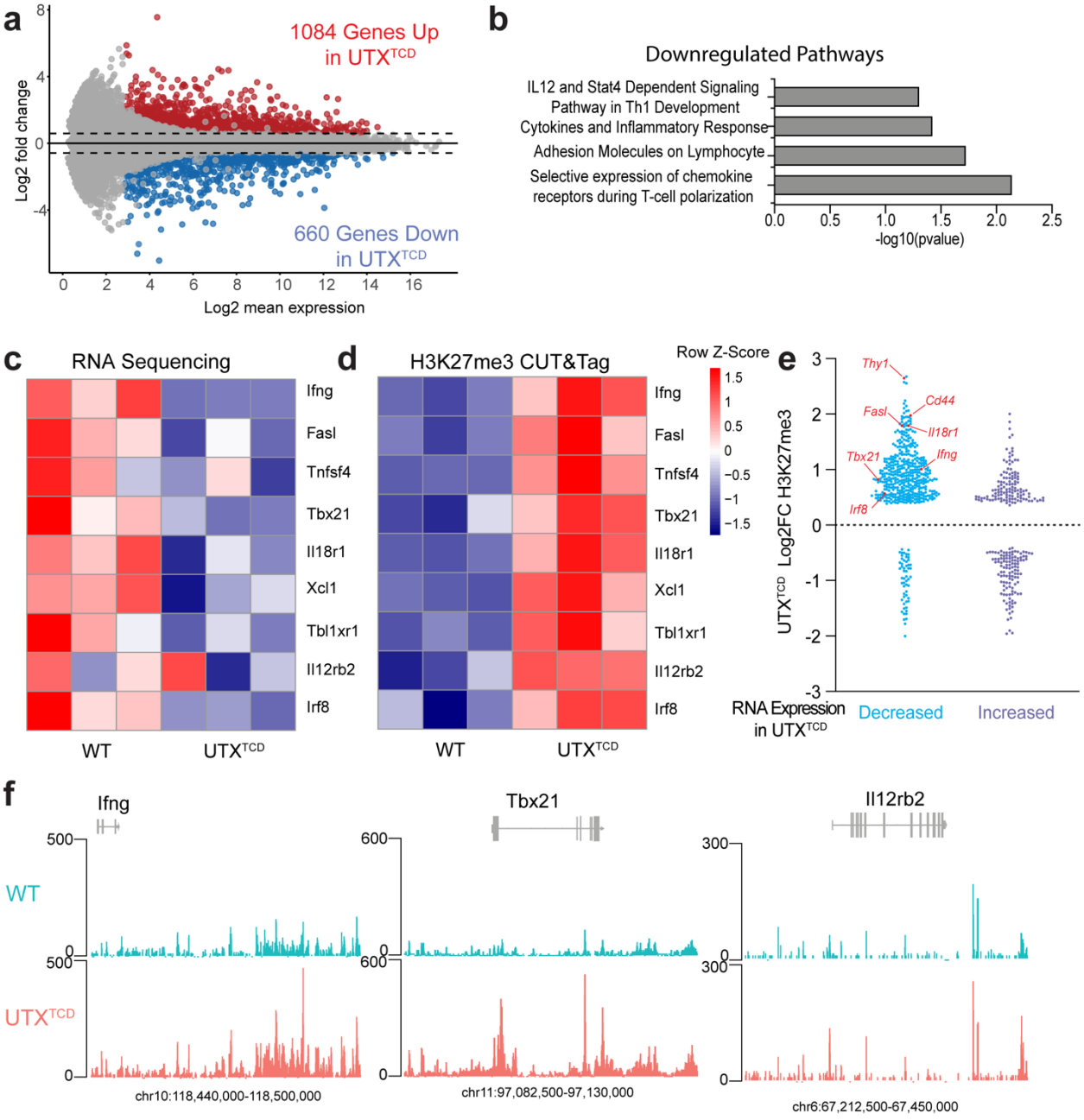

Figure 4: UTX promotes Th1 gene expression through removal of H3K27me3. Splenic T cells were sorted for RNA-seq library preparation (n=3 per group) from WT or UTX^{TCD} T cells. **a)** Volcano plot of total differentially expressed genes in T cells from WT vs. UTX^{TCD} plotted with Log2FC (y axis) and Log2 Mean Expression (x-axis). Red dots indicate genes that are significantly increased and blue dots indicate genes that are significantly decreased, gray dots are not significant.

b) Pathway analysis of significantly downregulated RNA-seq genes using DAVID with $-\log_{10}$(p-value) plotted on x-axis. Heatmaps of target genes in Th1 gene pathways that are **c)** significantly differentially expressed by RNA-seq or **d)** significant differential levels of H3K27me3 by CUT&Tag of WT or UTX^{TCD} T cells. **e)** Log2FC in UTX^{TCD} vs. WT of H3K27me3 levels (y-axis) plotted by either decreased (>-0.5 Log2FC) (blue) or increased (>+0.5 Log2FC) (purple) expression by RNA-seq (x-axis). **f)** Representative gene tracks from UCSC Integrated Genome Browser of H3K27me3 CUT&Tag of *Ifng*, *Tbx21*, and *Il12rb2* ; Y-axis depicts counts per million (CPM).

Materials and Methods

Mice

All mouse experimental procedures were approved by the University of North Carolina Institutional Animal Care and Use Committee (IACUC) and mice were housed and bred in sterile, specific pathogen-free mouse facilities. $Utx^{fl/fl}$ mice were back-crossed to C57BL/6J for > 5 generations and crossed to Lck^{Cre} mice as previously described (Cook et al *Immunity* 2015).

Experimental colitis and tissue harvesting

Mouse model of colitis 1: WT and UTX^{TCD} mice were injected with 50 ug of anti-CD3 antibody intraperitoneally (i.p.). After 48 hours, the small intestine was harvested for flow cytometry.

Mouse model of colitis 2: $CD4^+$ cells were enriched from $Utx^{fl/fl}$ (control) or $Utx^{fl/fl}Lck^{Cre}$ 8- to 12-week-old female donor spleens using the $CD4^+$ T cell Isolation Kit II (Miltenyi Biotec) according to manufacturer instructions. Cells were labeled and sorted for $CD4^+CD25^-CD45RB^{hi}$ cells by fluorescence-activated cell sorting. Cells (5×10^5) were injected i.p. into 4- to 7-week-old $Rag2^{-/-}$ recipient female mice. Weights were measured weekly from initial cell transfer. Lack of survival was defined as death or weight loss > 20%. Recipient mice were euthanized once weight loss was >20% of initial body weight or at 10 weeks after adoptive transfer and spleens, mesenteric lymph nodes (MLNs), and colons were harvested. Spleens and MLNs were macerated and filtered into a single cell suspension using a 10-mL syringe using 40um cell strainers (BD), followed by incubation with ACK Lysis Buffer (Gibco). Colons were digested in collagenase/dispase and DNase (Roche), followed by Ficoll gradient centrifugation. Lymphocytes were collected and used for flow cytometry analysis.

Colon histopathology

Colons were harvested at 10 weeks after adoptive transfer or earlier if weight loss of 20% was noted. Specimens were fixed in 10% formalin, sectioned (5 μm), and stained with H&E. Scoring for inflammation was performed as described (Ostanin *et al Am J Physiol Gastrointest Liver Physiol* 2009; Read *et al Curr Protocol Immunol* 2001) in a blinded fashion by a veterinary pathologist.

Flow cytometry and cell sorting

Cells were analyzed for cell surface markers using fluorophore-conjugated antibodies (BioLegend, eBioscience). Cell surface staining was performed in FACS Buffer (2% FBS and 2 mM EDTA in PBS) and intracellular staining was performed by fixing and permeabilizing using the eBioscience Foxp3/Transcription Factor kit for intranuclear proteins or BD Cytofix/Cytoperm kits for cytokines. Flow cytometry was performed using the Attune NxT Acoustic Focusing cytometer (Thermo) and data were analyzed with FlowJo v10.7.2 software (TreeStar). Cell surface and intracellular staining was performed using the following fluorophore-conjugated antibodies: TCRβ (H57-597), CD3 (17A2), IFN-γ (XMG1.2), UTX (N2C1 - GeneTex), Goat anti-rabbit H&L (Abcam - ab6717), Bim (c34c5). Isolated splenic T cells were sorted using Aria-H Cytometer (BD) to >95% purity.

Hypoxia and In vitro Th1 skewing assay

Splenic $CD4^{+}CD25^{-}$ naïve T cells of WT or UTX^{TCD} mice were sorted per manufacturer's instructions (StemCell) and cultured with cytokines (10 ng/mL IL-2 and 5 ng/ml of IL-2), anti-

CD28 (0.5 mg/ml), and plate-bound anti-CD3 (5ug/ml) for 4 days. Cells were moved out of anti-CD3 and anti-CD28 into a new well with fresh media and cytokines on day 2. IFN-γ+ CD4+ T cells were accessed using intracellular cytokine staining on day 4. Cells were either incubated in normoxia (20% O_2) or hypoxia (1% O_2). Normoxia conditions were places in a 37C 5% CO_2 incubator in normal oxygen conditions. Hypoxia was simulated using a modular hypoxia incubator chamber that is purged and injected with a mixture of 1% O_2, 5% CO_2 balanced with nitrogen for 5 minutes at 20 liters/min. The hypoxia chamber was placed within the same 37C incubator as the normoxia condition.

RNA-seq library construction

RNA was isolated from 50,000 sort-purified NK cells per sample using RNeasy Mini kit (Qiagen). RNA quality was verified using High Sensitivity RNA Screen Tape and excluded samples with a RINe <6.0. RNA-seq libraries were sequenced using Illumina HighSeq 4000 platform (single end, 50bp).

CUT&Tag Library Preparation

For anti-H3K27me3 CUT&Tag library preparation, nuclei were isolated with cold nuclear extraction buffer (20 mM HEPES, pH 7.9, 10 mM KCl, 0.1% Triton X-100, 20% glycerol, 0.5 mM spermidine in 1X protease inhibitor buffer) and incubated with activated concanavalin A (ConA) coated magnetic beads (Polysciences - 86057-3) in PCR strip tubes at room temperature for 10 minutes. A 1:100 dilution of primary antibody (anti-UTX Cell Signaling Rabbit mAb #33510 or IgG Isotype Control: Cell Signaling Technology #3900S) in antibody buffer (20 mM HEPES pH 7.5; 150 mM NaCl; 0.5 mM Spermidine; 1X Protease inhibitor cocktail (Roche) ;

0.05% Digitonin, 2 mM EDTA, 0.1% BSA) was added and nuclei were incubated with primary antibodies overnight at 4C. The next day, the strip tubes were incubated on a magnetic tube holder and supernatants were discarded. Secondary antibody (Guinea Pig anti-Rabbit IgG Fisher Scientific - NBP172763) was added diluted 1:100 in Dig-Wash (20 mM HEPES pH 7.5; 150 mM NaCl; 0.5 mM Spermidine; 1X Protease inhibitor cocktail; 0.05% Digitonin) and nuclei were incubated for 1 hour at room temperature. Nuclei were washed four times in Dig-Wash and then incubated with a 1:20 dilution of pAG-Tn5 adapter complex (EpiCypher) in Dig-300 buffer (1x Protease inhibitor cocktail, 20 mM HEPES pH 7.5, 300 mM NaCl, 0.5 mM spermidine) for 1 hour at room temperature. To stop tagmentation, 25 uL Dig-300 buffer with 10 uL 1 M MgCl, 7.5 uL 0.5 M EDTA, 2.5 uL 10% SDS, and 5 uL 10 mg/mL proteinase K was added to each reaction and incubated at 55 degrees for 1 hour. DNA was extracted by phenol:chloroform:isoamyl alcohol separation. DNA was barcoded and amplified using the following conditions: a PCR mix of 25 uL NEBNext 2X mix, 2 uL each of barcoded forward and reverse 10 uM primers, and 21 uL of extracted DNA was amplified at: 58C for 5 min, 72C for 5 min, 98C for 45 sec, 16x 98C for 15 sec followed by 63C for 10 sec, 72C for 1 min. Amplified DNA libraries were purified by adding 1.3x volume of KAPA pure SPRI beads (Roche) to each sample and incubated for 10 minutes at room temperature. Samples were placed on a magnet and unbound liquid was removed. Beads were rinsed twice with 80% ethanol, and DNA was eluted with 25 uL TE buffer. All individually i7-barcoded libraries were mixed at equal molar proportions for sequencing on an Illumina NovaSeq 6000 sequencer.

Sequencing Data Analysis

H3K27me3 CUT&Tag fastq files were trimmed to remove low-quality reads and adapters using Cutadapt (version 2.3). The reads were aligned to the reference mouse genome (mm10) with bowtie2 (version 2.2.9). Peak calling was performed with MACS2 (version 2.1.1). Peaks/regions identified as H3K27me3-bound (UTX CUT&Tag) were annotated using the annotatepeaks.pl function from the HOMER analysis package. To determine the distance to the nearest TSS (transcription start site), we used the default settings in annotatepeaks.pl, which utilizes RefSeq transcription start sites to determine the closest TSS. For genomic annotation, we used the "Basic Annotation" output provided by the assignGenomeAnnotation program in annotatePeaks.pl. The TSS was defined from -1kB to +100bp, and TTS (transcription termination site) was defined from -100 bp to +1kB. "Basic Annotation" is based on alignments of RefSeq transcripts to the UCSC hosted mouse genome file (mm10). HTseq (version 0.9.1) was used to count the number of reads that overlap each peak per sample. The peak counts for ATAC-seq were analyzed with DESeq2 (version 1.24.0) to identify differentially accessible genomic regions. Peaks with adjusted p-value < 0.05 were considered significantly differentially accessible. The peak counts for H3K27me3 CUT&Tag were visualized with Integrated Genome Browser (version 9.1.8) using mouse genome 2011. RNA sequencing analysis was carried out by first checking the quality of the reads using FastQC. Then, they were mapped with HISAT2 (version 2.2.1) to the mouse genome (mm10). The counts for each gene were obtained by HtSeq. Differential expression analyses were carried out using DESeq2 (version 1.24.0) with default parameters. Genes with adjusted p value <0.05 were considered significantly differentially expressed. Sequencing depth normalized counts were used to plot the expression values for individual genes.

Pathway analysis of clustered RNA-seq data was performed using DAVID. Top relevant pathways were selected from KEGG Biological Pathways and Gene Ontology Pathways (Biological Processes and Molecular Function).

Statistical Analyses

For graphs, data are shown as mean ± SEM, and unless otherwise indicated, statistical differences were evaluated using a student's t test. For graphs containing multiple groups, either one-way (one treatment or condition) or two-way (multiple treatments or conditions) ANOVA with Tukey's correction for multiple comparisons was used as stated. For Kaplan-Meir survival curve, samples were compared using the Log-rank (Mantel-Cox) test with correction for testing multiple hypotheses. A p-value < 0.05 was considered significant. Graphs were produced and statistical analyses were performed using GraphPad Prism and ggplot2 library in R. Spearman Correlation on best fit regression line was performed using ggpubr library in R.

References

1. Shmakova, A., Batie, M., Druker, J. & Rocha, S. Chromatin and oxygen sensing in the context of JmjC histone demethylases. *Biochem J* 462, 385-395, doi:10.1042/BJ20140754 (2014).

2. Semenza, G. L. Targeting HIF-1 for cancer therapy. *Nat Rev Cancer* 3, 721-732, doi:10.1038/nrc1187 (2003).

3. Labani-Motlagh, A., Ashja-Mahdavi, M. & Loskog, A. The Tumor Microenvironment: A Milieu Hindering and Obstructing Antitumor Immune Responses. *Front Immunol* 11, 940, doi:10.3389/fimmu.2020.00940 (2020).

4. Harris, N. R., Carter, P. R., Yadav, A. S., Watts, M. N., Zhang, S., Kosloski-Davidson, M. & Grisham, M. B. Relationship between inflammation and tissue hypoxia in a mouse model of chronic colitis. *Inflamm Bowel Dis* 17, 742-746, doi:10.1002/ibd.21423 (2011).

5. Caldwell, C. C., Kojima, H., Lukashev, D., Armstrong, J., Farber, M., Apasov, S. G. & Sitkovsky, M. V. Differential effects of physiologically relevant hypoxic conditions on T lymphocyte development and effector functions. *J Immunol* 167, 6140-6149, doi:10.4049/jimmunol.167.11.6140 (2001).

6. Shehade, H., Acolty, V., Moser, M. & Oldenhove, G. Cutting Edge: Hypoxia-Inducible Factor 1 Negatively Regulates Th1 Function. *J Immunol* 195, 1372-1376, doi:10.4049/jimmunol.1402552 (2015).

7. Bosselut, R. Pleiotropic Functions of H3K27Me3 Demethylases in Immune Cell Differentiation. *Trends Immunol* 37, 102-113, doi:10.1016/j.it.2015.12.004 (2016).

8. Chakraborty, A. A., Laukka, T., Myllykoski, M., Ringel, A. E., Booker, M. A., Tolstorukov, M. Y., Meng, Y. J., Meier, S. R., Jennings, R. B., Creech, A. L., Herbert, Z. T., McBrayer, S. K., Olenchock, B. A., Jaffe, J. D., Haigis, M. C., Beroukhim, R., Signoretti, S., Koivunen, P. & Kaelin, W. G., Jr. Histone demethylase KDM6A directly senses oxygen to control chromatin and cell fate. *Science* 363, 1217-1222, doi:10.1126/science.aaw1026 (2019).

9. Prickaerts, P., Adriaens, M. E., Beucken, T. V. D., Koch, E., Dubois, L., Dahlmans, V. E. H., Gits, C., Evelo, C. T. A., Chan-Seng-Yue, M., Wouters, B. G. & Voncken, J. W. Hypoxia increases genome-wide bivalent epigenetic marking by specific gain of H3K27me3. *Epigenetics Chromatin* 9, 46, doi:10.1186/s13072-016-0086-0 (2016).

10. Cook, K. D., Shpargel, K. B., Starmer, J., Whitfield-Larry, F., Conley, B., Allard, D. E., Rager, J. E., Fry, R. C., Davenport, M. L., Magnuson, T., Whitmire, J. K. & Su, M. A. T Follicular Helper Cell-Dependent Clearance of a Persistent Virus Infection Requires T Cell Expression of the Histone Demethylase UTX. *Immunity* 43, 703-714, doi:10.1016/j.immuni.2015.09.002 (2015).

11. Beyaz, S. *et al*. The histone demethylase UTX regulates the lineage-specific epigenetic program of invariant natural killer T cells. *Nat Immunol* **18**, 184-195 (2017).

12. Bregenholt, S *et al*. "In vitro activated CD4+ T cells from interferon-gamma (IFN-gamma)-deficient mice induce intestinal inflammation in immunodeficient hosts." *Clinical and experimental immunology* vol. 118,2 (1999).

13. Sin, Jun Hyung *et al*. "The epigenetic regulator ATF7ip inhibits *Il2* expression, regulating Th17 responses." *The Journal of experimental medicine* vol. 216,9 (2019).

14. Powrie, F., Carlino, J., Leach, M. W., Mauze, S. & Coffman, R. L. A critical role for transforming growth factor-beta but not interleukin 4 in the suppression of T helper type 1-mediated colitis by CD45RB(low) CD4+ T cells. *J Exp Med* 183, 2669-2674, doi:10.1084/jem.183.6.2669 (1996).

15. Qi, L., Chen, J., Yang, Y. & Hu, W. Hypoxia Correlates With Poor Survival and M2 Macrophage Infiltration in Colorectal Cancer. *Front Oncol* 10, 566430, (2020).

16. Garris, Christopher S et al. "Successful Anti-PD-1 Cancer Immunotherapy Requires T Cell-Dendritic Cell Crosstalk Involving the Cytokines IFN-γ and IL-12." *Immunity* vol. 49,6 (2018): 1148-1161.e7, (2018).

17. Wei, G., Wei, L., Zhu, J., Zang, C., Hu-Li, J., Yao, Z., … Zhao, K. Global mapping of H3K4me3 and H3K27me3 reveals specificity and plasticity in lineage fate determination of differentiating CD4+ T cells. *Immunity*, *30*(1), 155–167. (2009).

18. Roman, Jessica et al. "T-cell activation under hypoxic conditions enhances IFN-gamma secretion." *American journal of respiratory cell and molecular biology* vol. 42,1 (2010).

19. Mitchell, J.E. *et al*. UTX promotes CD8(+) T cell-mediated antiviral defenses but reduces T cell durability. *Cell Rep* **35**, 108966 (2021).

20. Gozdecka, M. *et al*. UTX-mediated enhancer and chromatin remodeling suppresses myeloid leukemogenesis through noncatalytic inverse regulation of ETS and GATA programs. *Nat Genet* **50**, 883-894 (2018).

21. Wang, C. *et al*. UTX regulates mesoderm differentiation of embryonic stem cells independent of H3K27 demethylase activity. *Proc Natl Acad Sci U S A* **109**, 15324-15329 (2012).

22. Wang, S.P. *et al*. A UTX-MLL4-p300 Transcriptional Regulatory Network Coordinately Shapes Active Enhancer Landscapes for Eliciting Transcription. *Mol Cell* **67**, 308-321 e306 (2017).

Chapter 4:

Concluding Remarks

Concluding Remarks

While major sex differences occur in both the innate and adaptive immune responses, only recently has sex been beginning to be considered as an important biological factor in treatment decisions. Given the importance of NK cells in anti-viral immunity, understanding the root causes of sex differences in NK cell biology will have far-reaching implications in optimizing endogenous effector responses. We demonstrated that lower UTX expression in male NK cells contributes to their increased numbers and decreased effector functionality. NK cell UTX is required for controlling NK cell fitness, modulating accessibility of transcription factor binding motifs, increasing chromatin accessibility at effector gene loci, and poising NK cells for rapid response to viral infection. Our findings suggest the possibility that UTX deficiency in human NK cells may contribute to decreased viral immunosurveillance observed in these patients, although future work will be needed to support this hypothesis. In males with severe viral illness, for instance, enhancing NK cell UTX activity may provide therapeutic benefit. We expect that these insights will be important not only in the setting of viral infections, but also in other infections and cancer, where NK cells also play an important role. These findings may also have important implications for adoptive cellular therapies, in which NK cells are the subject of intense interest. Additionally, deeper understanding of sex differences in NK cells can also set criteria for donors to develop off-the-shelf cellular therapies.

Furthermore, since deletion of UTX in T cells phenocopies the increased H3K27me3 accumulation and decreased IFN-γ production seen in hypoxia, one possible hypothesis is that UTX's demethylase activity is required for promoting IFN-γ production in T cells. However, additional studies using a demethylase-dead mutant of UTX in T cells would be beneficial in determining if these effects are dependent on UTX's catalytic activity. This contrasts with UTX's

activity in mouse NK cells in which demethylase activity is dispensable for productive IFN-γ secretion. This indicates UTX may display cell type specific activities. Further studies are needed to elucidate differential UTX-mediated mechanisms based on the cell type. Moreover, additional mechanistic studies are required to identify specific regions that UTX are bound to within the genome in $CD4^+$ T cells to determine direct UTX-mediated effects. Also, other protein-protein interactions between UTX and other transcription factors during hypoxia such as Hif-1α will be important to understand if they co-regulate each other.

In summary, our work here has delineated two mechanisms of epigenetic regulation of immune cell homeostasis and effector processes by UTX. First, we described sex differences mediated by increased expression of UTX in females due to escape from X-inactivation. We identified major sex differences in NK cell number mediated by resistance to apoptosis and defective effector mechanisms of cytokine production and cell cytotoxicity in male NK cells compared to female. Additionally, we defined UTX's oxygen sensor capabilities in the context of hypoxia in T cells since both hypoxia and loss of UTX in T cells resulted in decreased Th_1 differentiation and IFN-γ production. Furthermore, specific loss of UTX in T cells protected from two models of autoimmune colitis but also was detrimental in colon cancer challenged mice. These advances have not only added to the basic understanding of NK cell and T cell regulatory mechanisms during various immune challenges but have given us further insight into how to boost endogenous immune responses for future therapeutic approaches.